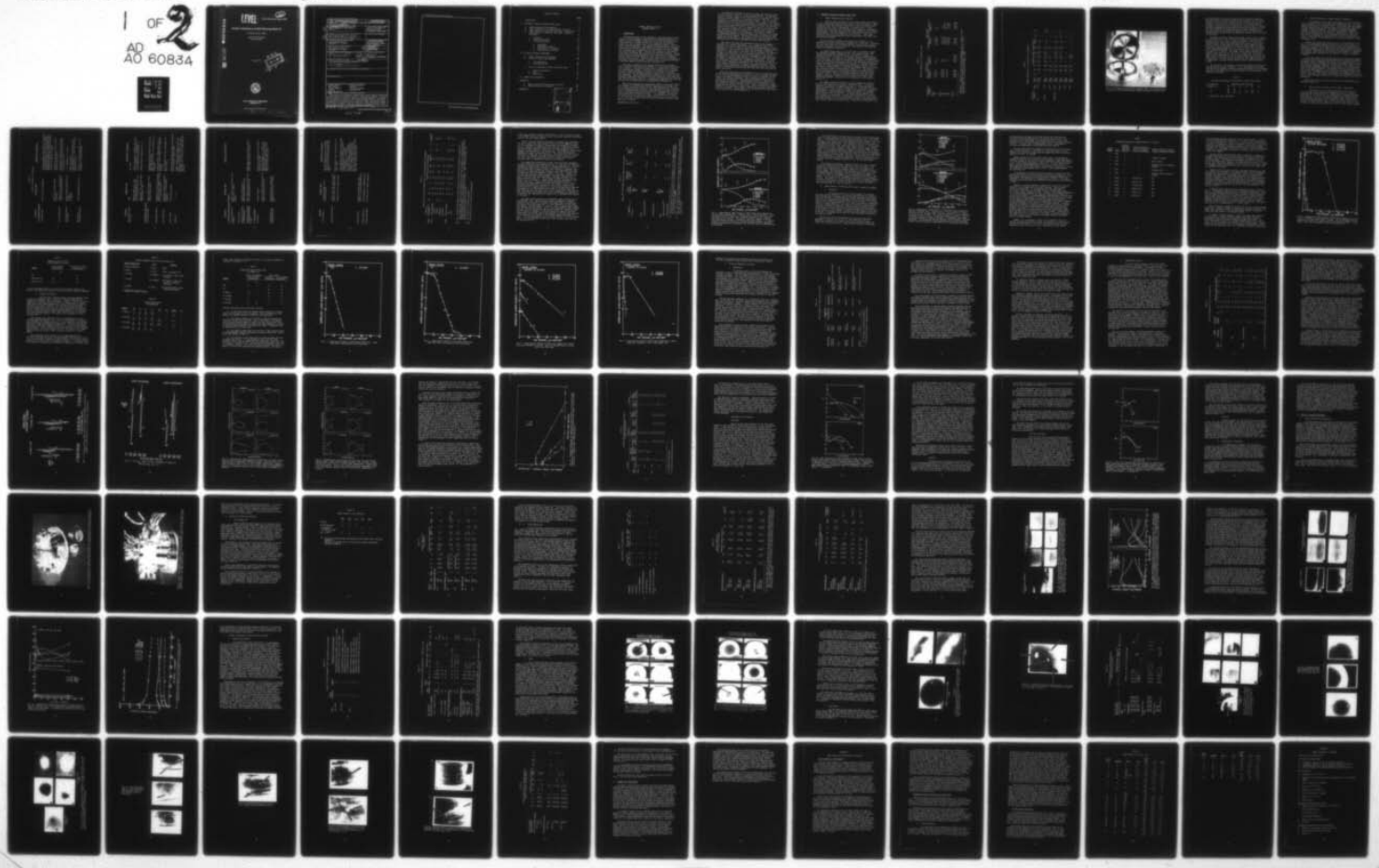
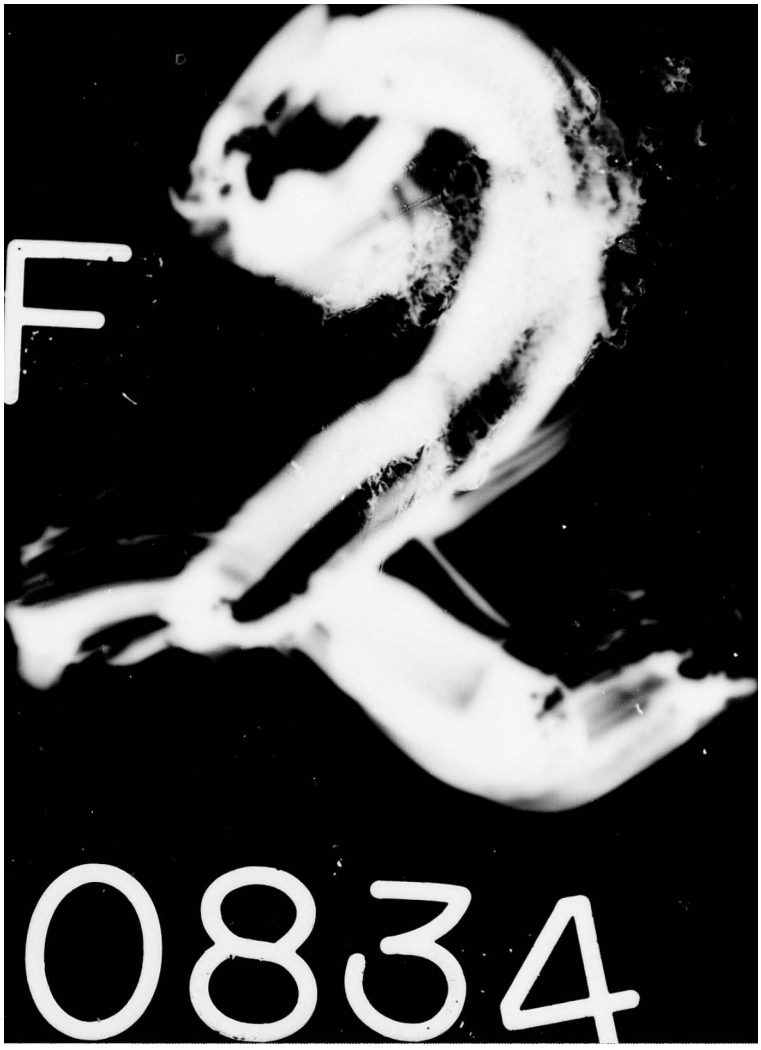
AD-A060 834 NAVAL RESEARCH LAB WASHINGTON D C F/G 13/9
SURFACE CHEMISTRY OF BALL BEARING STEELS II.(U)
AUG 78 J S MURDAY, E G SHAFRIN

UNCLASSIFIED NRL-MR-3850 NL

1 OF 2
AD
AO 60834




F
0834

AD A060834

DDC FILE COPY

LEVEL II

NRL Memorandum Report 3850

Surface Chemistry of Ball Bearing Steels II

J.S. Murday and E.G. Shafrin

Surface Chemistry Branch
Chemistry Division

DDC
RECEIVED
NOV 3 1978
F

August 1978

NAVAL RESEARCH LABORATORY
Washington, D.C.

Approved for public release; distribution unlimited.

78 10 23 055

SECURITY CLASSIFICATION OF THIS PAGE *(When Data Entered)*

REPORT DOCUMENTATION PAGE

READ INSTRUCTIONS BEFORE COMPLETING FORM

1. REPORT NUMBER: NRL Memorandum Report 3850 (14) NRL-MR-3850
2. GOVT ACCESSION NO.
3. RECIPIENT'S CATALOG NUMBER

4. TITLE *(and Subtitle)*: Surface Chemistry of Ball Bearing Steels II. (6)
5. TYPE OF REPORT & PERIOD COVERED: Report on One Phase of a Continuing Problem
6. PERFORMING ORG. REPORT NUMBER

7. AUTHOR(s): James S. Murday and Elaine G. Shafrin (10)
8. CONTRACT OR GRANT NUMBER(s)

9. PERFORMING ORGANIZATION NAME AND ADDRESS: Naval Research Laboratory, Washington, D. C. 20375
10. PROGRAM ELEMENT, PROJECT, TASK AREA & WORK UNIT NUMBERS: NRL Problem C02-31.101; Program Element 61153N-13; Project RR0130143

11. CONTROLLING OFFICE NAME AND ADDRESS: Naval Research Laboratory, Washington, D. C. 20375 (11)
12. REPORT DATE: August 1978
13. NUMBER OF PAGES: 99

14. MONITORING AGENCY NAME & ADDRESS *(if different from Controlling Office)*: (16) RR013011 (12) 99p.
15. SECURITY CLASS. *(of this report)*: Unclassified
15a. DECLASSIFICATION/DOWNGRADING SCHEDULE

16. DISTRIBUTION STATEMENT *(of this Report)*: Approved for public release; distribution unlimited. (17) RR013011A3

17. DISTRIBUTION STATEMENT *(of the abstract entered in Block 20, if different from Report)*

18. SUPPLEMENTARY NOTES

19. KEY WORDS *(Continue on reverse side if necessary and identify by block number)*

Surface analysis	Surface treatments
Ball bearing	Silicones
Surface chemistry	Tricresyl phosphate
Cleaning	Bearing steels
Auger spectroscopy	

20. ABSTRACT *(Continue on reverse side if necessary and identify by block number)*

The lifetime and performance characteristics of ball bearing surfaces and sliding contacts are determined in part by their surface chemistry. This work is in the nature of a survey to identify the important aspects of the various bearing preparation techniques, using newly available analytical tools which are sensitive to the surface layers. Examples of Auger spectroscopic surface analyses will be presented which illustrate the surface compositional changes due to different aspects of specimen preparation: cleaning techniques, specimen handling procedures, and chemical treatment technology.

DD FORM 1 JAN 73 1473 EDITION OF 1 NOV 65 IS OBSOLETE S/N 0102-014-6601

SECURITY CLASSIFICATION OF THIS PAGE *(When Data Entered)*

251950

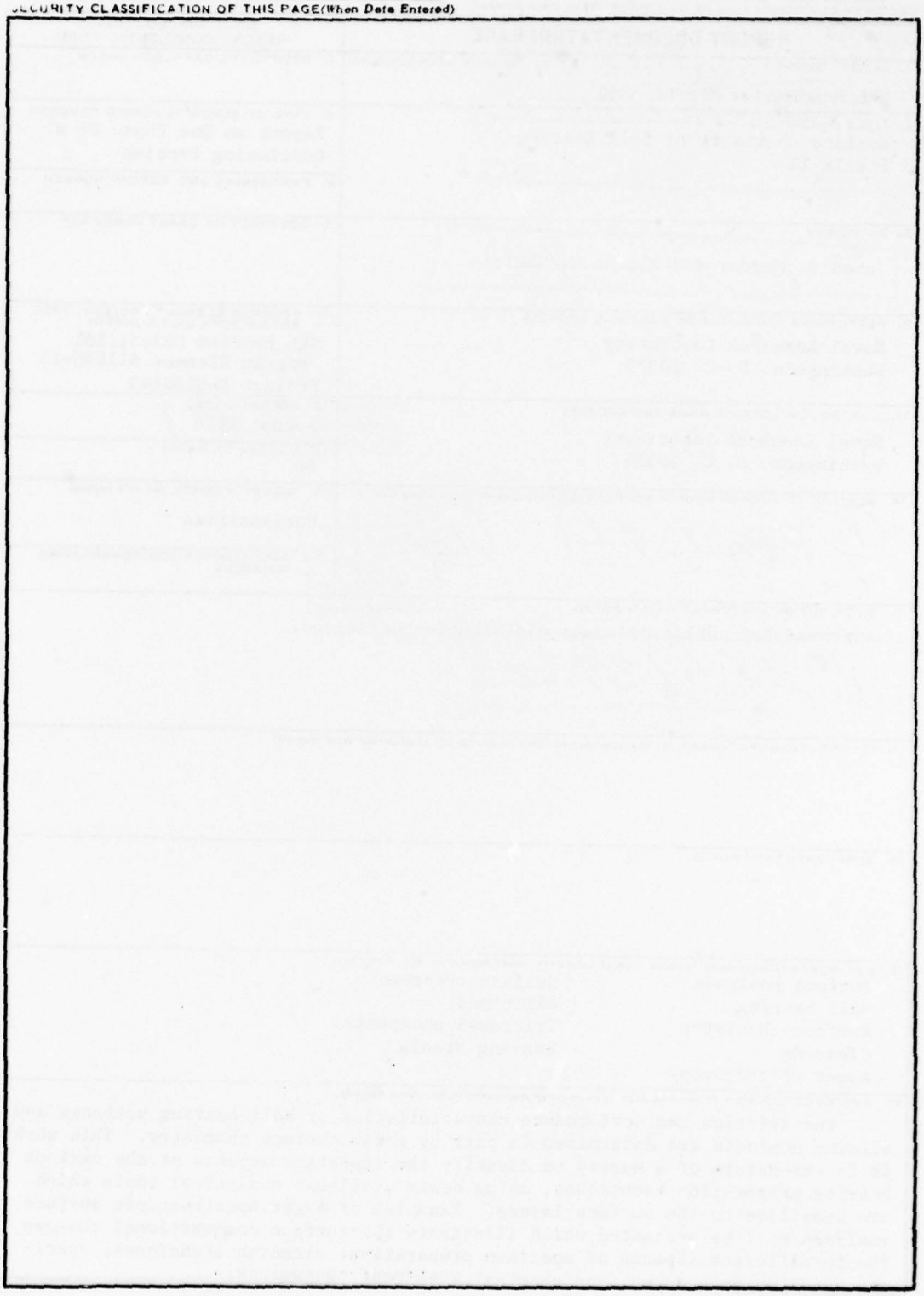


TABLE OF CONTENTS

		Page
I.	INTRODUCTION	1
II.	REFERENCE STUDIES ON BEARING STEEL DISKS	3
	A. Sample Preparation and Handling	3
	B. Auger Fingerprints of Common Chemical Treatments	8
	C. Auger Analysis of 52100 and 440C Steel: Oxide Films	8
	D. Auger Analysis of 52100 and 440C Steel: Chemical Treatments	17
	1. Silicones	17
	2. Lapping Environment	23
	3. Tricresyl Phosphate	30
	a. Background	30
	b. Experimental Results	34
	c. Discussion of TCP Results	44
	d. Relationship to Bearings	49
III.	STUDIES OF BEARING COMPONENTS	50
	A. Sample Preparation and Handling	50
	B. Studies of Operational Bearings	53
	1. 2171 Bearing Set	53
	2. G-200 Bearing Set	56
	C. Studies of Bearings in Final Production Stage	67
	1. General Observations	67
	2. Balls	70
	3. Inner Races	73
IV.	SUMMARY AND CONCLUSIONS	85
APPENDICES		
	A. Auger Spectroscopy/Experimental Procedure	87
	B. Sample Preparation Procedures	92
REFERENCES		94

ACCESSION for
NTIS White Section
DDC Buff Section
UNANNOUNCED
JUSTIFICATION
BY
DISTRIBUTION/AVAILABILITY CODES
Dist. SPECIAL
A

SURFACE CHEMISTRY OF BALL BEARING STEELS II

I. INTRODUCTION

A pervasive concept in all tribology is the elastoplastic interaction at the microscopic irregularities on engineering surfaces (1). Implicit in this statement is the observation that tribological processes depend on a complex interaction of physical and chemical properties, some of them related to bulk material behavior, some of them to surface phenomena. The rapidly developing concepts in surface science can be expected to make important contributions to tribology, but as Fischer (2) has pointed out for catalysis, our present rudimentary understanding of simple surfaces will translate to the complex tribological processes only in certain well-defined instances. One of these instances is the measurement of the composition of surface films. Surface films on bearing metals can play a major role in reducing friction and wear (3,4). Further, these same films are instrumental in protecting the surface against corrosive attack (5) and in protecting a lubricant against surface-catalyzed degradation (6).

The role of surface films on bearing metals will be enhanced under conditions of boundary lubrication, i.e. when surface asperities are in contact. This can occur when there is insufficient lubricant (or contamination) present to maintain the separation of two bearing surfaces or when the bearing is moving at slow speeds (as during start-up) where the elastohydrodynamic properties of a liquid lubricant are inadequate. These considerations are important for instrument ball bearings, especially those used in inertial gyroscopes where the bearing must retain positional stability to hundreds of Angstroms over long time periods with a minimum amount of unreplenishable lubricant (7).

While X-ray Photoelectron Spectroscopy (XPS) is the better analytical technique for defining the chemical composition of surfaces, the use of Auger spectroscopy (AES) has one clear advantage for the study of ball bearing surface chemistry; that advantage is spatial definition. This is important because precision miniature bearings such as the R-4 class of instrument bearings are small ($\sim$ 2 cm diameter) and the wear track widths are less than 100 microns. The composition of films in the wear track is of particular interest since it is in the vicinity of the track that friction, wear and surface-catalyzed lubricant breakdown can be expected.

Manuscript submitted August 8, 1978.

An additional advantage in the use of Auger spectroscopy is that an electron beam is used to excite the Auger process. The secondary electron emission created by the electron beam can be detected to give secondary electron images of the surface which are identical to those produced by a scanning electron microscope (SEM). Thus, the surface composition may be correlated with position on the sample. The lateral resolution (i.e. the electron beam diameter) available from the electron gun in the NRL Auger spectrometer is 5 microns at best, far from high quality SEM resolution, but it is adequate to resolve features on the ball bearings, including the wear track. Further, with a scanning Auger microscope (SAM) it is possible to obtain spatial images of elemental distributions from the samples. This feature is very useful in establishing whether an observed composition is localized or homogeneous across the sample. The facility to provide the SEM and SAM images was obtained late in the program, after it became apparent that meaningful data on bearing components required these features.

This report will show the usefulness of AES in the analysis of instrument ball bearing performance - as a diagnostic for failed bearings, as a quality check in the manufacturing processes, or as an analytical tool in a controlled study of bearing steel surface chemical modification. The work did not pursue any one aspect of bearing chemistry in great detail, but rather tried to establish the potential of Auger as an analytical tool for bearing studies and to lay the groundwork for further, more specific investigation. The report is organized into two principal sections. The first reports the results of studies on samples prepared in laboratory conditions. This work was performed to establish the fundamental understanding of bearing steel surface chemistry as observed by AES. The second section of the report details the results of studies on bearing components. These studies include observations on bearing components taken from various stages in the manufacturing process and from controlled life tests at Draper Laboratory.

Since the calculation of stoichiometry via AES is semiquantitative and the chemical interpretation of AES is not well developed, the work in the first section develops standards on which to evaluate the data taken on the bearing components. The processing procedures used to convert the raw data into a semiquantitative measure of composition are detailed in Appendix A. The processed data are presented in the form "normalized Auger intensities" which will be contracted to Auger intensities for the rest of this report. These intensities are directly related to the percentage of atomic composition if certain approximations are fulfilled. A discussion of the approximations as they relate to this work can be found in Appendix A.

II. REFERENCE STUDIES ON BEARING STEEL DISKS

A. Sample Preparation and Handling

Special disks of 52100 and 440C bearing steels were prepared so that careful Auger spectroscopic studies could be performed. These studies provided the reference information by which the observations on bearing parts could be interpreted. The disks were $\sim$ 2 cm in diameter and 3 mm thick; these dimensions were chosen as a compromise between ease of handling and size restrictions imposed by the spectrometer geometry. The bulk composition of 52100 and 440C steels is presented in Table 1 in both weight and atomic percent. Since Auger spectroscopy inherently measures atomic concentration, the latter will be used in this report.

Unless specified otherwise the buttons were prepared by hand lapping with 3 micron alumina grit suspended in a water base. Following the lap, the buttons were processed through a three-solvent-cleaning procedure which goes by the acronym TSC. The details of the TSC procedure are defined in Appendix B.

It became evident early in the study that a considerable amount of carbonaceous residue remained on many TSC-cleaned buttons. The residue could possibly interfere with, or more likely confuse the interpretation of, the study of the various chemical treatments which were under study. An alternative "cleaning" procedure, via exposure to a glow discharge, was chosen to provide samples which were significantly more free of surface carbonaceous residue. The description of glow discharge processing (GD) is presented in Appendix B. The glow discharge process was very successful in removing carbonaceous residue, but it was found to deposit aluminum on the button surfaces unless the buttons were correctly located in the discharge chamber (8). The excellent results achieved with the proper sample location are demonstrated by the surface compositions of the buttons prepared on the later dates listed in Table 2. The glow discharge process did more than remove unwanted carbonaceous residues from the surface; the surface oxide layers were altered. This point will be addressed in more detail in Section II C.

The sample cleanliness evident in the data presented in Table 2 reflects more than just an efficient cleaning process. It was also necessary to transport the samples from the C.S. Draper Laboratory (CSDL) in Boston, Mass. to NRL in Washington, D. C. without incurring contamination. At the program's inception the buttons were transported individually in acid-cleaned petri dishes and mounted in a standard sample holder at NRL for analysis. It quickly became apparent that this procedure was inadequate. Several other variations of transport and handling were tried until the procedure evolved to its final state which was mounting on an acid-cleaned metal carrier at Draper Laboratory. This carrier, which is pictured in Fig. 1 along with its transport case,

Table 1

Nominal Composition of Bearing Steels

Constituent: Element	52100 Steel (High-Carbon Chrome Alloy) Weight %*	Atomic %	440C Steel (Hardenable High-Carbon Stainless) Weight %	Atomic %
Major:				
Fe	96.5-97.3	93	77.2-81.2	74
Cr	1.3-1.6	1.5	16.0-18.0	17
Minor:				
C	0.95-1.10	4.5	0.95-1.20	4.7
Mn	0.25-0.45	0.3	1.00 max	1.0 max
Mo	-	-	0.35-0.75	0.3
Si	0.20-0.35	0.5	1.00 max	1.9 max
Ni			0.75 max	0.7 max
Trace:				
P	0.025 max	0.04 max	0.04 max	0.06 max
S	0.025 max	0.04 max	0.03 max	0.04 max

* Reference: "Aerospace Structural Metals Handbook, Vol. I, Ferrous Alloys", Air Force Materials Laboratory, Mechanical Properties Data Center, Belfour Stulen, Inc., Traverse City, Mich., 1970.

Table 2

Sample Composition as a Function of "Cleaning"

Preparation Method	Date	Metal	Cr	Normalized Auger Intensities Fe	O	C	S	Cl	Ca	Na/Zn	Al	Si
Lap	11/74	440C	?	23	16	61	0.2	0.1	0.1	-	-	-
		52100		29	24	45	0.3	0.4	0.1	0.8	-	-
Lap+TSC	11/74	440C	2	37	35	24	0.3	0.1	0.2	-	-	0.6
		52100		39	29	31	0.2	0.2	0.2	0.6	-	0.2
	2/76	440C	2	45	45	7	0.6	-	0.6	-	-	-
		52100		48	44	5	-	-	3	-	-	-
Lap+TSC+GD	10/74	440C	-	40	45	8	0.3	0.4	0.3	1	5	-
		52100		43	44	7	0.2	0.2	0.2	0.8	4	-
	11/74	440C	-	46	46	7	0.2	0.1	0.2	-	0.4	0.1
		52100		49	45	4	0.1	-	0.4	0.5	1	-
	4/75	440C	-	50	50	-	-	-	-	-	-	-
		52100		52	48	-	-	-	-	-	-	-
	2/76	440C	-	42	58	-	0.06	-	-	-	-	-
		52100		49	51	-	0.05	-	-	-	-	-

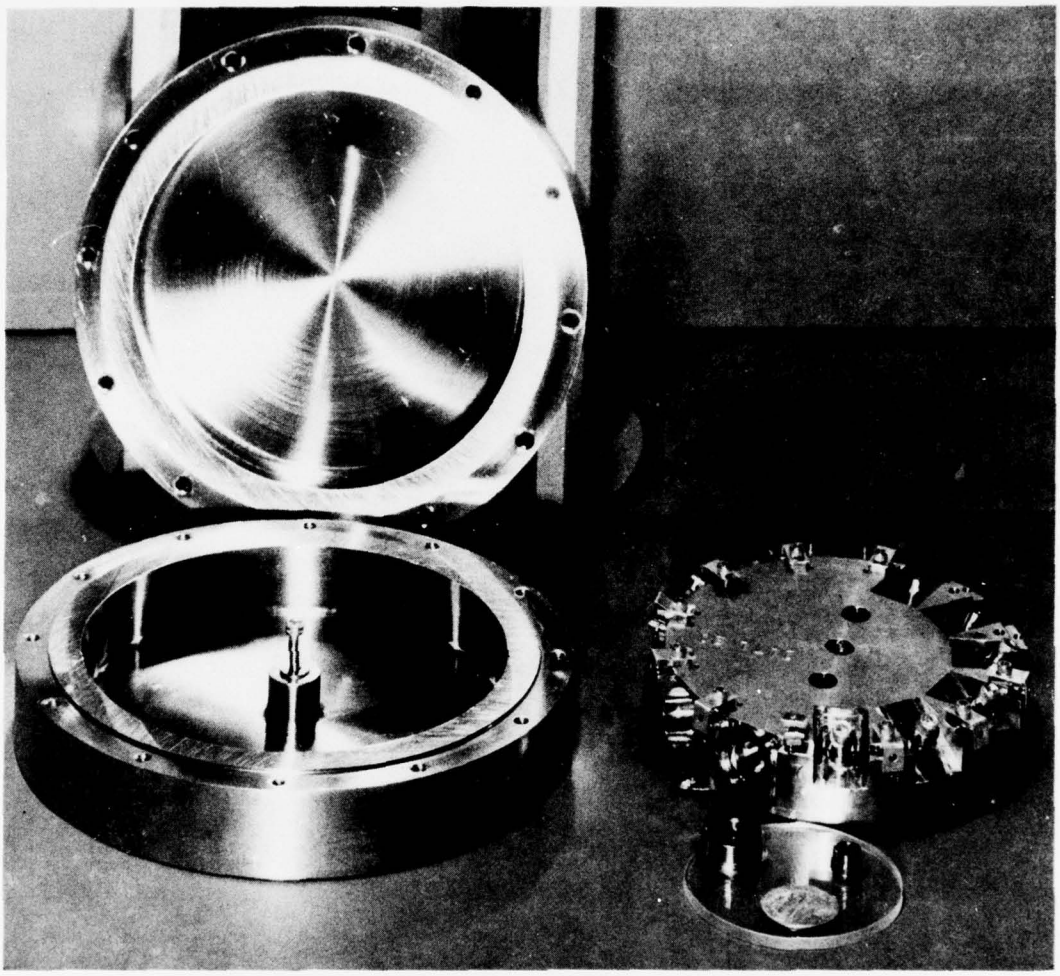


Fig. 1 - The sample carrier and its transport case. Note the flat, mating edges of the case which prevent ready circulation of ambient air.

has been designed to accept the samples with a minimum of handling. That handling is all done with acid-cleaned equipment and with gloved operators. When ready for shipment the carrier is bolted onto the transport case which is in turn bolted shut. The mating edges are polished to reduce entrance of external air into the case; in this way external contaminants are prevented from reaching the sample. At NRL the case is opened, the carrier picked up by acid-cleaned tongs inserted into the two off-axis holes evident in Fig. 1, mounted onto the spectrometer sample holder and immediately plunged into the waiting vacuum system.

Contamination of the samples while under vacuum is also a problem. At a pressure of 10^{-8} Torr, a sufficient number of molecules strikes a surface in one hour to cover it with a monolayer if all those gas molecules stuck. That such contamination did in fact occur is illustrated in Table 3 which shows the growth of carbon signal intensity with time in the vacuum system. To minimize this problem the vacuum system was routinely baked out for 10 hrs. at 150°C prior to opening it to receive the samples. The base pressure prior to opening was in the high 10^{-10} or low 10^{-9} Torr range. After sample insertion the pressure would return to the low 10^{-9} Torr range after 12-24 hours. When a careful measurement of the surface composition was desired, the Auger spectra were taken as soon as possible after insertion into the vacuum system. One full initial spectrum for each sample surface in a complete set of twelve buttons required about 8 hours from start to finish.

The efficacy of the cleaning, transport and handling procedures is demonstrated by the data in Table 2. It is interesting to note that both TSC and GD cleaning procedures became more effective as the program progressed, presumably due to constant feedback raising awareness of the need for careful work.

Table 3

Specimen* Contamination During Time in Auger Vacuum System

Time in System (days)	Normalized Auger Intensity					
	Fe	O	C	S	Cl	Ca
0	52	48	-	-	-	-
1	48	44	7	0.5	0.2	1
8	45	42	10	1	0.5	2

* 52100 steel, after lap+TSC+GD

B. Auger Fingerprints of Common Chemical Treatments

An important use for Auger spectroscopy is in the identification of chemical states on bearings with unknown histories. For Auger identification to be of greatest value it is necessary that the different chemical treatments of the bearing steels leave a distinct fingerprint, a unique surface constituency. The number of chemical treatments designed to improve 52100 and 440C steels performance is manifold; each has a particular goal to achieve, a raison d'etre. Some of the more common treatments and their designated purposes are listed in Table 4. Also included are such potential sources of inadvertent exposure to chemicals as the degradation of the lubricating oils, effects of humidity, etc.

Program time limitations precluded the full investigation of very many of the treatments, especially since both the outer surface composition and the composition depth profile should be determined for a meaningful analysis. As an indication of the possibilities, the outermost surface composition for four of the most common chemical treatments was examined. These four can be broken into two classes: a) exposure to phosphate-based treatments and b) exposure to chromic acid-based treatments.

All of the samples used for this aspect of the study were prepared at the same time so that any observed differences following the various treatments could be reasonably attributed to the treatment itself. In particular, prior to treatment all samples were lapped, solvent cleaned, and then glow discharge "cleaned". At the time of this aspect of the work the glow discharge process was depositing Al at a 1% constituency level on the sample surfaces. The aluminum signal was observed on the GD, TCP and ZDTP samples; it was missing from the samples treated with chromic acid. Evidently the latter removed the aluminum as part of its surface reactions. The surface constituencies are presented in Table 5. The Al is not included in Table 5 as it would not normally be part of the fingerprint.

Sample spectra and a detailed discussion of the differences were reported earlier (8).

C. Auger Analysis of 52100 and 440C Steel: Oxide Films

The ability of AES to identify the various forms of iron oxide has been studied by several investigators (9-13). Similar relationships can be expected for chromium and its oxides; published Auger data for Cr and Cr_2O_3 do show the same type of changes as seen in Fe and Fe_2O_3 (14, 15). The most extensive Auger study of iron oxides has been performed by Seo, Lumsden and Staehle (SLS) (9), who measured the Auger dN(E)/dE spectra of the Fe_{MVV} lines (30-60 eV) for a number of carefully grown thick oxide films. Their observed changes

Table 4

Surface Treatment of Bearings

Function	Chemical Type	Additional Information
A- Lubricant Additive		
Anti-Wear Agent	TCP (tricresyl phosphate)	Anti-wear additive; EP additive; also used to passivate mild steel so as to inhibit catalytic pyrolysis of ester-based oils; passivating treatment involves immersion of steel in TCP at 500 to 525°F for about 24 hours in absence of oxygen.
	ZDTP (zinc dialkyl dithio-phosphate)	All-purpose anti-wear and anti-oxidant additive; widely used
Anti-Foaming Agent	Silicone; e.g., high molecular weight polydimethylsiloxane	Dow Corning, DC-200; General Electric SF-96; used in concentrations of parts per million of oil
Corrosion Inhibitor (for steel)	Barium dinonylnaphthalene sulfonate	R. T. Vanderbilt Co. product.
	a) neutral	Fully neutralized
	b) basic	Half neutralized; remaining hydroxyl group available to react with any acids generated in oil
Vapor-Phase Corrosion Inhibitor	Dicyclohexylammonium nitrite	Shell, No. 226; has potential for dry packaging of cleaned bearings

Function	Chemical Type	Additional Information
Anti-Oxidant Agent (for oil)	ZDTP	See above
	Phenolic type; e.g., tert-butyl-methyl phenol, BHT, tert-butyl-phenyl phenol, etc.	"Ionol" from Shell; "Vanlube PCX" from R. T. Vanderbilt; a chemically well-defined material used in KG-80
	Amine type; e.g., phenyl-alpha-naphthylamine, PANA	Eastman Organic Chemicals, No. 351
B- Lubricant Base Stock		
KG-80 Base Fluid	Super-refined, dewaxed, hydro-generated hydrocarbon	Available only from Kendall Refining Co. (now owned by Witco). NOTE: KG-80 is about to be phased out of production
MB-20B Base Fluid	Combination of polyol esters and diesters (polyol component likely to be pentaerythritol)	Available from H. Ravner, NRL; this is successor to MIL-L-6085A for instrument bearings
MIL-L-6085A Base	Basically a diester (initially, comparable to diethylhexyl sebacate)	Specifications have been down-graded in many respects
Krytox Fluid	Perfluorinated ether	duPont; has some potential for high temperature lubrication (above 500°F)
"Sanotrac"	--------	A high traction fluid which is used for bands, -- automatic clutches, etc.; requirements are that it not be too good a lubricant, but it must be a good anti-wear material

Function	Chemical Type	Additional Information
C- Lubricant Degradation Products		
Diester Hydrolysis Products	Adipic and/or other dibasic acids Half esters of above Alcohol	
Polyol Esters		
Degradation Products of Hydrocarbons	Aliphatic hydrocarbons Short-chain aliphatic acids	
Degradation Products of Fluorinated Base Fluids	Short-chain perfluorinated acids; e.g., perfluorobutric acid	AVOID; high toxicity ratings; likely to be highly corrosive to steel
D- Miscellaneous		
Surfactant	"Viodex" duPont	Could not be identified from duPont literature at NRL.
	Aerosol OT-100% (dioctyl ester of sodium sulfosuccinic acid)	American Cyanamid Co.; a 100% concentration, solid, anionic wetting agent; the most effective wetting agent of the Aerosol series.
Solvents Used in Cleaning Bearings	Stoddard Solvent, chlorinated hydrocarbons, Freons, acetone, etc.	

Function	Chemical Type	Additional Information
Barrier Films	Perfluorooctanoic acid or perfluorooctanol	Barrier films are inert and should not react with steel; any reaction would come from perfluorinated fragments
Boundary Lubricants*	Palmitic acid (16 carbon atoms) Stearic acid (18 carbon atoms) Behenic acid (22 carbon atoms)	Most commonly used; representative of whole class * See "Aircraft Propulsion Lubricating Film Additives; Boundary Lubricant Surface Films," C. M. Allen, E. Drauglis, W. A. Glaeser, C. A. Alexander, R. J. Jakobsen (Battelle, Columbus Laboratories), Technical Report AFAPL-TR-73-121, Vol. II, Air Force Aero Propulsion Laboratory, Wright-Patterson Air Force Base, Ohio 45433, January 1975
Cutting Fluids	Mineral oils with high sulfur content; chlorine-containing oils	
Moisture Effects	Humid atmosphere; condensed water	
Saline Environment	Air-borne salts, humid atmosphere	

Table 5

Bearing Steel Surface Composition for Various Chemical Treatments

Steel	Chemical Treatment[1]	Normalized Auger Intensities										
		Cr	Fe	O	C	S	Cl	Ca	N/Cd[2]	K	P	Na/Zn[2]
440C	Glow Discharge	-	45	46	7	0.2	0.4	0.2	0.7	-	-	1
	TCP[3]	-	28	27	24	0.7	-	1	0.4	0.8	6	12_N
	ZDTP[4]	<0.4	40	43	12	0.5	0.1	0.2	0.2	-	1	3_Z
	Chromerge	2	35	38	25	0.7	-	-	0.3	-	-	-
	Passivate	2	18	21	59	0.2	0.2	0.2	0.4	-	-	-
52100	Glow Discharge	-	45	46	7	0.2	0.2	0.2	0.7	0.3	-	0.8
	TCP	-	26	27	35	0.6	-	0.8	0.5	0.2	5	5_N
	ZDTP	-	43	41	9	0.3	0.1	0.1	0.2	0.3	1	2_Z

(1) For a complete description of the preparation procedures and treatments see Appendix B.

(2) The principal Auger lines for Na/Zn and N/Cd are too close in energy to easily discriminate between them when signal to noise conditions are poor. If the signal is sufficiently strong secondary features can be used to identify the element. Where this was possible, the identification is noted by a subscript.

(3) TCP stands for tricresyl phosphate.

(4) ZDTP stands for zinc dialkyl dithiophosphate.

in the Fe_{MVV} spectral features (see footnote a, Table 6) and the oxygen-to-iron ratio provide an empirical basis on which to identify the chemical state of the iron-oxygen system.

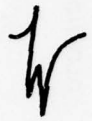
Table 6 presents schematic drawings of the Auger Fe_{MVV} lineshape for the Fe, Fe_2O_3 and Fe_3O_4 chemical forms as well as numerical values for the parameters SLS chose to characterize the changes in the Auger spectra. Because our observations were made with a different spectrometer and slightly different conditions, the same parameters were remeasured on bulk samples of Fe_2O_3 and Fe_3O_4. The parameter values differ somewhat from those of SLS (see Table 6) but confirm the essential differences between the Fe_2O_3 and Fe_3O_4. The large O/Fe ratio for the bulk Fe_2O_3 as compared to the SLS film may be due to waters of hydration (9).[3] Both the SLS and present data are taken from surfaces sputtered until an equilibrium condition was attained.

The composition profiles for solvent cleaned and glow discharge "cleaned" 52100 steel are presented in Fig. 2. This data was taken with simultaneous Auger analysis and sputter etching (Appendix A). The glow discharge process not only provides a carbonaceous-free surface, but also an oxide layer thicker by about 30 Å. The Fe_{MVV} signature, both separation of minima and Fe_2/Fe_1 intensity ratio, for the outer layer is consistent with that observed in Table 6 for Fe_2O_3. However, the observed oxygen-to-iron signal intensity is about unity, larger than that for the reference Fe_2O_3 materials. This may correspond to a higher hydration state (9).[3] The interface between the Fe_2O_3 and the metallic iron is marked by a region where the Fe_{MVV} signature is consistent with Fe_3O_4. Boggs, Kachik and Pellissier (16) found a $Fe_2O_3/Fe_3O_4/Fe$ progression in an oxide film formed on iron at 350°C. The oxide composition and thickness for the solvent cleaned 52100 chrome steel are roughly equivalent to oxide films measured by Coad and Cunningham (17) on unspecified chrome steels by combined Auger/XPS. They concluded that the oxide film on their samples was a thin layer of Fe_2O_3 overlying a Fe_3O_4 oxide layer, that the chromium was depleted at the surface, and that there was a region rich in chromium oxide adjacent to the metal.

The carbon Auger spectra for hydrocarbons versus carbides can be distinguished (18). The superficial carbon contaminant is removed quickly and is replaced by a carbide type signal when the oxygen concentration drops below about 40%, i.e. when penetration of the oxide film begins. The peak amount of carbon, $\sim$ 20%, is substantially larger than the nominal bulk amount, 5 at %. This discrepancy in part reflects the fact that the carbon Auger sensitivity factor for carbide is twice that of carbon in graphite. Since the latter was used for the data normalization the actual carbon concentration is one-half that recorded in the Tables and the figures in the carbide regions throughout the text. Coad and Cunningham do report as much as 20 at % C in the surface layers of an unidentified chrome steel; their estimate came from both XPS and AES data (17).

Table 6

Fe_{MVV} Auger Lineshape Characteristics of Iron Oxides

Species	Fe_{MVV} Lineshape	Separation of Minima (eV)	$\frac{Fe_2}{Fe_1}$ (a)	$\frac{O_{510}}{Fe_{650}}$ (b)
Fe metal		-	-	-
Fe_2O_3				
sputtered film[9]		7.5-8	17.-1.8	0.58-0.60
sputtered bulk		7.5	2.0	0.88
Fe_3O_4				
sputtered film[9]		4.5	0.4	0.53
sputtered bulk		5.0	0.8	0.59

a) Fe_2/Fe_1 is defined (13) as the ratio of the lengths of the line segments between the two minima of the Fe_{MVV} spectra; as drawn above Fe_2 is the righthand segment, Fe_1 is the lefthand segment.

b) The ratio of peak to peak intensities of the oxygen 510 and iron 650 eV Auger dN(E)/dE spectrum, divided by a scale factor of 4 to correspond to the data as plotted in the depth profile figures.

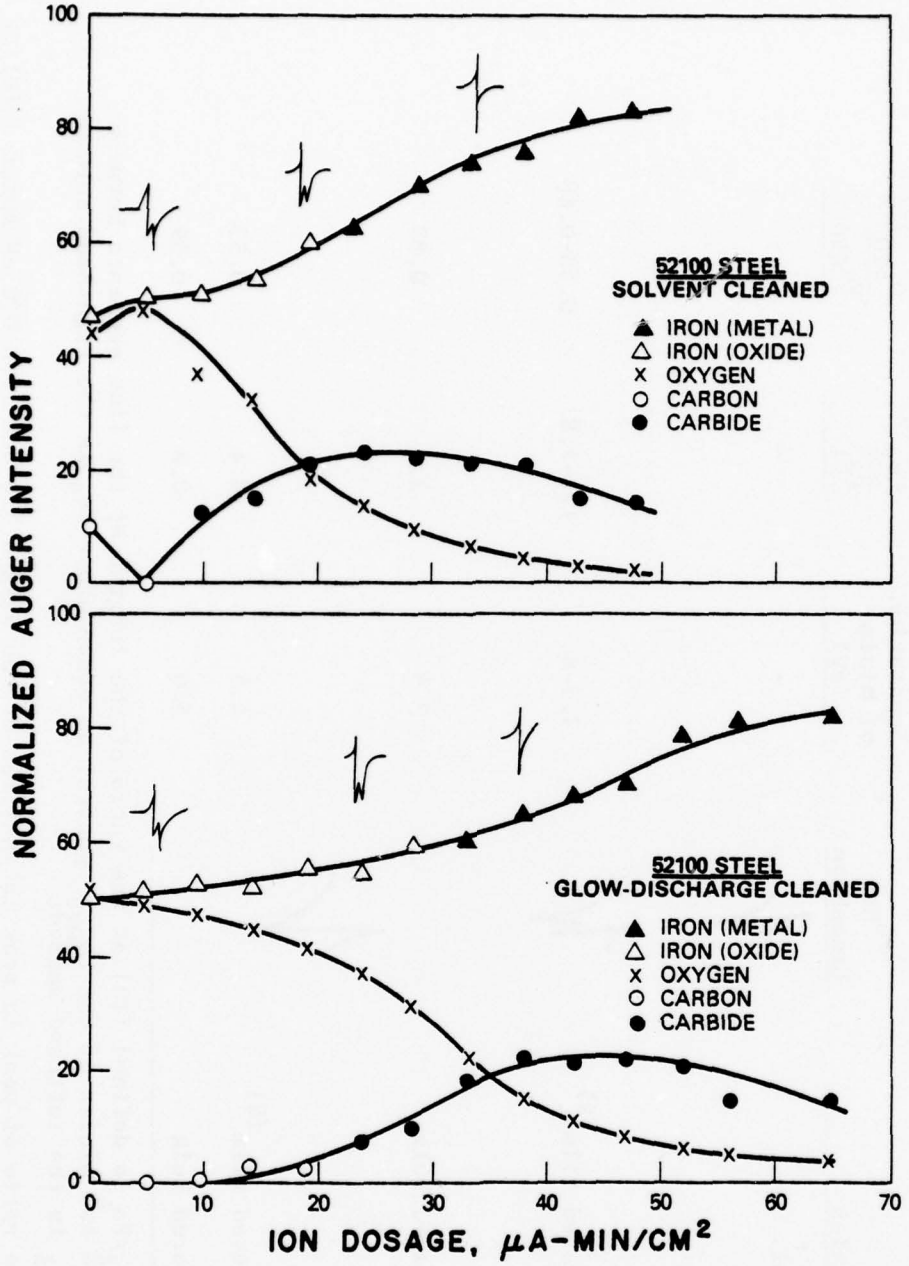


Fig. 2 - Auger/sputter depth profile of 52100 steel after lapping and the indicated cleaning step. [Sputter rate ~ 2 Å/(μA min/cm²).] Inset sketches portray the Fe_{MVV} Auger lineshape observed at the corresponding points in the profile. (a) Surface cleaned by organic solvents. Some carbonaceous residue is present on iron oxide surface. (b) Surface cleaned by solvents followed by a glow-discharge "cleaning" procedure. No carbonaceous residue is observed, but the oxide layer is approximately 30 Å thicker.

The observations on the 440C steel are similar to the 52100 except that the larger chromium content plays an important role in the passive layer. The interference of larger spectral features (Fe_{MVV} in the Cr_{MVV} and O_{KLL} in the Cr_{LMM}) obscure the chromium features and make their interpretation less certain. The composition profiles for solvent and GD prepared buttons of 440C steel are shown in Figure 3. The essential features are an iron oxide outer layer, again with the Fe_{MVV} spectra consistent with Fe_2O_3, backed by a mixed iron/chromium oxide or carbide layer. As the oxygen concentration begins to drop below 30% the lineshapes of both the iron and chromium MVV spectra begin the metamorphosis from oxidized to metallic form. Ferrante (19) has shown that the surface oxide composition of a modified 440C steel changes from iron oxide to chromium oxide with increasing temperature. His room temperature oxide is about the same thickness observed here for the solvent-cleaned sample.

The oxygen glow discharge "cleaning" results in a 30 Å increase in the iron oxide layer for the 440C as it did in the 52100. The oxygen/iron intensity ratio is again larger than that expected for ferric oxide, indicating the probably presence of a hydrate or other excess oxygen. The thickness of the apparent Fe_2O_3 layer on the glow discharged samples is different from the observations of Boggs, et. al (16) and Coad and Cunningham (17) on atmosphere grown oxides. Presumably it is due to the use of oxygen at one point in the discharge process. This change in the oxide layer effected by the glow discharge process is reflected in a slower surface reaction rate experienced by the bearing steels when treated with TCP and in shorter lifetimes in operating bearings (7) (see text below).

D. Auger Analysis of 52100 and 440C Steel: Chemical Treatments

1. Silicones

The adverse effects of silicone presence in bearings have been widely publicized. The military specification for precision ball bearings used in instruments and rotating components specifically restricts the use of silicone lubricants except for those applications which involve temperature extremes (Ref. 20, Section 10.4). The investigation of the surface chemistry of silicones is therefore an important aspect of bearing chemistry. One effect of silicone on bearing metals is readily observed by exposing a cleaned surface to silicone fluid, removing the silicone by the TSC procedure and observing the spread of an oil droplet. In the absence of silicone exposure, the oil drop will spread across the metal surface increasing the drop diameter noticeably in minutes. An exposed surface does not show appreciable spreading on the same time scale.

Previous work (8) has established that 440C and 52100 steels, submerged in silicone for one hour at room temperature and then immediately cleaned by a procedure using three different organic solvents, show poor wetting by oil. Auger analysis was used to determine

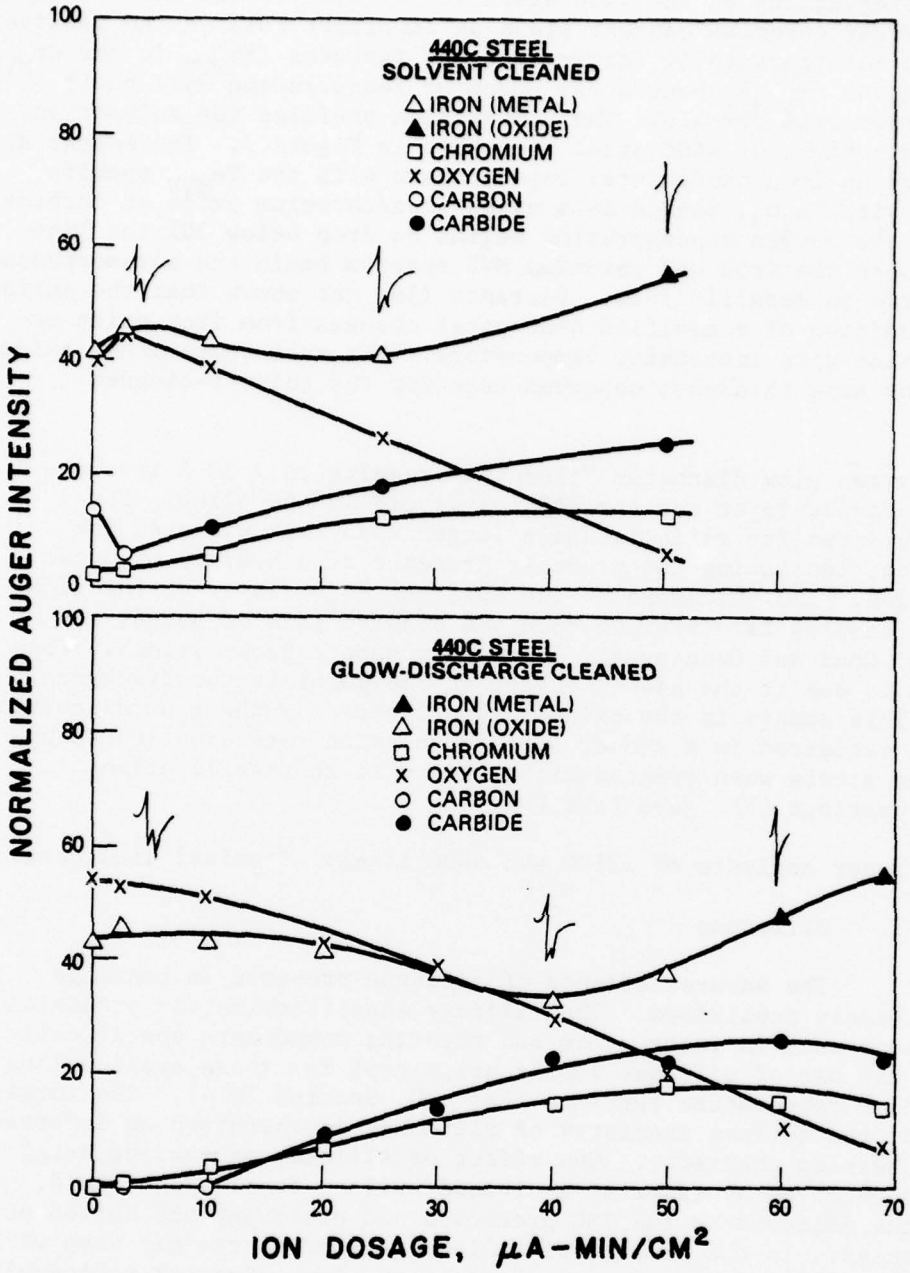


Fig. 3 - Auger/sputter depth profile of 440C steel after lapping and indicated cleaning step. [Sputter rate ~ 2 Å/(μA min/cm^2).] Inset sketches portray the Fe_{MVV} Auger lineshape observed at the corresponding points in the profile. (a) Surface cleaned by solvents. Some Carbonaceous residue is present; outer layer is principally iron oxide. (b) Surface cleaned by solvents followed by a glow-discharge "cleaning" procedure. No carbonaceous residue observed, but the glow-discharge process caused the growth of approximately 30 Å additional iron oxide.

the presence of silicones on the steel surface and found that the silicone presence as determined by the silicon Auger spectral line was barely or not detectable. The marginal detection is due to the combined effects of low concentration and spectral interferences between Fe and Si. An upper limit of approximately 20% of a monolayer of silicone was established as the minimum detectable amount.

The work reported below examines the effectiveness of the solvents used to remove silicones. The efficacy of silicone removal is also examined as a function of aging time and temperature after the silicone exposure but prior to cleaning.

Sample buttons of 440C and 52100 chrome steel were prepared by lapping, followed by TSC and finally by GD cleaning. Auger examination of a 440C surface at this state of sample preparation showed the presence of Fe, O and a barely perceptible trace of Ca. No other elements were seen. The peak-to-peak magnitude of the Fe_{MVV} line near 80 eV was correlated with the Fe 650 eV line to give a ratio of $Fe_{80}/Fe_{650} = 0.048$; this compares to the average value of $0.057 \pm .006$ reported earlier for 440C steel (8).

A polydimethyl siloxane (Dow Corning DC-200) was deposited by submerging the buttons in a dilute solution of DC-200 in benzene for 1 hour. Upon removal from solution all buttons showed oleophobic behavior as evidenced by the retraction of the benzene into droplets. The sample preparation from that point was different for each button and is reported in Table 7.

Samples 1 to 6 were prepared to examine the efficacy for silicone removal of the solvents used in the TSC procedure. The following conclusions were drawn: 1) as determined from the magnitude of the Si 83 eV (LVV) line and confirmed by the Si 1619 eV (KLL) line, the solvent efficacy ranking is Freon > toluene > 50% acetone/50% methanol; 2) the Freon solvent used in this work left substantial residues of C and Sn on the surface. An acetone/methanol wash following the Freon wash removed some of this residue; 3) TSC usually reduced the silicone concentration below the level needed for positive Auger identification; 4) the oxygen-to-iron ratio is either unaffected by the sample treatment procedures examined to this point or it decreases slightly. A simple model for the effects of silicone exposure would picture the silicones adsorbed onto the steel surface without significantly affecting the outermost iron oxide. If this were true, then the oxygen/iron ratio should increase with silicone exposure since silicones contain oxygen which can mask both the Fe and O of the clean surface. A decrease in the oxygen/iron ratio is explained on the basis of chemical changes in the steel surface or on the basis of non-oxygen bearing contaminants left on the steel surface.

Samples 7 to 12 reported in Table 7 were prepared to test for chemical reactions which might increase the difficulty in removing the silicone from the surface. One set of two samples was left at room temperature (25°C) for 3 and 21 hours, respectively, after removal

Table 7

Preparation History of Samples Exposed to Silicone

Sample Number	Steel	Silicone Exposure time (hrs at 25°C)	Temperature/Time in Air After Exposure Prior to Cleaning	Solvents Used in Cleaning (5 min. ultrasonic in each)
1	440C	0	-	-
2	440C	1	-	toluene, toluene
3	440C	1	-	Freon, Freon
4	440C	1	-	methanol/acetone, methanol/acetone
5	440C	1	-	toluene, Freon
6	440C	1	-	toluene, Freon, methanol/acetone
7	52100	1	25°C/3 hrs	TSC
8	52100	1	218°C/3 hrs	TSC
9	52100	1	25°C/21 hrs	TSC
10	52100	1	218°C/21 hrs	TSC
11	52100	1	218°C/1 hr	TSC
12	52100	1	119°C/1 hr	TSC

from the benzene solution and before three solvent cleaning. Another set of three samples was subjected to 1, 3, and 21 hours, respectively, at 218°C in the same way. These latter samples showed visual discoloration which is believed to be due to oxidation of the steel surface. No definitive observation of silicon was made on any of these 5 samples following TSC. The Fe_{MVV} line structure (40-60 eV) does show differences, presently not interpretable, between the oxidative state of the 25°C versus 218°C samples.

Sputter profile data have been taken to examine for changes in surface composition due to prolonged exposure of 52100 to polydimethyl siloxane. Two 52100 buttons were prepared by the standard lap, TSC and GD procedure. The buttons were submerged in DC-200 for 3 hours at 25°C and then solvent cleaned. One sample shows no trace of silicon; on the other silicon was detected at the 3% level on the surface. Since TSC normally leaves an undetectable amount of silicon this sample must be considered an anomaly.

Figure 4 shows the carbon, silicon and oxygen intensities plotted as a function of ion dosage. The oxygen intensity does not immediately decrease upon the inception of sputtering. After an increase which reflects the removal of a contaminant overlayer, the oxygen shows a region of constancy which can be interpreted as the ion dosage required to sputter-remove an oxide layer thicker than the AES sampling depth. The point of intercept of the exponential decay line with the constant intensity line (Fig. 4) defines an ion dosage which is the approximate measure of oxide thickness ($1\mu A\ min/cm^2$ is $\sim$ 2Å, see Appendix A) reported in Table 8.

A halflife can be defined for the decreasing intensity regions in Fig. 4. The meaning of this halflife is discussed in Appendix A. Note that both silicone-exposed samples have a rapidly removed carbon layer, but the sample on which silicon was detected shows a carbon component with a longer halflife which is equal to the silicon halflife. This suggests the longer halflives of C and Si are correlated, as would be expected if they are part of a silicone molecule. Both are removed from the surface long before the oxide layer is penetrated. This shows they are part of a surface film on top of the oxide.

Table 8 presents a summary of the data for the two silicone-exposed samples and a reference sample not exposed but otherwise identical. The oxide layer thicknesses on the silicone-exposed samples are somewhat larger than that found on the reference sample.

In summary, silicone exposure of the two bearing steels examined here can result in surface chemical changes that affect lubricant spreading but were usually not identified by these AES studies. If the DC-200 silicone is present in amounts greater than 20% of a monolayer, the AES can identify its presence via the silicon Auger. Whereas simple solution deposition does not incorporate AES-detectable silicon, lapping the bearing steel with a grit suspended in silicone incorporates

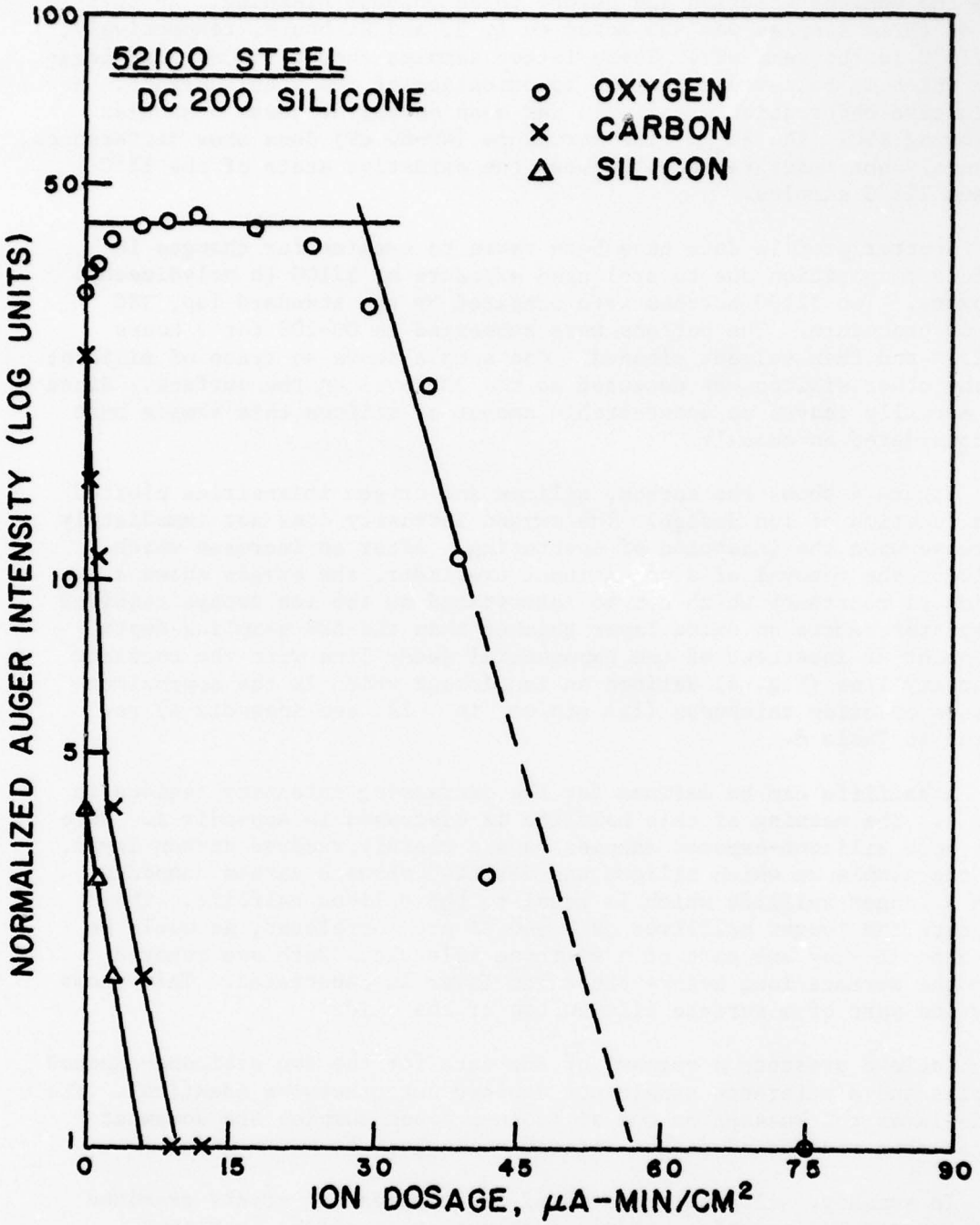


Fig. 4 - Auger/sputter depth profile of 52100 steel exposed for 3 hours at 25°C to DC-200, a polydimethyl siloxane. The TSC cleaning after exposure did not remove all evidence of silicon from this sample. A summary of this data is presented in Table 8, GD+DC-200 (2).

Table 8

Composition Depth Profile
52100 Exposed to Silicone

Sample	Decay Halflife (μA-Min/cm^2)		"Thickness" of $_2$Oxide (μA-Min/cm^2)
	C	Si	
GD	-	-	20
GD+DC-200 (1)	0.6	-	30
GD+DC-200 (2)	0.6/3	3	35

an easily detected amount of silicon into the surface layers of the steel. This subject is treated in the next section on lapping compounds.

2. Lapping Environment

The last metal removal process in bearing component manufacture is frequently a lap. A variety of lapping compounds are commercially available for this purpose. A series of 52100 buttons were prepared to study what effects the choice of lapping grit or vehicle might have on the surface composition. The grit and vehicles used for this work are listed in Table 9. The 52100 buttons were polished, solvent cleaned (TSC), and subjected to the glow discharge "cleaning" prior to a hand lap with the various lapping compounds. Following the lap the buttons were again solvent (TSC) cleaned but not put through the glow discharge cleaning. The samples were transported to NRL in the usual way.

These samples were examined prior to the availability of the scanning Auger spectrometer. As a result any observation of imbedded grit particles was a random event, i.e. it was observed if the electron beam fortuitously irradiated an imbedded area. The electron beam size was small, $\sim$ 200 micron diameter, and only 2 - 3 areas on each sample were analyzed; it was not known how many observations of a grit particle would be made. In fact there were only two. One occurred on a sample lapped with the Acco-Craft 15 MOS; the other occurred on a control sample.

The composition depth profiles for the lapped samples were analyzed in the same way as the silicone-exposed 52100 (Section II D 1), i.e. via oxide layer thickness and decay halflives. The surface compositions prior to sputter etch are presented in Table 10. The profile data were obtained by sequentially sputtering and lapping for a complete Auger

Table 9

Lapping Compounds used for the Lap Sample Set

Sample Designation	Grit	Vehicle
(normal procedure)	3μ Al_2O_3	Water
A (Nujol)	3μ Al_2O_3	Nujol (a mineral oil)
B (15 MWS)	15μ diamond	Acco-Craft* 15 MWS (water soluble)
C (15 MOS)	15μ diamond	Acco-Craft* 15 MOS (oil soluble) (contains silicone)
D (DC-200)	3μ Al_2O_3	Dow Corning DC-200 (poly-dimethyl siloxane)

* Commercial lapping compound

Table 10

Surface Composition
Lap Sample Set

Sample	Fe	O	C	S	Cl	Ca	Na/Zn	Si
A (Nujol)	42	34	23	0.4	-	-	0	-
	9	31	29	0.6	-	-	0.2	-
B (15 MWS)	44	36	19	0.5	-	-	-	-
	45	37	17	0.6	0.08	-	0.4	-
C (15 MOS)	46	35	19	0.4	0.08	-	-	-
	43	34	22	0.6	0.4	-	0.4	-
D (DC-200)	34	27	30	1.	-	-	-	7
	36	28	27	0.5	-	-	-	8

trace. The results are presented in Table 11 and several examples are presented in Figures 5 - 8.

Table 11

Composition Depth Profile Data
Lap Sample Set

Sample	Surface Contaminant Decay Halflife (μA-min/cm^2)		Oxide Layer Thickness (μA-min/cm^2)	Decay Halflife (μA-min/cm^2)
	C	Si		
TSC	< 1	-	10	10
GD	-	-	20	10
A (Nujol)	1.5	-	10	12
B (15 MWS)	2	-	13	19
C (15 MOS)	1	-	6	6
D (DC-200)	13	14	5	21

Several conclusions can be drawn from the data.

(1) As one would expect the lapping process removed the thicker oxide layer produced by the GD treatment. This is manifested by the smaller ion dosages necessary to penetrate the oxide film.

(2) The lapping compound with DC-200 as a vehicle incorporated carbon and silicon into the oxide. This is reflected by the observation that the oxide thickness is smaller than the silicon decay time. In the previous section where the sample was simply exposed to silicone the silicon signal observed on the sample was shown to disappear prior to penetration of the oxide layer.

(3) The samples lapped with the Acco-Craft 15 MWS compound showed no distinguishable chemical differences from those lapped with 3 micron Al_2O_3 (see lap+TSC in Table 2).

(4) The halflife of the oxygen decay for the lap sample set must be viewed with caution. It was observed on the GD and TSC 52100 reference samples that the oxygen halflife became much longer when data was taken in a sequential (i.e. alternating sputter/analyze) rather than a simultaneous fashion. The GD and TSC sputter profile data shown in Figs. 2, 5, and 6 were taken with simultaneous analysis. The data on

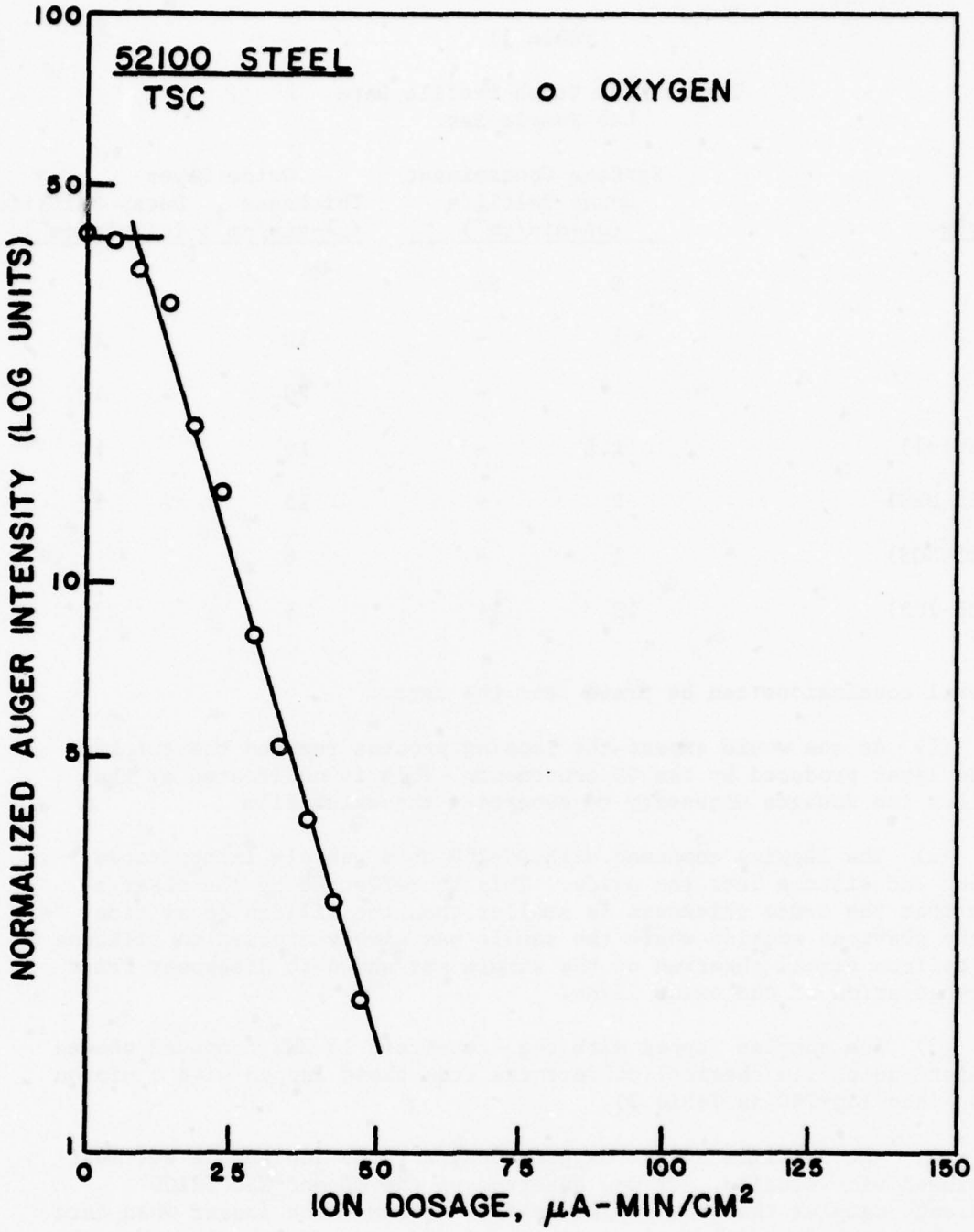


Fig. 5 - Auger/sputter profile of TSC-cleaned 52100 steel. Auger data taken simultaneously while sputtering.

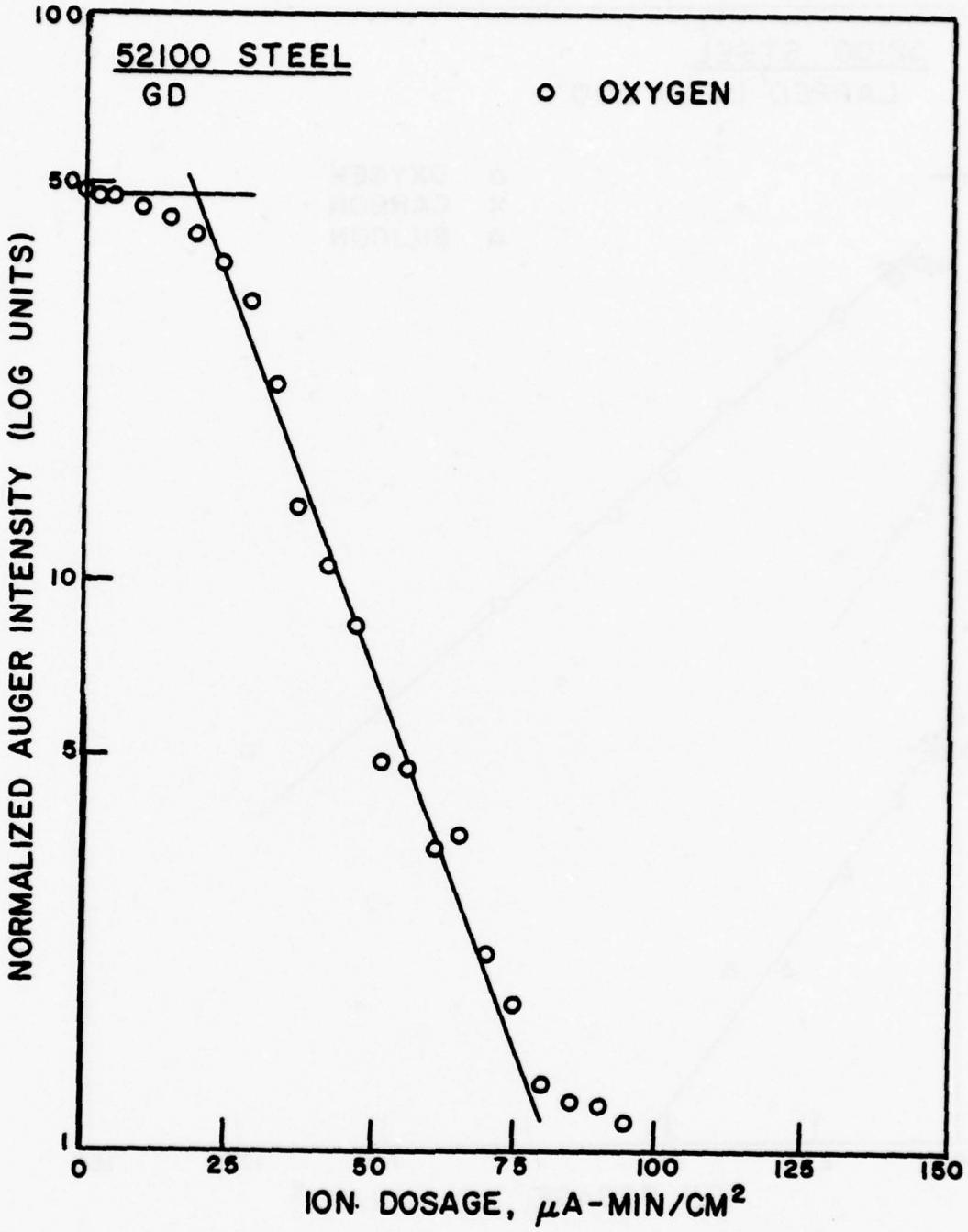


Fig. 6 - Auger/sputter profile of GD-cleaned 52100 steel. Auger data taken simultaneously while sputtering.

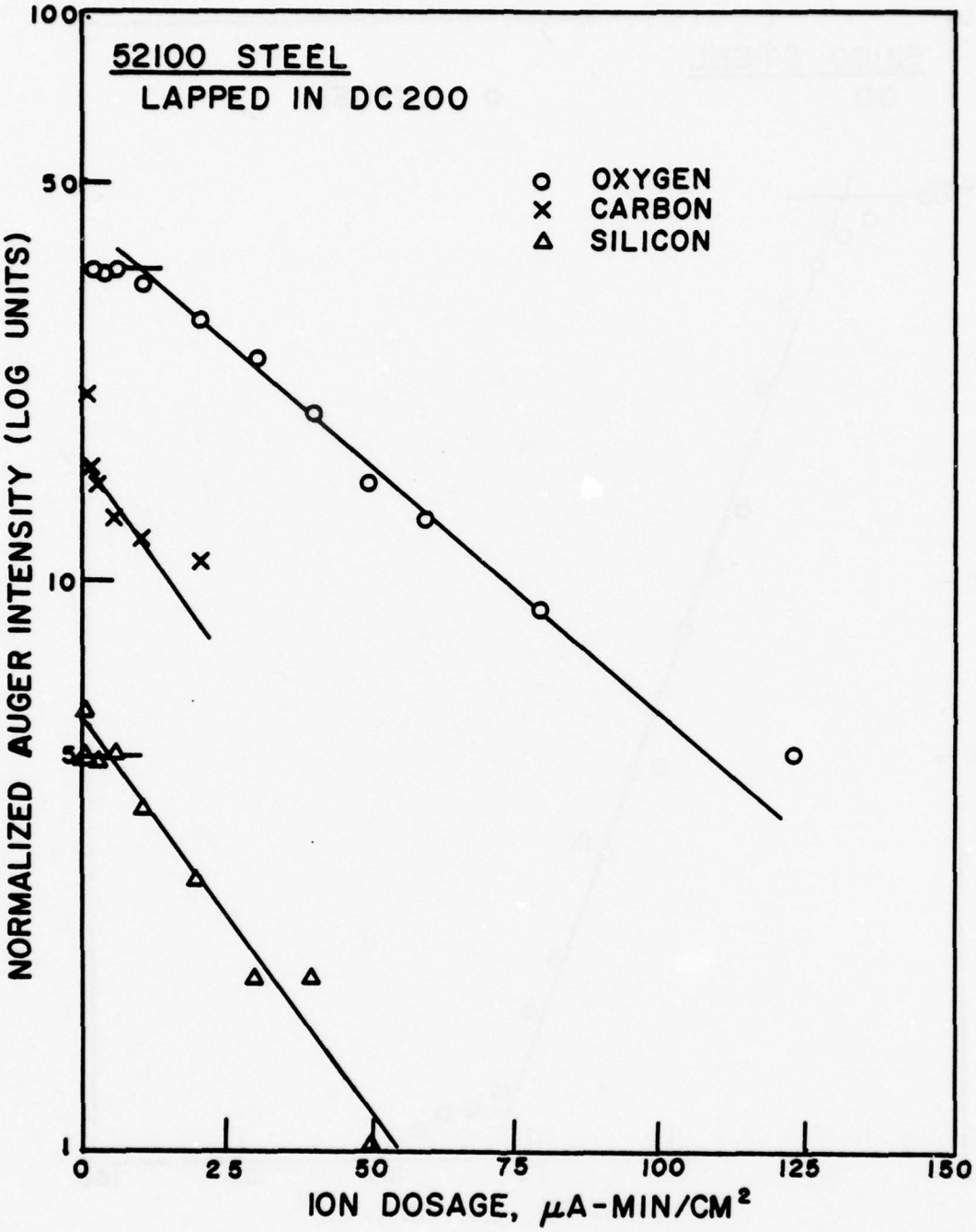


Fig. 7 - Auger/sputter profile of 52100 steel lapped with 3 micron Al_2O_3 grit suspended in DC-200. Note the incorporation of silicon beyond the oxide layer.

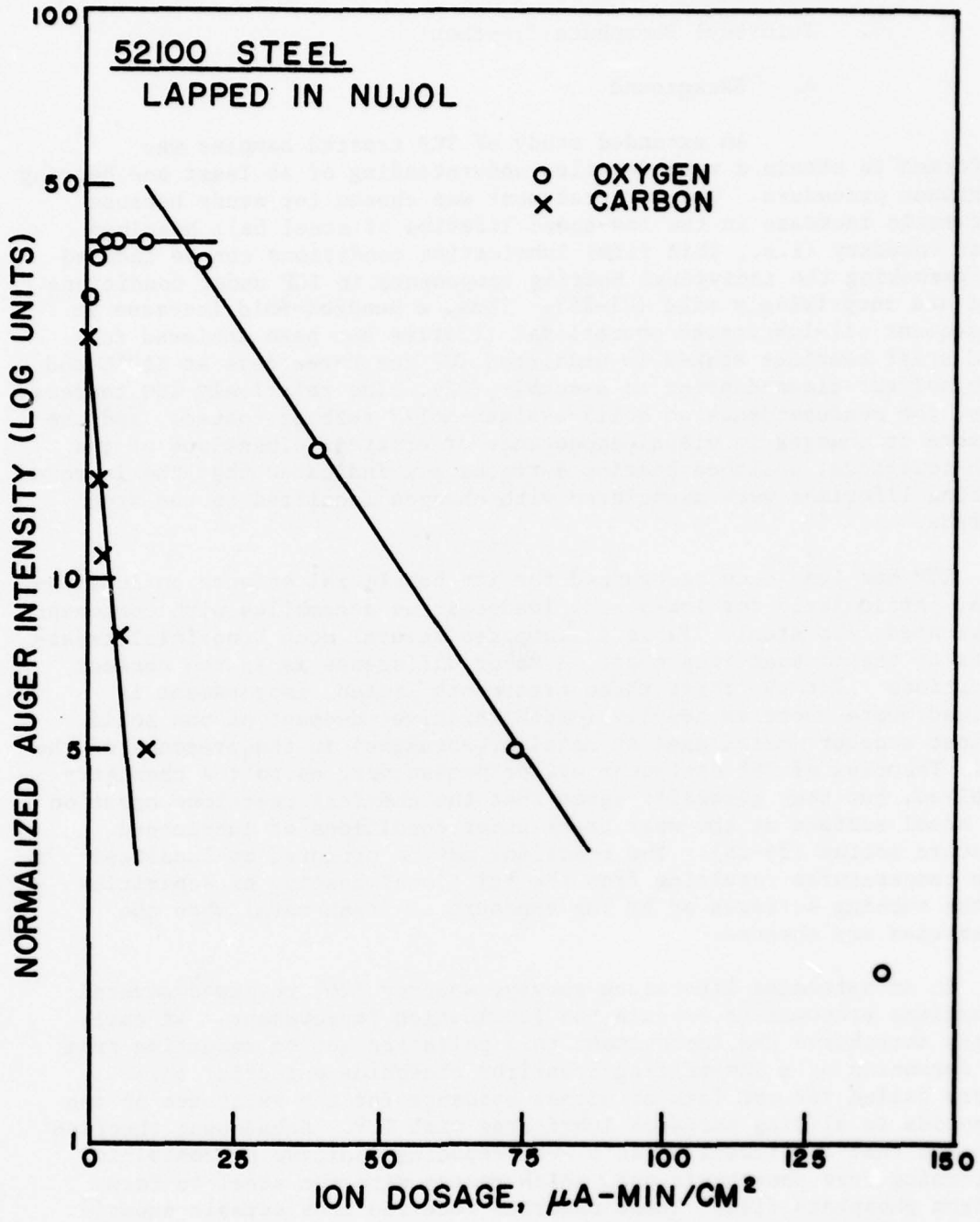


Fig. 8 - Auger/sputter profile of 52100 steel lapped with 3 micron Al_2O_3 grit suspended in Nujol (USP mineral oil).

samples A-D were taken with alternating sputter etch/analysis and may have an apparent longer halflife due to experimental reasons.

3. Tricresyl Phosphate Treatment

a. Background

An extended study of TCP treated samples was performed to obtain a more detailed understanding of at least one bearing treatment procedure. The TCP treatment was chosen for study because a dramatic increase in the low-speed lifetime of steel ball bearings under boundary (i.e., thin film) lubrication conditions can be induced by presoaking the individual bearing components in TCP under conditions that are surprisingly mild (21-25). Thus, a hundred-fold increase in subsequent oil-lubricated operational lifetime has been achieved for 440C steel bearings soaked in undiluted TCP for three days at 110°C and then solvent cleaned prior to assembly (22). The relatively low temperature, the nondependence on solid-against-solid rubbing contact, and the absence of changes in visual appearance or critical dimensions of the high-tolerance, polished bearing surfaces all indicated that the improved bearing lifetimes were associated with changes localized to the steel surface.

TCP has long been recognized for its beneficial effects on lubrication, particularly for low-speed, load-bearing assemblies with components fabricated from steel. Table 12 compares several such beneficial treatments to the presoak treatment. A major difference is in the contact conditions. For the first three treatments listed, improvement is noticed where there is heavily loaded relative movement of one solid against another (metal against metal or abrasive) in the presence of the TCP. Theories of TCP anti-wear effectiveness vary as to the chemistry involved, but they generally agree that the chemical reactions occur on the steel surface at the wear track under conditions of lubricated relative motion (26-28). The reactions may be promoted by localized high temperatures resulting from the frictional heating of asperities on the rubbing surfaces or by the exposure of fresh metal when the asperities are sheared.

In an extensive literature survey, Godfrey (26) reviewed several mechanisms proposed to explain the lubrication improvement. An early theory attributed the improvement to a polishing action resulting from the formation of a low-melting iron/iron phosphide eutectic; this theory failed for the lack of direct evidence for the existence of the phosphide in sliding surfaces lubricated with TCP. Subsequent theories proposed that TCP functions as a wear-reducing additive by containing or forming free phosphoric acid which reacts with the steel to form an iron phosphate film. These theories received considerable experimental support from a variety of research approaches, including the friction, wear, and electron diffraction surface analyses of Godfrey(26). He was able to identify a mixture of $FePO_4$ and $FePO_4 \cdot 2H_2O$ in the film formed when steel sliding on steel was lubricated with the TCP.

Table 12

TCP Treatments in Lubrication of Steel[a]

Application	Conditions: Contact	Conditions: TCP Concentration	Conditions: Temperature	Purpose
Lubricant additive	Metal/ metal	~ 3% in oil	Operational[b]	Anti-wear agent for petroleum-based oils
Prerun	Metal/ metal	Neat	Warm[b]	Surface run-in of asperities Chemical coating
Lapping vehicle	Metal/ abrasive	Neat	Ambient[b]	Finishing process
Passivation	Metal/ no O_2	Neat	260-275°C	Inhibit catalytic pyrolysis of ester-based oils
Presoak	Metal	Neat	110°C	Increase bearing lifetime

[a] For low-speed, load-bearing assemblies

[b] Localized hot-spots at rubbing asperities

Combined radiotracer and wear studies using P^{32}-radiotagged TCP_{32} led Bieber et al. to suggest (27,28) that most, if not all, of the P^{32} they reported as chemically reacted at the bearing metal wear scar may have originated from polar P^{32} impurities and not from the tagged TCP. They postulated adsorption of the polar materials as a precursor to the chemical reaction but did not identify the chemical nature of the ultimate reaction products.

Distinct from the above, a treatment involving the contact of TCP with nonrubbing steel surfaces also has been reported as improving subsequent frictional behavior. Pretreatment of individual bearing parts with hot TCP has been recommended to passivate the mild steel surfaces so that they do not catalyze pyrolysis of ester-based lubricating oils (29,30); this extends the lifetime of the lubricant and protects the metal surfaces from deleterious effects from the pyrolytic degradation products of the lubricant. The catalytic inhibition was associated with the generation of a characteristic iron oxide of an inert spinel type (30). The recommended passivation conditions (Table 12) are far more rigorous than those of the TCP presoak, however.

The effectiveness of the TCP-presoak treatment in extending bearing performance lifetimes under adverse conditions, coupled with the fact that the presoak is applied to the bearing components independent of their assembly, makes this treatment attractive for direct incorporation in the manufacturing process and for inclusion in subsequent rework stages.

The effectiveness of several chemical presoak treatments and the appropriate conditions of application leading to maximum benefits for each chemical have been reported previously by CSDL (21-25). The performance characteristics were evaluated for the chemically treated steels both in the pin-on-disk test configuration and as assembled bearings. For each treatment a companion "control" experiment was run in which the steel components were immersed in V-78 lubricant at the same temperature and for the same length of time as in the presoak chemical; subsequently both the control and the chemically presoaked systems were operated while flooded with V-78. A uniform presoak temperature of 110°C was chosen in order to increase the reaction rate without compromising the metallurgical properties of the steels. In the pin-on-disk tests, simultaneous measurements were made of the electrical resistance and the coefficient of friction under a 1 Kg load at 5 cm/sec over a 2-hour period; at the conclusion of each run visual observations were made on the wear scars, particularly those of the pins. The bearing assemblies were subjected to low-speed dynamometer (LSD) tests at 1 rpm, milliwattmeter measurements at high-speed (24,000 rpm), and visual examination for surface deterioration.

The results on pin-on-disk tests on presoaked 52100 steel indicated that the minimum presoak time required to achieve essentially maximum improvement in performance corresponded qualitatively to the reactivity of the presoak chemical with the 52100 steel. Thus, a minimum time of 7 days sufficed for the reactive chemical, acid phosphite, whereas a 15-day presoak was required to achieve maximum benefits from treatment with the less reactive TCP. The improvements were manifested by lesser wear, lower frictional resistance, and higher electrical resistance across the sliding contacts.

The identical chemical treatments were also applied to 52100 bearing components. Of four chemical soaks used, all but the TCP-treated components failed at least one of the assembled-bearing tests at a relatively early stage of lifetime testing. However, bearings treated for 15 days (or longer) with TCP were able to survive hundreds of hours of LSD runs with no sign of deterioration; under the same conditions, the control bearings failed in a matter of hours.

Essentially similar results were observed with 440C steels, except that effective treatment times were shorter. Photographs of pins from the pin-on-disk studies showed heavy wear scars on the controls but virtually no scarring on pins pretreated with TCP for as little as 2 days. The results of various measurements led to the conclusion that TCP treatment was superior to the other chemical soaks (i.e., isopropyl oleate, acid phosphite, and a polyester turbo oil) and that the optimum improvement in the performance of 440C steel was achieved in a minimum of 2 days exposure. The appearance of occasional pitting on 440C steels after a 14-day exposure, however, suggests that the performance of this steel could be degraded by excessive treatment.

Surface cleanliness is important in bearing preparation. For example, bearings which were contaminated (as identified by their non-wetting by V-78 oil) prior to the TCP soak exhibited far shorter lifetimes than did those which had passed the wettability test (24). From this it was concluded that the TCP treatment was less effective than normal because of the contaminating surface film. The results cited previously were obtained for steels which had been given a solvent treatment between the last metal removal step (lapping) and the chemical soak. In the search for an alternate cleaning procedure, recourse was had to the glow discharge process, a technique which had proved itself in the cleaning of gas bearings (31). Comparable chemical treatments and bearing evaluation tests were therefore run on glow-discharged surfaces for comparison with the solvent-cleaned surfaces. However, the bearing performance of the glow-discharged steels exposed to TCP proved ambiguous.

b. Experimental Results

The tri-p-cresyl phosphate used in the presoak treatment for this work was a commercial product, used neat, and containing less than 2% of the ortho isomer. An analysis by atomic absorption showed impurity levels of 51 ppm Na, 4 ppm K, and 12 ppm Ca. The liquid was preheated to the reaction temperature of 110°C before immersion of the freshly prepared steel flats. At the end of the reaction period the specimens were withdrawn from the warm liquid, allowed to cool to room temperature in air, and then subjected to TSC treatment.

Parallel sets of experiments were run on the two bearing steels cleaned by TSC alone or by TSC followed with GD. Surface compositions were analyzed for both the cleaned steels and those that had been TCP-treated. TCP exposure times were chosen to: (i) bracket the minimum period determined necessary to obtain maximum improvement in bearing performance of each alloy, and (ii) permit sufficient overlap of the treatment times so that direct comparisons could be made between the treated steels. For each alloy six buttons were prepared, one set of three being TSC-treated, the other set GD-treated. All twelve freshly cleaned buttons were immersed in TCP at the same time, but were withdrawn pairwise after the appropriate immersion times had elapsed. For the 52100 steel, one button each from the TSC- and GD-treated sets was removed after 3, 15, or 21 days; the corresponding immersion periods for the 440C steel were 1, 3, and 15 days. Immediately after withdrawal, the buttons were cooled to room temperature and, regardless of previous cleaning history, TSC-treated to remove any entrained liquid. The dry buttons were then mounted and shipped to NRL for AES analysis.

The results of the analysis of both clean and TCP-soaked steel surfaces prior to sputter etching are presented in Table 13. Iron and oxygen are the only elements common to all of the cleaned surfaces (i.e. before TCP treatment). Evidence that the surface carbon was not introduced by the solvent cleaning comes from comparisons with the various TCP-treated surfaces; no carbon was found on glow-discharged 440C steel even though the final treatment had been solvent cleaning to remove gross TCP. The striking, and consistent,differences in the observed surface carbon content between the two TCP-treated alloys therefore must reflect major differences in their surface reactions with the TCP.

None of the other elements, including phosphorus, known to be present in the bulk alloy (Table 1) were detected in the cleaned surfaces. Phosphorus was, however, detected in the outermost surface of every steel specimen that had been exposed to TCP. The concentration of P was roughly equivalent (around 5 at.%) regardless of the type alloy, its cleaning history, or the length of its TCP exposure. Although presoak time had little effect on the surface concentration of P, it did influence the chemical state, as shown by the changes in position and lineshapes of the low-energy Auger spectral features corresponding to

Table 13

Surface Composition Prior to Sputter Etch

Metal	Sample Cleaning	Exposure to TCP (days)	Normalized Auger Intensities								
			Cr	Fe	O	P	C*	K	Ca	Na	S
440C	Glow discharge	-	0.5	44	55	-	-	-	-	-	0.1
		1	-	38	45	6	-	4	2	4	-
		3	-	36	43	4	-	7	2	7	0.6
		15	-	33	36	5	-	9	2	14	1
	TSC	-	3	42	40	-	14	-	0.5	-	0.2
		1	-	34	34	5	17	4	2	5	0.2
		3	-	29	34	7	15	5	2	7	0.2
		15	-	30	35	6	0.6	8	2	14	0.4
52100	Glow discharge	-	-	48	52	-	-	-	-	-	-
		3	-	32	34	6	19	5	1	3	0.4
		15	-	26	30	4	32	2	0.6	4	0.2
		21	-	16	26	4	48	2	0.3	4	0.3
	TSC	-	-	44	40	-	15	-	0.6	0.4	0.1
		3	-	20	24	6	41	3	0.8	4	0.1
		15	-	24	30	6	36	2	0.6	2	0.2
		21	-	26	34	4	31	2	0.4	2	0.2

* In the presence of 5% potassium, concentrations of carbon below 2% could not be identified.

transitions involving the valence band. This is demonstrated by Fig. 9 where those features for both phosphorus and iron are reproduced for 52100 steel after three different exposure times. After the 3-day presoak, the minimum in the P Auger signature occurred at the same electron energy (119 eV) as that of a well-defined iron phosphide (32), but neither its lineshape nor that of the iron matched those for the iron phosphide (see Figure 10). After 21-days presoak, the minimum shifted to lower energy and the general features of the P signature were consistent with those observed for iron phosphates. Further, there was some correlation between the lineshape of the iron from the TSC 52100 exposed for 21 days and that from known iron phosphates. The possible presence of iron phosphate will be discussed later in more detail.

Of the remaining elements in Table 13, the Na, K and Ca are known to be present at the parts per million range in the liquid TCP. Therefore, their appreciable concentration on the TCP-treated steels indicates preferential deposition or adsorption on the solid surface. The remaining element, sulfur, is an ubiquitous contaminant (particularly in high vacuum systems) and its recurrence in low concentrations is not a matter of concern.

Composition depth profiles for the TCP-treated steels are presented in Figs. 11 and 12 for 52100 and 440C steels, respectively, after three different presoak times. For clarity, smoothed curves are used to present the changes in surface elemental concentration as a function of sputter time, and the display is limited to major elements (Fe, O, C, and P for 52100, with Cr added for 440C steel). As in the case of the clean steels, changes in elemental concentration were often accompanied by shifts in Auger spectral features indicative of an altered chemical environment. On the curves corresponding to carbon concentrations, a vertical tick marks the sputter time required for emergence of a carbide signal. Although several changes occur in the valence band spectral feature of iron with progressive profiling, only the emergence of the signature identified with metallic iron has been marked on the iron concentration curves. The assignment of a comparable tick to mark the transition to metallic chromium was not attempted because of spectral interference. For 52100 steel the length of sputtering required to reach the metallic iron is directly related to the length of the TCP presoak; the correlation is less well defined for the 440C.

A feature common to the profiles for all surfaces with large initial concentrations of carbon is the artifactual suppression of the concentrations of the remaining elements. Accordingly, many of the profiles show a sharp initial rise in concentrations as early sputtering removes the contaminating carbon overlayer. With continued ion etching more representative relations develop; the oxygen concentration decreases and the iron concentration rises to approach an asymptotic value related to the alloy composition ($\sim$ 80 at.% for 52100 and $\sim$ 60 at.% for 440C). The corresponding concentration of carbon, in carbide form, usually

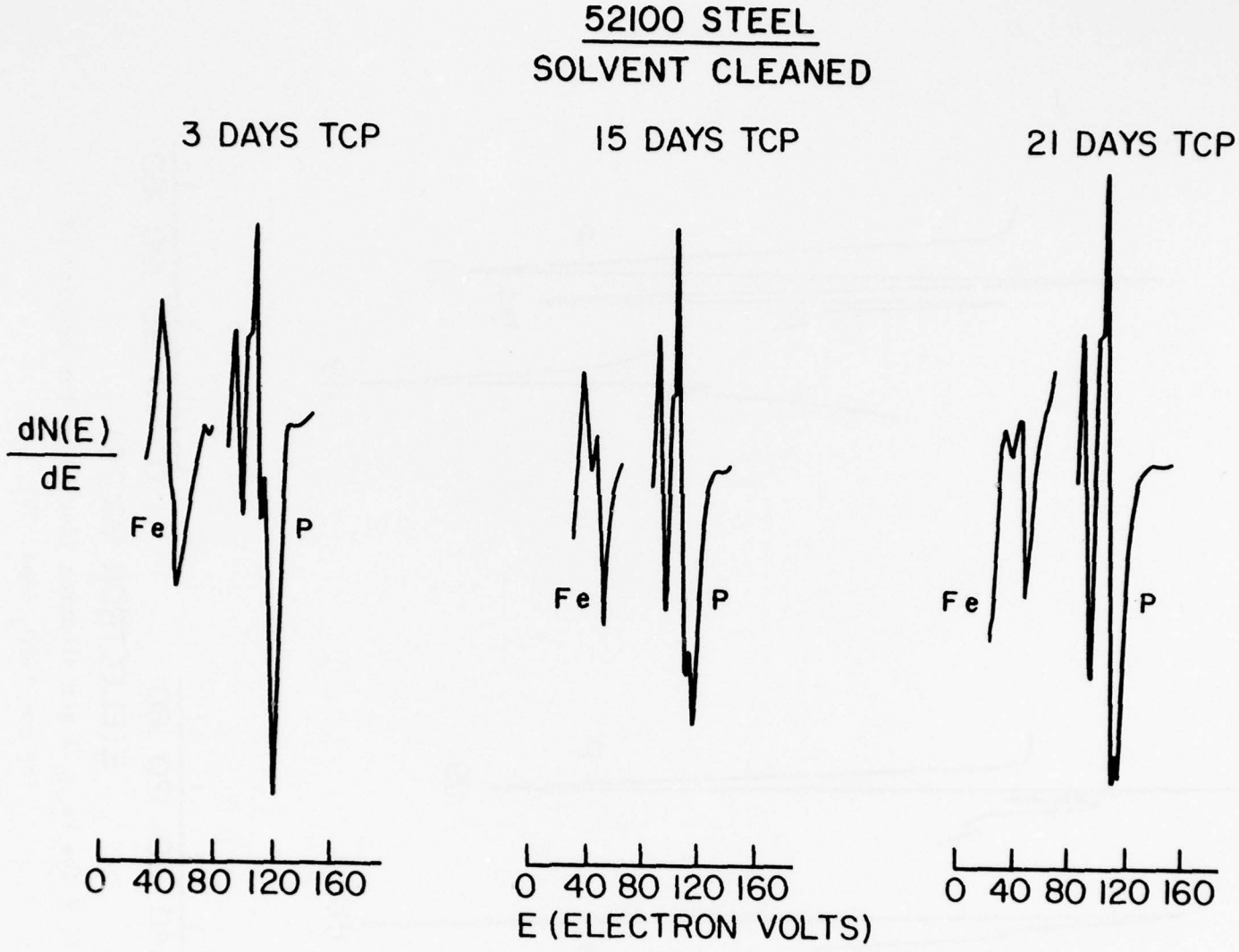


Fig. 9 - The Fe_{MVV} and P_{LVV} Auger electron lineshapes for samples of 52100 steel exposed to TCP at 110°C for 3, 15, and 21 days, respectively.

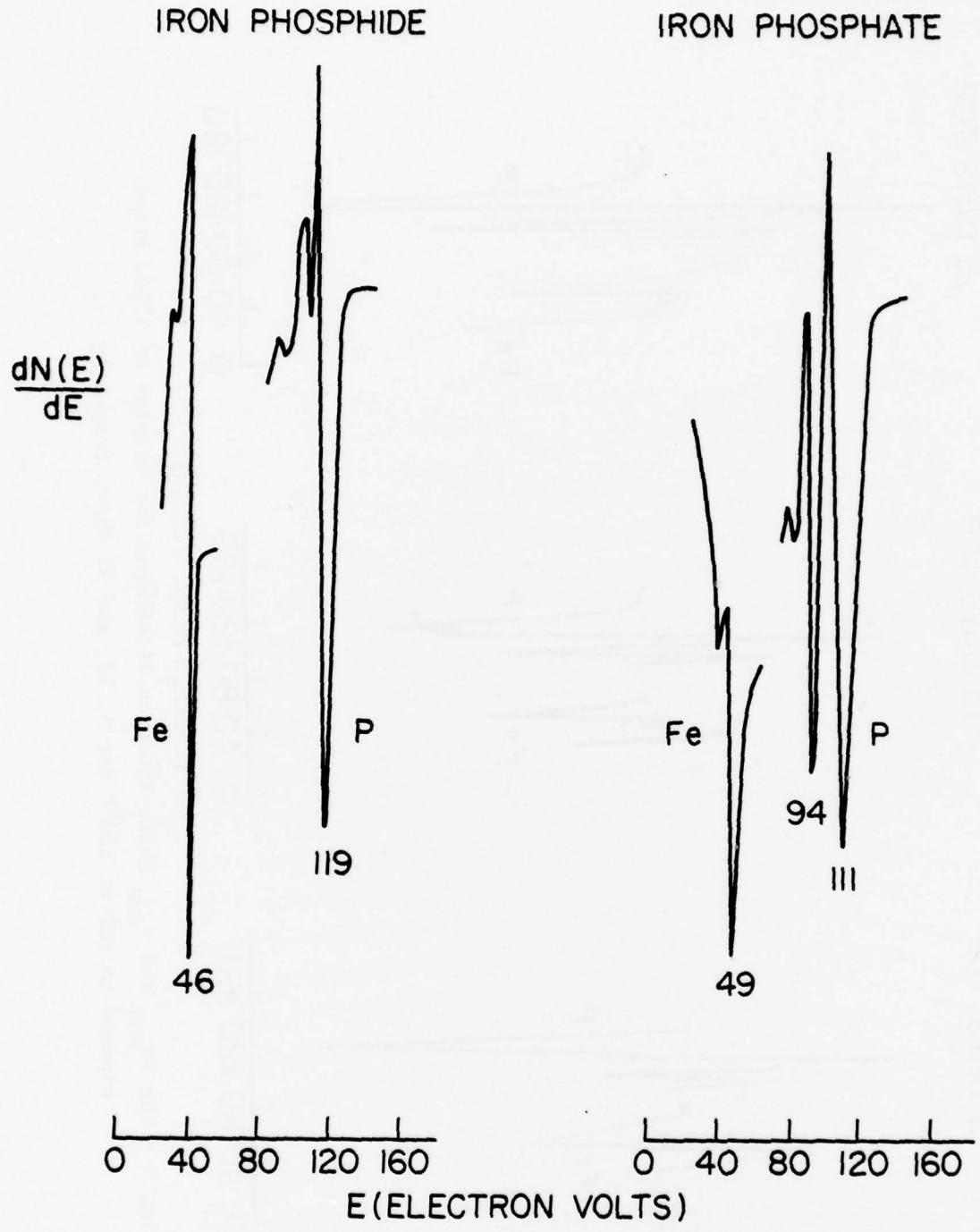


Fig. 10 - The Fe_{MVV} Auger electron lineshapes for samples of FeP and $FePO_4$ (Ref. 32).

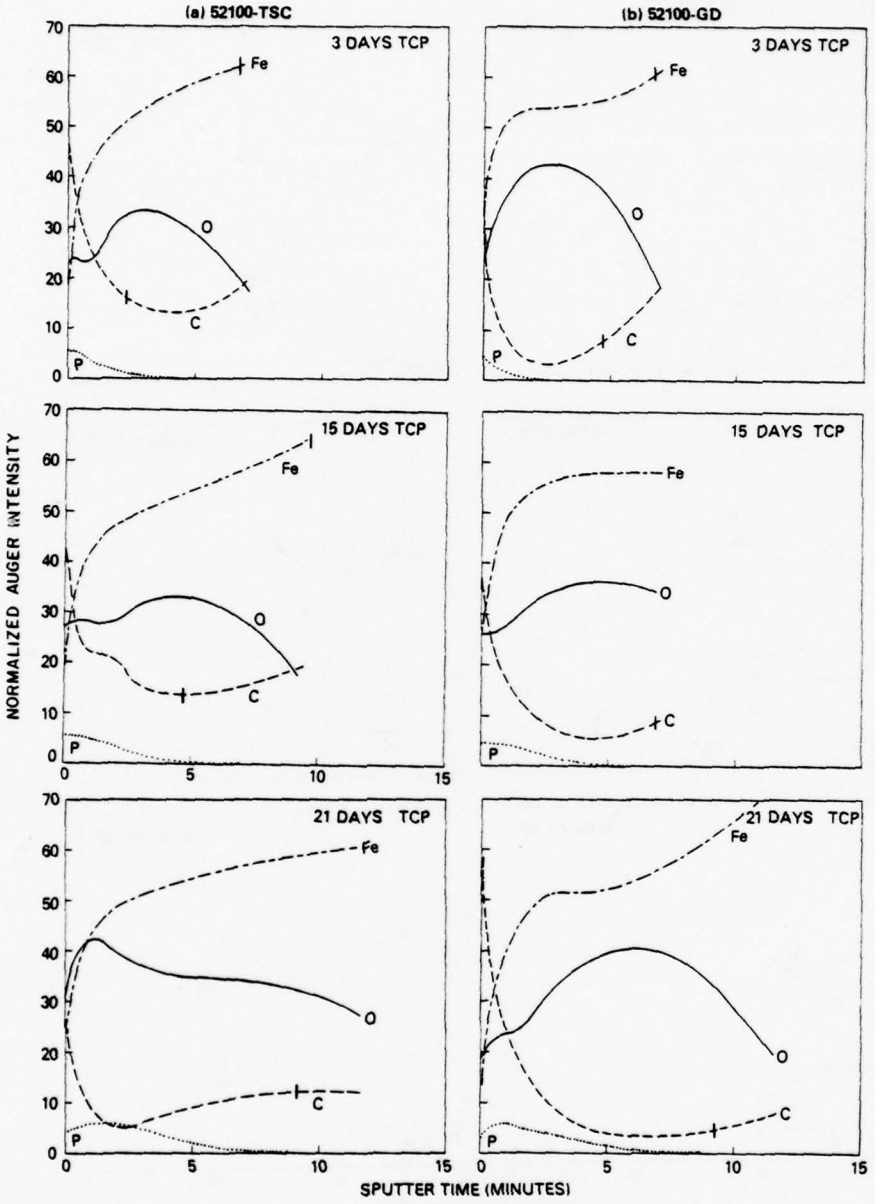


Fig. 11 - Auger/sputter depth profiles of 52100 steel (a) after solvent cleaning and (b) after glow discharge treatment, each followed by exposure to TCP at 100°C for 3, 15, and 21 days, respectively. (Sputter rate ~ 10 Å per minute.) Tick on iron profile marks first appearance of metallic iron spectral feature; tick on carbon profile, appearance of carbide.

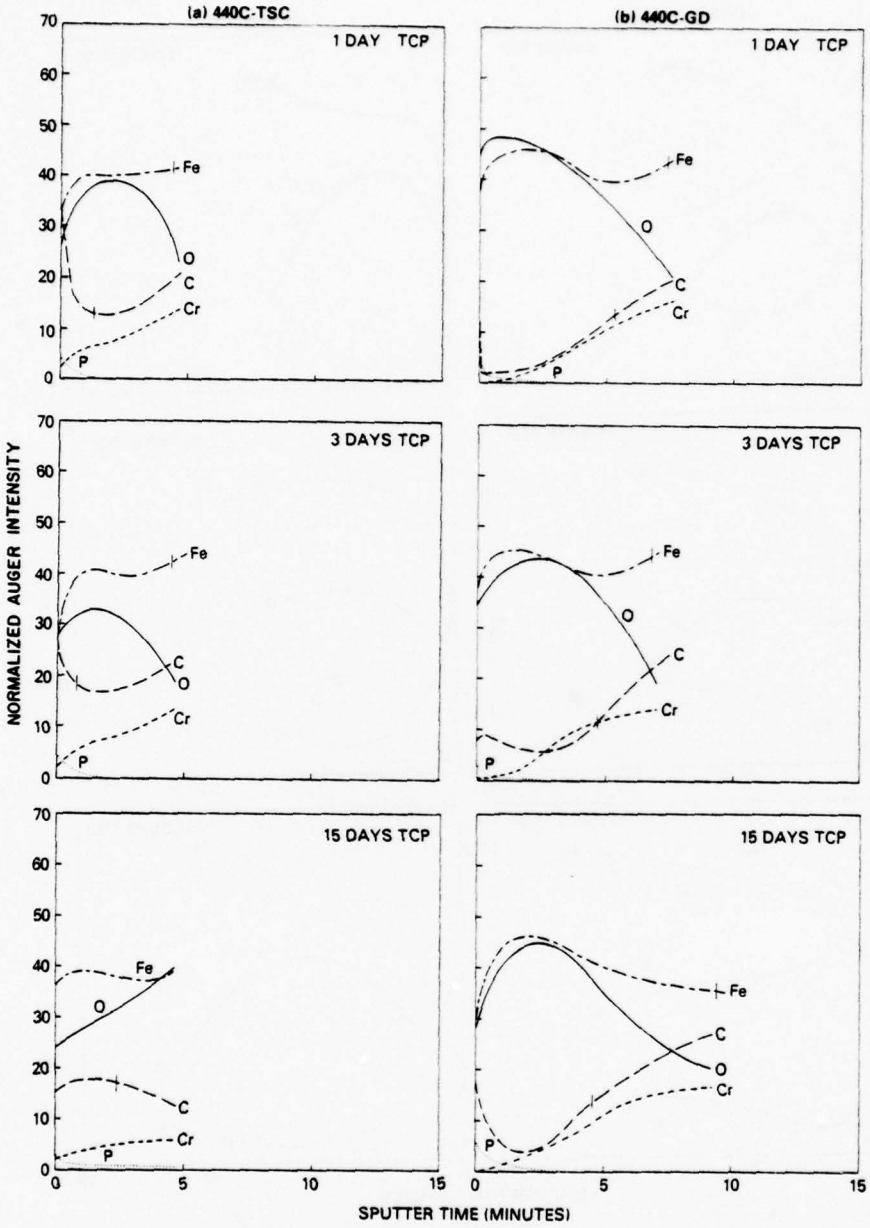


Fig. 12 - Auger/sputter depth profiles of 440C steel (a) after solvent cleaning and (b) after glow discharge treatment, each followed by exposure to TCP at 110°C for 1, 3, and 15 days, respectively. Sputter rate ~10 Å per minute.) Tick on iron profile marks first appearance of metallic iron spectral feature; tick on carbon profile, appearance of carbide.

exceeds the nominal C concentration for the bulk alloy. (It is known that the carbon Auger signal from carbide is $\sim$ 2X more intense than that from graphite. The normalization procedure did not take this into account; most of the discrepancy could be removed by utilizing a carbide sensitivity factor for carbon.)

Attention now turns to the element phosphorus and the changes that occur for it as the TCP-treated surfaces are etched. Changes occur in the P Auger signature with sputtering; the possibility of sputter-ion beam damage cannot be ruled out, but sputtering for 10 minutes on $FePO_4$ resulted in no change in its P signal shape.

From the depth profiles of Fig. 1 for 52100 steel gross correlations emerge for phosphorus. Not only is its initial surface concentration limited to about a 5% maximum, but that same level is maintained to a considerable depth into the surface; further, the persistence depth appears related to the length of the chemical presoak for a given alloy. The relatively low concentrations involved make it difficult to quantify these correlations, however. It therefore proved instructive to employ a semi-logarithmic display of the data for phosphorus and for the other elements present in low concentration on the TCP-treated steels. The semi-logarithmic form was chosen since simple sputtering models predict an exponential decay for the removal of submonolayer quantities. A typical graph is shown in Fig. 13, presenting the data obtained on TSC-cleaned 52100 steel exposed to TCP for 15 days. The log of the atomic percentage of each low-concentration element is plotted against sputter time; segments of straight lines are then fitted to the individual data points. Not only is the persistence of the P concentration at the same level highlighted by the horizontal line segment, but the subsequent rate of decay is found to be exponential (i.e. linear on a semilog plot). The intersection of the two linear segments which, together, completely describe the data provides a physically significant numerical value (convertible to film thickness) for data comparisons such as those of Table 14.

In Table 14 are tabulated the plateau concentrations, persistence depths, and decay halflives for phosphorus on TCP-treated steels. Data for the 52100 specimens confirm the correlation of increased persistence depth of the maximum phosphorus concentration with increasing TCP exposure. They also reveal the consistently greater persistence depth on TSC- than on GD-treated steels for equivalent TCP exposure. Presumably this relates to the greater oxide thickness on the latter. For the 440C steel, on the other hand, the initial concentrations of phosphorus tend to be low and there is no evidence of a plateau concentration. The P concentration does, however, decrease at two different rates, the early rate being much faster than the later (Table 14). The lower initial concentration and shorter decay halflife for the 440C as compared to the 52100 steel given the same TCP treatment again testify to the differences in their reactivity.

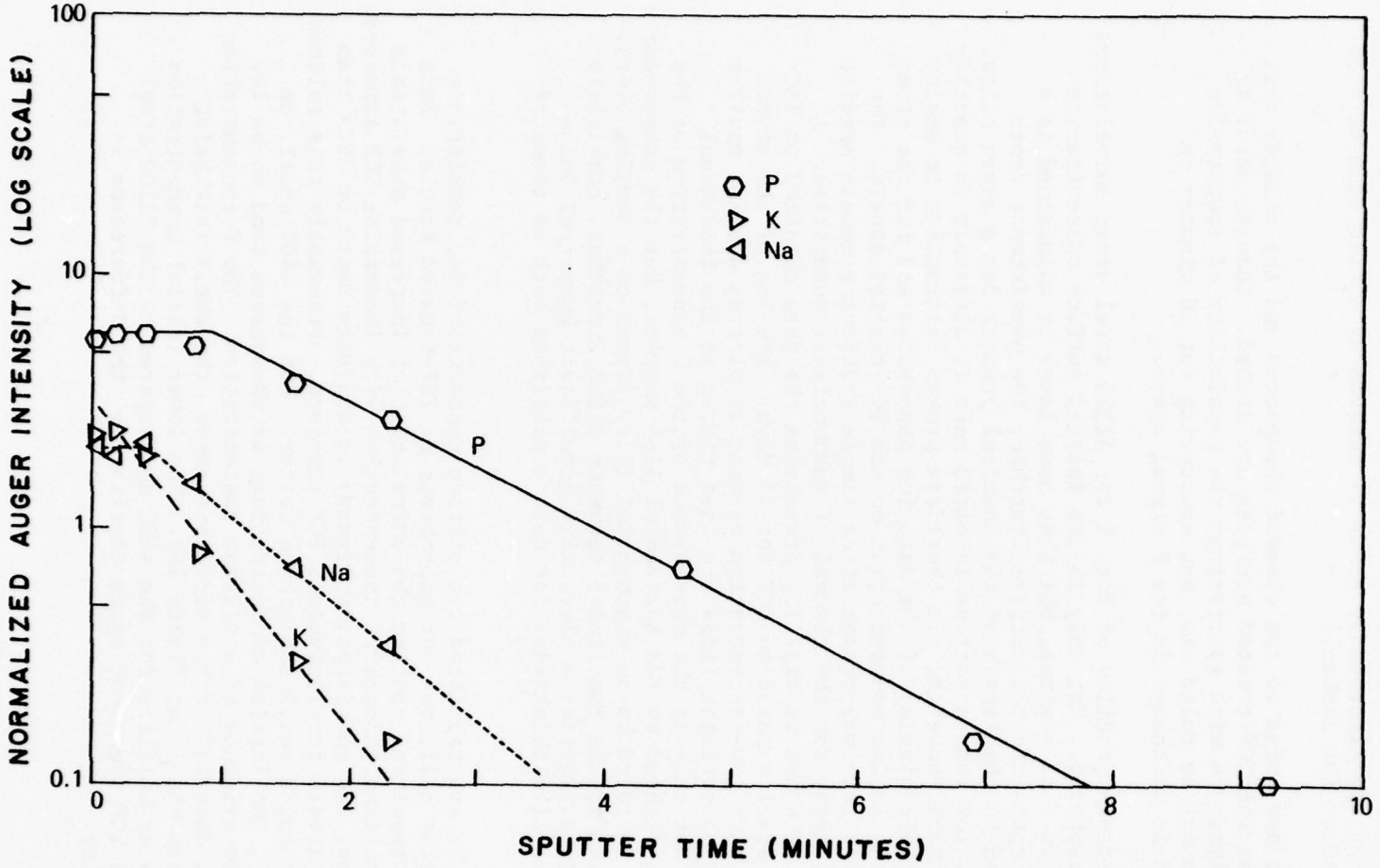


Fig. 13 - Semilogarithmic graph of Auger/sputter depth profiles of low-concentration elements in surface of 52100 steel, solvent cleaned and then exposed to TCP at 110°C for 15 days. (Sputter rate ∿ 10 Å per minute.)

Table 14

Parameters Describing Low-Concentration Elements
on Steels Treated with TCP

Specimen			Phosphorus					Potassium	
Steel Alloy	Cleaning	TCP Exposure (days)	Thickness 5%-P Region (minutes of sputter)	Normalized Auger Intensities	Decay Halflife (minutes of sputter)	Normalized* Auger Intensities	Decay* Halflife (minutes of sputter)	Normalized Auger Intensities	Decay Halflife (minutes of sputter)
52100	TSC	3	0.5	6	0.7			4	0.3
		15	1.0	6	1.2			3	0.4
		21	3.0	5	1.2			3	0.8
	GD	3	0	4.6	0.5			3	0.2
		15**	0.9	5	1.2			3	0.5
		21	1.2	6	1.6			4	0.5
440C	TSC	1	-	3.5	0.45	0.9	< 0.1	3	0.2
		3	-	3.8	0.5	1.2	< 0.1	5	0.2
		15	-	1.5	4.3	2.3	0.1	6.6	0.65
	GD	1	-	2.3	0.8	2.2	0.1	3	0.3
		3	-	1.6	0.8	2.3	0.1	6	0.2
		15	-	3.8	0.8	2.3	0.1	8	0.25

* For rapidly decreasing species.

** Data suspect; see Discussion Section II D3c.

The results for phosphorus are to be compared with those in Table 14 for potassium, an element present as an impurity in the bulk TCP at the low level of 4 ppm. Although the initial concentrations are roughly equivalent, there is no evidence for a plateau in the potassium concentration profile. That fact, coupled with the extremely short decay halflives, indicates the potassium to be a true surface contaminant, rather than an integral part of the surface layer as is the phosphorus.

The behavior of sodium is ambiguous. Although present at an order of magnitude greater impurity level than potassium in the liquid TCP, its initial concentration on the TCP-treated steels (Table 13) is never more than twice that of potassium. There is slight evidence for a plateau concentration level, but the persistence depth never equals that for phosphorus. Caution must be exercised in interpreting the sodium data because sodium ions are known to migrate under the influence of a beam of charged particles in silicon dioxide (33). The larger ionic radius and greater mass of potassium would make it less susceptible to such influence.

c. Discussion of TCP Results

52100 TSC

Since the data base developed for the 52100 steel presents a more consistent, interpretable picture, it will be analyzed first. It will be most convenient to describe the surface film by starting at the bulk metal phase and progressively analyzing the surface film constituency as it changes as one moves closer to the external surface. This is, of course, the reverse order from which the data is actually taken. Figure 14a presents the O/Fe ratio observed as a function of sputtering time for the three 52100 TSC samples exposed to TCP. This particular representation of the data has been chosen to identify three regions in the surface film. These regions are identified, in order of occurrence starting next to the bulk metal, as an oxide layer, a transition layer, and a layer consisting of some kind of iron-oxygen compound containing $\sim$ 5% phosphorus. In the same order they are identified in Fig. 14 by the region where the O/Fe ratio drops below $\sim$ 0.6 for the longer sputtering times, the region where the phosphorus concentration drops from 5% to less than 1% (lower limit of detection), and the surface region where the phosphorus concentration is essentially constant at 5%. A fourth region, a surface contaminant layer, might also be defined; it is not obvious in Fig. 14 but shows in the elemental depth profile plots (Fig. 10) as a rapid decrease in carbon and a rapid increase in P, Fe and O. Some of the carbon contaminant deposited while the samples were in the vacuum system. This is evident by comparison of the compositions in Table 13 which were measured immediately after entry into the vacuum system and the compositions presented in Fig. 11 which were measured at a later time.

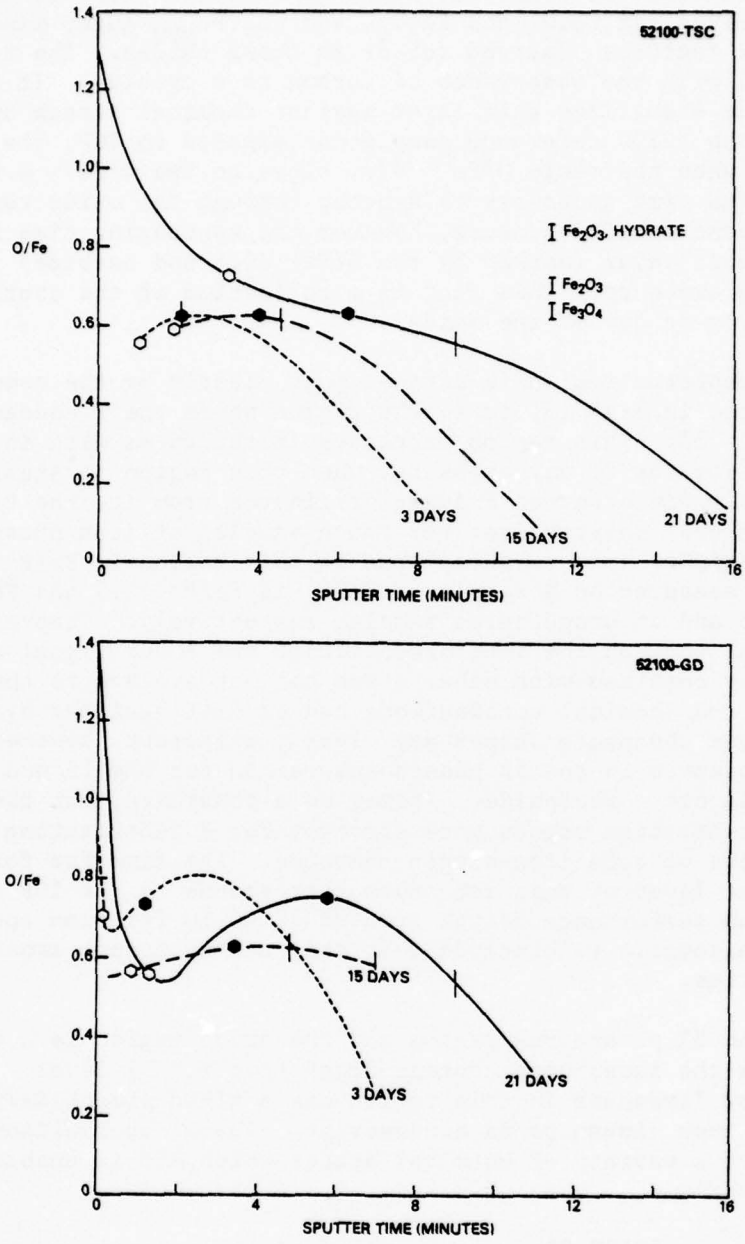


Fig. 14 - O/Fe concentration ratio profiles for 52100 steel (a) after solvent cleaning and (b) after glow discharge treatment, each followed by exposure to TCP at 110°C for indicated number of days. (Sputter rate ~ 10 Å per minute.) Vertical tick indicates appearance of carbide. Open symbol indicates persistence depth of 5%-phosphorus region; closed symbol, < 1% phosphorus.

On the 52100 TSC samples the oxide region is so identified because there is no detectable P, K, or Na, the O/Fe ratio of $\sim$ 0.6 is consistent with those observed for Fe_2O_3 and Fe_3O_4, and the Fe_{MVV} Auger lineshape has the general features observed for Fe in those oxides. The region is also correlated with the observance of carbon as a carbide. It may be that the carbide stabilizes this layer against chemical attack by the TCP soak. On the 52100 reference sample not exposed to TCP, the carbon became carbide when the ratio O/Fe $\sim$ 0.7, close to the O/Fe $\sim$ 0.6 observed here. The time necessary to sputter through the oxide region is fairly independent of TCP exposure, however the sputtering time necessary to reach its outer layer (marked by the O/Fe $\sim$ 0.6 and carbide) increased with increasing exposure. This fact is a reflection of the continuing growth of a layer on top of the oxide.

The 5% phosphorus region is defined most clearly by the composition profile presented in Fig. 13; it is the region where the P concentration is constant at $\sim$ 5%. This region increases in thickness with increasing TCP exposure. For the 21 day exposure, when this region is significantly thick so that all the observed P Auger originates from it, the P signal shape resembles that observed for reference samples of iron phosphate. However, the ratio of iron to phosphorus in this region is Fe/P $\sim$ 8-10. The same ratio measured on a sample of $FePO_4$ is Fe/P $\sim$ 1.5 and Fe/P $\sim$ 1 for a sputtered and an unsputtered sample, respectively. Theoretical and experimental work on the interpretation of the Auger signal shape for P chemically combined with other atoms has not evolved to the point where the many P-O chemical combinations can be distinguished by Auger. The phosphide and phosphate shapes are clearly different, however, and the P signal observed in the 5% phosphorus region for the 15 and 21 day TCP exposures is not a phosphide. It may be a phosphate, but the 5% limit on P concentration argues more strongly for P substituting into lattice vacancies of some iron-oxygen compound. The time for formation of a significant layer of this substance corresponds to the TCP exposure time for optimum performance of the treated 52100 in friction and wear tests; it is reasonable to conclude that this new substance imparts the desired properties.

Between the 5% phosphorus region and the oxide region is a transition zone where the phosphorus content drops from its 5% level. The phosphorus Auger lineshape in this region has a mixed phosphide/phosphate character; the iron lineshape is nondescript. These observations probably reflect a variety of chemical states which AES is unable to distinguish clearly.

52100 GD

The O/Fe ratio as a function of sputter time for two GD 52100 samples exposed to TCP is presented in Fig. 14b. The data for the GD 52100 sample exposed to TCP for 15 days has not been included in the analysis because it behaves similarly to the 52100 TSC sample exposed to TCP for 15 days and does not conform to the pattern established by the 3 and 21 day exposures. On the basis of its similarity

to the 52100 TSC sample, we suspect that the glow discharge preparation step for that button was not successful.

The same three regions can be identified on the GD 52100 as were on the TSC 52100 samples. However the initially thicker oxide layer has slowed the reaction rates. This is reflected in the much thinner 5% - phosphorus layer at equivalent TCP exposure and the disappearance of the phosphorus well before the carbon shows up as a carbide.

The fact that the thicker oxide layer slows the formation of the 5% - phosphorus layer implies that the principal reaction is not between iron oxide and the TCP bath. Rather it argues for the reaction to be limited by either the migration of iron through the oxide (or defects therein) to react with the bath, or for P and O to diffuse inward to the metal.

The reactant contributed by the TCP soak is not defined by the data. However, the tendency for the hydrocarbon-like carbon to rapidly decrease with sputtering accompanied by an increase in phosphorus (see Fig. 11, 52100 TSC and GD exposed 21 days) argues against activity by the cresyl groups. This observation will be made once more, with more obvious impact, on the 440C samples.

The slower reaction rate of the GD 52100 samples with the TCP bath prevents the formation of the 5% phosphorus layer during a 15 day soak. This corresponds to the observations on bearing tests at CSDL where the 15 day TCP soak of GD treated bearings did not result in satisfactory performance.

440C Glow Discharge

With the 440C steel the glow discharge prepared samples provide the more convenient set for analysis. In place of O/Fe, the ratio of O/(Fe + Cr) is plotted as a function of sputtering time in Fig. 15b for the three GD 440C samples exposed to the TCP bath. The sum of the iron and chromium was chosen rather than just iron because both transition metals play a major role in the surface oxide. The GD process results in an outer layer of about 30 Å of iron oxide, nearly free from chromium. This 30 Å layer is similar to that formed on the GD 52100 reference sample. This oxide layer on the 440C evidently is a barrier to reaction with the TCP bath. Examination of the profiles in Fig. 15b shows that the oxide layer is substantially intact even after 15 days exposure. No 5% phosphorus region forms; with the onset of sputtering the phosphorus disappears first rapidly and then more slowly to below the 1% level (see Table 14). The rapidly departing phosphorus may originate in an adsorbed layer whereas the slower departing species probably reflects some reaction with the oxide. The phosphorus Auger signal shows a mixed phosphide/phosphate lineshape.

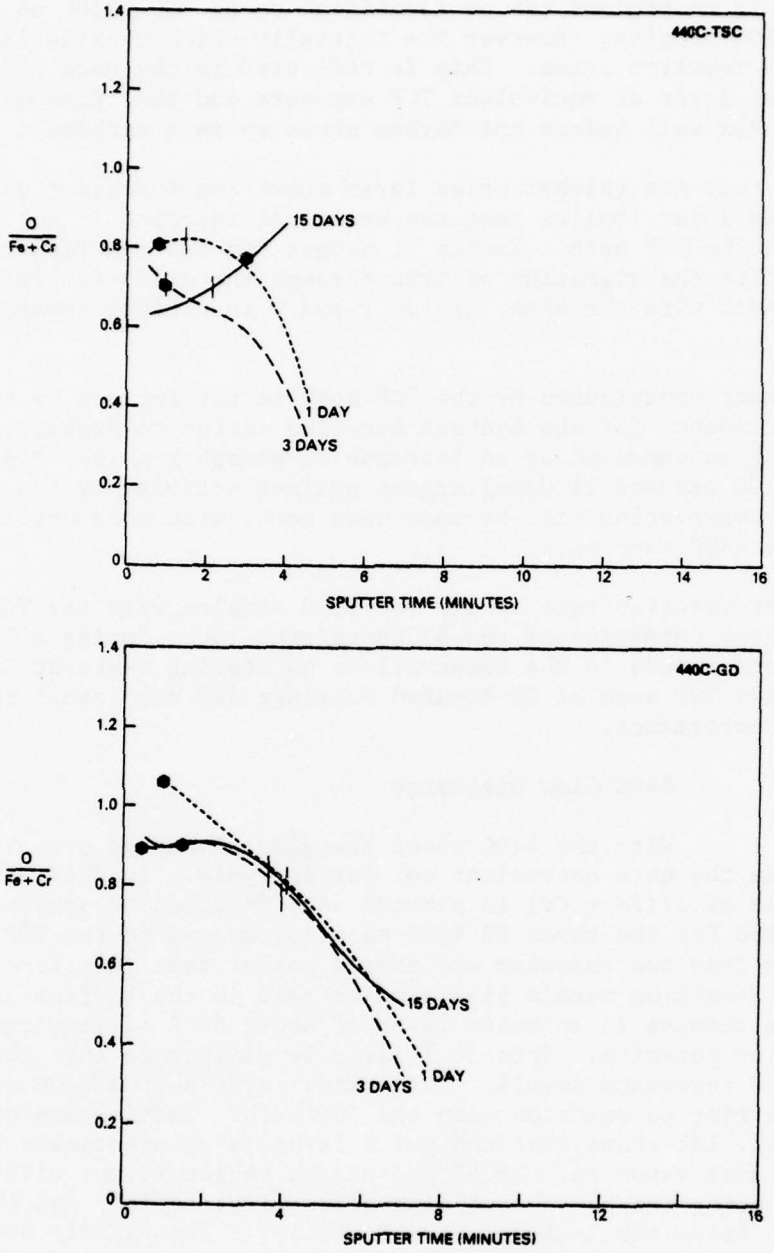


Fig. 15 - 0/(Fe + Cr) concentration ratio profiles for 440C steel (a) after solvent cleaning and (b) after glow discharge treatment, each followed by exposure to TCP at 110°C for indicated number of days. (Sputter rate ∿ 10 Å per minute.) Vertical tick indicates appearance of carbide. Open symbol indicates persistence depth of 5%-phosphorus region; closed symbol, ∿ 1% phosphorus.

The initial composition of the surfaces of all three samples showed less than 2% carbon (the detection limit due to spectral interference from the K signal) even after the 15 day exposure. This observation and the depth profile information are in stark contrast to the 52100 samples where evidence for chemical changes were abundant. Since the glow discharge process resulted in a similar oxide region on the outer surface of both 52100 and 440C, the difference in the reaction rate must lie in the presence of the chromium at the back edge of the oxide film. The chromium may stabilize a nonreactive iron oxide passivation layer or it may block the migration of iron to the surface where it can react with the TCP bath.

The concentration on the GD 440C surface of K and Na, impurities in the bath at 4 and 51 ppm, is as large as that of the P. Since no carbon is observed on the surface, the cresyl groups are not present. These two facts lead one to conclude that the phosphorus present on the 440C surface may well be due to polar impurities in the TCP, as suggested by Klaus and Bieber (27).

440C TSC

The data summary for the TSC 440C samples, presented in Fig. 15a, does not lend itself to easy interpretation. It is clear that the reaction rate of the TSC 440C is greater than that observed for the GD 440C samples and less than that observed for the TSC 52100 samples. However no discernable layer formation has been identified. The 440C is known to form etch pits with 14 day exposures to the TCP bath. This suggests that the somewhat anomalous behavior of the TSC 440C exposed to TCP for 15 days is an artifact arising from the Auger spectroscopy sampling both relatively unreacted areas and reacting etch pits. The data from that situation would not reflect the simplistic layer analysis which worked with the 52100.

d. Relationship to Bearings

It is important to recognize that the presoak treatment may have an entirely different effect on the surface chemistry of steel than that which results from interactions in the presence of heavily loaded rubbing surfaces, the conditions which obtain for many of the widely used TCP lubrication improvement methods. Conversely, the surface chemistry may be identical in both cases, but the reaction and its products may be distributed more uniformly during the presoak rather than radiating from individual reactive asperities where metal/metal contact occurs.

No comparisons are made here between compositional profiles for TCP-treated research flats and those of used TCP-treated bearing components because of the unavailability of the latter from recently operated bearings. However, it is instructive to refer to the results of analyses in Section III B 2 on the wear scars of bearings which had been treated with a related phosphate chemical, zinc dialkyldithiophosphate (ZDTP).

The work described in Section III B 2 and this Section provide evidence for both the TCP and the ZDTP presoak systems that improved low-speed bearing endurance is associated with the presence of a persistent, though modest, concentration of phosphorus in the outermost atomic layers of a surface which is otherwise principally an iron oxide. The effectiveness of such a relatively low surface concentration in extending useful bearing lifetimes suggests that the phosphorus plays an important role in stabilizing the outermost iron oxide layer against attack, mechanical or chemical. Thus, the major contribution of the various phosphate treatments may be the establishment of just such a layer: the presoak treatment operating by developing the layer in sufficient depth that a reservoir of phosphorus is available from within the metal surface to replenish the surface layer during subsequent bearing operation, whereas the lubricant additives operate by forming and continually replenishing the layer by the slow release of phosphorus from the liquid reservoir during operation.

III. STUDIES OF BEARING COMPONENTS

A. Sample Preparation and Handling

The sample preparation and handling procedures for the bearing components were similar to those developed for the reference button samples. After their final treatment and cleaning the components were mounted in a specially designed carrousel designed to hold each part at the proper alignment for analysis. A picture of the carrousel is shown in Fig. 16. An aluminum tab with a hole drilled in it was placed over the ball for samples prepared early in the project. The tab was placed so as to facilitate positioning the ball on the analyzer axis, i.e., if aluminum was seen in the Auger then the sample was not centered properly. When the scanning Auger spectrometer was installed, the need for the tabs disappeared and they were discontinued. The carrousel was in turn mounted into a shipping container similar to the one shown in Fig. 1.

Except where noted, the spectrometer used for the bearing component studies was a scanning Auger system. The scanning system was not available until the last few months of the study. As a result there is limited information on bearing components. Some attempts had been made to analyze components with the fixed beam Auger (see Section III B 1) but it was not possible to accurately determine where the analyzed spot was on the samples. This information is critical to examine wear track chemistry.

A specially designed bell jar and sample holder were constructed by Draper Lab to permit the rotation of inner and outer races in vacuo in such a way as to keep the ball groove (or wear track) in the analyzer focal plane. This bell jar is pictured in Fig. 17. The jar was designed

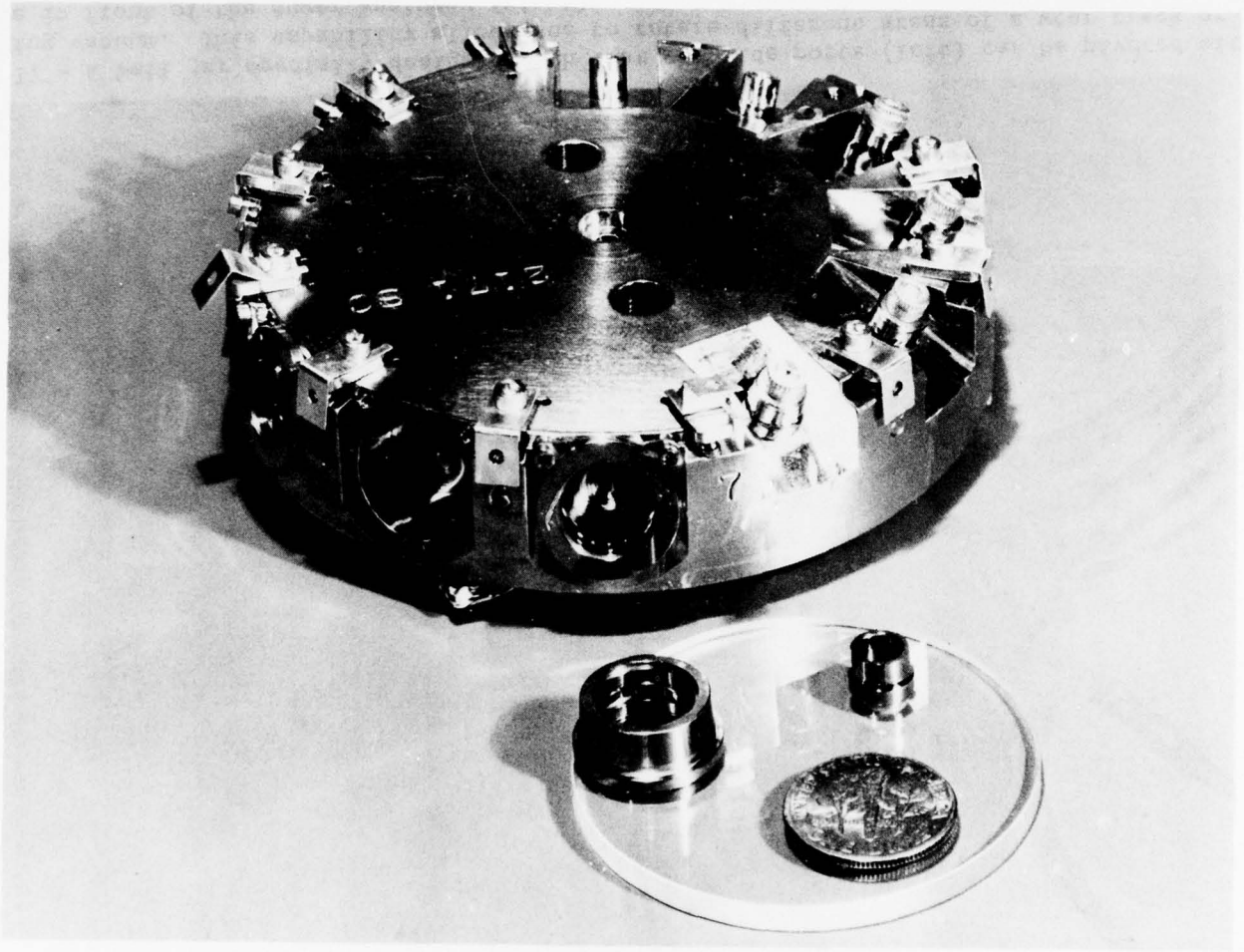


Fig. 16 - Close-up view of sample carrier designed to hold miniature ball bearing components. The Al tabs shadowing the balls were removed after the scanning Auger spectrometer was acquired.

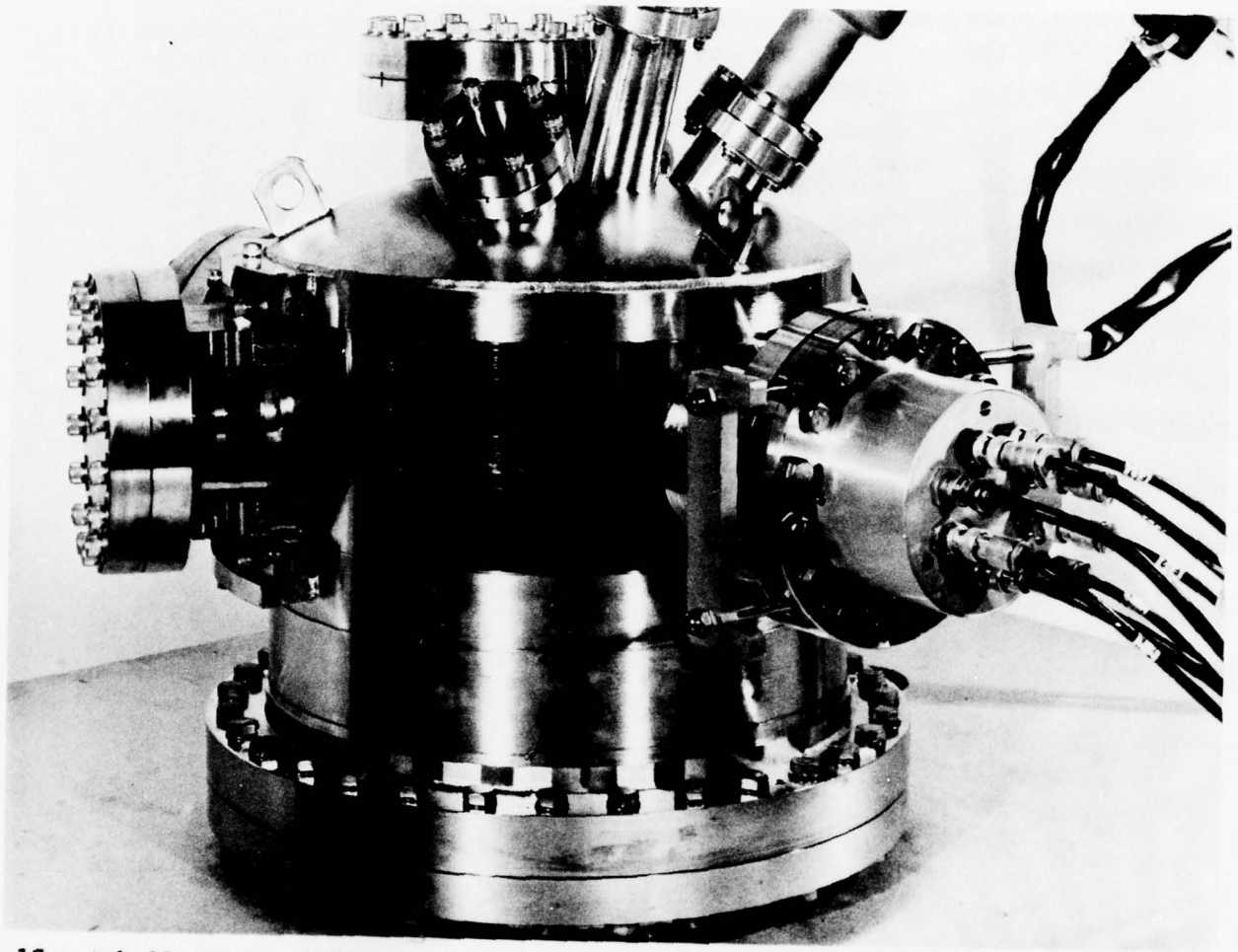


Fig. 17 - A bell jar specially designed such that the side ports (left) can be pivoted without breaking vacuum. This capability allows one to rotate different areas of a wear track or ball groove in front of the Auger analyzer (right).

prior to the availability of the scanning Auger analyzer. As a result, the access port for the analyzer was not the correct size for the scanning analyzer. Since scanning capability was found indispensable, this bell jar was not used. With a relatively simple modification however,it could be altered to accept the scanning analyzer and should prove invaluable for future studies.

B. Studies of Operational Bearings

1. 2171 Bearing Set

Draper studied the performance of 2171 bearings (52100 steel) prepared with certain procedures which were suspected of being detrimental to bearing lifetimes. Table 15 summarizes the history of these bearings. Bearings 35 and 36 were run as a pair with: 1000 hours under standard conditions of 24,000 rpm outer race rotation, 4 lbf preload, 100°F and 1 atmosphere He; exposure to DC-200 silicone to make them nonwettable; 2000 hours additional running to show faint lubricant breakdown. Bearings 55 and 56 were exposed to a 4% solution of Joy in water and showed significant lubricant breakdown in about 200 hours of running. Bearing 57 was exposed to DC-200 but had no running.

Unfortunately, this bearing set required analysis prior to acquisition of the scanning Auger by NRL. Thus, positioning difficulties resulting from sample geometry were compounded by uncertainties as to the precise location of analysis sites relative to the wear tracks on inner and outer races. The data collected from the outer race (OR) originated from a side of the bearing not even in the ball groove; the inner race (IR) data is believed to be from the ball groove. Even the use of perforated aluminum tabs (Section IIIA) to target the bearing balls was only partially successful. Despite attempts to position the balls so as to minimize (zero if properly positioned) the Al Auger signal, in practice a small amount of Al was observed in much of the ball data (Table 16).

Since it was impossible to accurately locate the spot analyzed, no sputter depth profiles were taken on these samples. The measured surface compositions are presented in Table 16.

Prior studies (Section II D) have established that we should not observe the silicones and that prediction is borne out by the data for the silicone-exposed bearings No. 35, 36 and 57. Bearing No. 57 which was not run showed no unusual characteristics. Bearings No. 35 and 36, however, did show significant amounts of phosphorus (with lineshape consistent with a phosphorus - oxygen moiety - see Section II D 3b), cadmium and tin. The origin of these three elements has not been accounted for.

Table 15

Known History of 2171 Bearings

	#35	#36	#57	#55	#56
Pre-run	X	X			
DC-200 Exposure	X	X	X		
Joy Exposure (4% salt in H_2O)				X	X
Run to LBD[1]	X	X		X	X

(1) The pair #35 and #36 were run 2000 hours and showed faint lubricant breakdown.
The pair #55 and #56 were run 200 hours and showed significant lubricant breakdown

Table 16

Surface Composition
2171 Bearings

Bearing ID	Part	# Spots	Normalized Auger Intensities Fe	O	C	S	Cl	Ca	P	Na/Zn	Si	N/Cd	Sn	Al
Silicone Exposed, NOT Run														
#57	Ball	1	28	25	44	2	0.2	0.1	-	-	-	-	-	1
	IR	2	32	26	39	1	0.1	0.5	0.1	0.1	-	-	-	-
	OR	1	32	27	40	0.8	-	0.4	-	-	-	0.2	-	-
Silicone Exposed, Run														
#35	Ball		No Reliable Data											
	IR	3	28	26	43	0.5	-	0.2	0.4	0.2	0.3	0.3(Cd)	0.2	-
	OR	3	27	28	42	0.7	0.2	0.6	0.5	0.4	0.6	0.3	0.2	-
#36	Ball		No Reliable Data											
	IR	4	31	27	41	0.6	-	0.1	0.3	0.2	-	-	-	-
	OR	2	29	26	43	0.6	0.1	0.3	0.4	0.3	-	0.7	-	-
Joy Exposed, Run														
#55	Ball	1	32	29	37	1	-	0.1	0.3	0.1	-	-	-	1
	IR	1	33	27	39	0.5	0.2	0.1	-	0.1	-	0.2	-	-
	OR	3	31	27	39	0.7	0.2	0.6	0.2	0.3	0.8	0.7	-	-
#56	Ball	1	37	33	28	1	0.7	0.1	0.2	0.1	-	-	-	1
	IR	1	36	31	31	0.6	0.2	0.3	0.1	-	0.2	-	-	0.5
	OR	1	31	26	40	0.6	0.2	0.2	-	-	0.9	1	-	-

The two bearings exposed to Joy, No. 55 and 56, are not distinguished by any anomalous surface composition. The Draper studies have shown that the agent in Joy which causes the LBD is a minor anionic constituent in the generic class, glyceryl ether sulfonate. Other than C and O which are present in copious quantities normally, sulfur is the only element of this constituent. The data for bearings No. 55 and 56 do not show any evidence of unusual S concentrations. Careful studies, similar to that performed on the TCP effects on bearing steels (Section II D 3), evidently will be required to establish the degradation action of Joy on the bearing steels.

B. 2. G-200 Bearing Set

The 2171 bearing set discussed in the previous section was a carefully prepared set which was well documented, but was surface analyzed by fixed-beam Auger. The G-200 bearing set (440C steel) represents a sample set whose history was quite varied, but one for which the scanning Auger capability was available.

Over a period of time, Draper had collected and stored R-4 bearings and bearing parts which had shown unacceptable behavior either in pre-run or post-run wetting tests. A set of these parts was examined with the Auger spectrometer to investigate the usefulness of Auger for discriminating surface composition differences which might correlate with poor performance characteristics. As will be seen below, significant differences were detected among the various parts themselves and between the parts and the reference specimens. Table 17 describes the chemical history for all of the examined parts; not included in the Table is the fact that all were three-solvent cleaned (TSC) just prior to shipment to NRL. For the most part the observed surface compositions of the bearings reflect their preparation; but there are significant discrepancies. The surface compositions of the bearing parts are presented in Table 18.

The predominant feature of all the bearing part surface compositions is the presence of carbon. The amount of carbonaceous overlayer is essentially the same for all samples; no substantial differences are observed between different bearing sets or between balls, inner races or outer races. The amount of carbon is substantially larger than that observed on those reference specimens which had been three solvent cleaned (TSC) prior to shipment to NRL for Auger examination (see Table 19).

The second most striking feature observed on many samples was the magnitude of the Cr Auger intensity. Cr is present at $\sim$ 15 atomic % in 440C, but as evident from the data on the reference specimens, (Section II B and C), it has not usually been observed at that concentration in the outer layers of the 440C. Work by Ferrante (19) has demonstrated that under his experimental conditions 440C steel forms a

Table 17

Known History of R-4 Bearing Parts

Treatment	Bearing 801			Bearings M1C + M999B			Misc. Parts		
	Ball	IR	OR	Ball	IR	OR	Ball	IR	OR
Passivated	X	-	X	X	?	?	X	?	?
Chromerged	-	-	-	X	-	-	-	-	-
Tricresyl Phosphate	X	-	X	-	?	?	X	-	-
Zinc Dialkyldithiophosphate	X	X	X	-	-	-	-	-	-
Fail wetting test							X	X	X
Assemble and run as bearing	X	X	X	X	X	X			
Fail post run oil distribution test	X	X	X	X	X	X			

Table 18

Surface Composition
440C Steel R-4 Bearings

Matched Bearing Sets	Normalized Auger Intensities							
	Cr	Fe	O	C	S	Ca	P	Na/Zn[1]
801								
Ball	0.1	5.5	14	68	1	0.5	3	7_z
Inner Race	0.9	4	16	63	1.5	0.8	3	11^z
Outer Race	1.5	4.5	19	54	1.5	1	3.5	15^z_z
M1C								
Ball	5.5	13.5	20	59	0.8	0.3	-	0.1
Inner Race	3.5	9	15	72	0.4	0.2	-	-
Outer Race	7	10	17	65	0.5	0.4	0.1	-
M999B								
Ball	3.5	13.5	19	62	0.6	0.2	0.1	0.1
Inner Race	3	18	13	75	0.3	0.3	0.8	0.2
Outer Race	7.5	9	16	65	0.8	0.4	0.04	0.4
Miscellaneous Bearing Parts								
Balls	0.2	14	18	65	0.1	0.2	2	0.6
Inner Race	6	9.5	18	63	0.4	0.6	1.5	0.8
Outer Race	5.5	9.5	14.5	69	1	0.6	0.1	-

(1) The principal Auger lines for Na and Zn are too close in energy to easily discriminate between them. If the signal has sufficient signal to noise ratio, secondary features can be used to identify the element. Where this was possible, the identification is noted by a subscript z for zinc and n for sodium.

Table 19

R-4 Bearings with Known Treatments Compared to Auger Fingerprints(1)

Treatment/Specimen	Cr	Fe	O	C	S	Ca	K	P	Na/Zn	Fingerprint Elements
TSC										
Reference	2	45	45	7	0.6	0.6	-	-	-	
IR from Misc.	6	10	18	63	0.4	0.6	-	1.5	0.8	
OR from M999B	7	10	17	65	0.5	0.4	-	0.04	0.4	
Chromerge										
Reference	2	35	38	25	0.7	-	-	-	-	Cr, S
Ball from M1C	6	14	20	59	0.8	0.3	-	-	0.1	
Ball from M999B	4	14	19	62	0.6	0.2	0.1	-	0.1	
TCP										
Reference	-	28	27	24	0.7	1	0.8	6	12	P,Na,K,Ca
Ball from Misc.	0.2	14	18	65	0.1	0.2	-	2	0.6	
ZDTP										
Reference	0.4	40	43	12	0.5	0.2	-	1	3	Zn, P, S
Ball from 801	0.1	5	14	68	1	0.5	-	3	7	

(1) Reference Auger composition taken from Table 2 and Table 5

stable, predominantly iron oxide outer layer below 600°C. Our previous data on 440C samples are in agreement with that conclusion (see Fig. 3). The observation of such large Cr signal intensities is therefore surprising. The inner and outer races have much larger Cr signals than do the balls except in the cases of the M1C and M999B bearings where the balls had been subjected to a Chromerge treatment. In no other cases was a Chromerge treatment reported and furthermore the reference flat which was Chromerge-treated did not show nearly as much Cr (as measured by the Cr/Fe signal ratio) as is shown by these bearing parts. These observations beg an answer to the question of what final treatments these bearings received in the manufacture. The possibility of wear processes exposing the Cr is discounted since a) the 801 balls do not show the large Cr in spite of running and b) the miscellaneous parts were never assembled or run as bearings but still have large Cr signals.

The Fe/O ratio is seen to be nearly unity in the reference specimens. In the bearing parts this ratio often deviates significantly from unity but, except for the 801 parts, where it does so, the sum of the Fe/O and Cr/O ratios is approximately unity. This observation leads to the conclusion that the Cr is in an oxide form. The phosphorus signal intensity is strongest on those parts which have been exposed to a TCP or ZDTP submersion treatment, i.e., the 801 parts and the miscellaneous balls (see Table 19). The signal shapes are of the form observed for oxyanions of phosphorus. Phosphorus, again consistent with an oxygen-phosphorus moiety, is found on the miscellaneous IR and OR parts and on the M999B parts. Here the source of phosphorus is presumed to be the TCP additive to the lubricant for extreme pressure (EP) protection. If the lubricant TCP additive is the source for the M999B, the absence of phosphorus on the M1C parts is not understood since these two bearing sets had similar histories.

As a set, the 801 bearing parts show a surface composition considerably different from the other R-4 bearing parts and have a close correspondence to the reference specimens treated with ZDTP (see Table 19). This particular set had been run as a bearing to lubricant breakdown. The characteristic features of the 801 set are the large Zn, P, and S signals. As a signature of three characteristic elements, these match with the reference specimen treated with zinc dialkyldithiophosphate (ZDTP) which also contains these three elements. Further, the ZN/P/S intensity ratios are approximately the same for the 801 parts and the ZDTP-treated reference specimen.

The scanning Auger micrographs shown in Figure 18 show that the distribution of Zn, P, S, and C is not homogeneous and that the wear track has a significantly different composition from the remainder of the ball groove. Sputter profile measurements of the composition in and next to the wear track provided the depth profiles presented in Fig. 19. In the wear track (Fig. 19a) the profile is similar to a solvent-cleaned 440C sample, with the exceptions of a thicker oxide layer, some phosphorus ($\sim$ 5 at %) and zinc ($\sim$ 2 at %) in the first few atomic

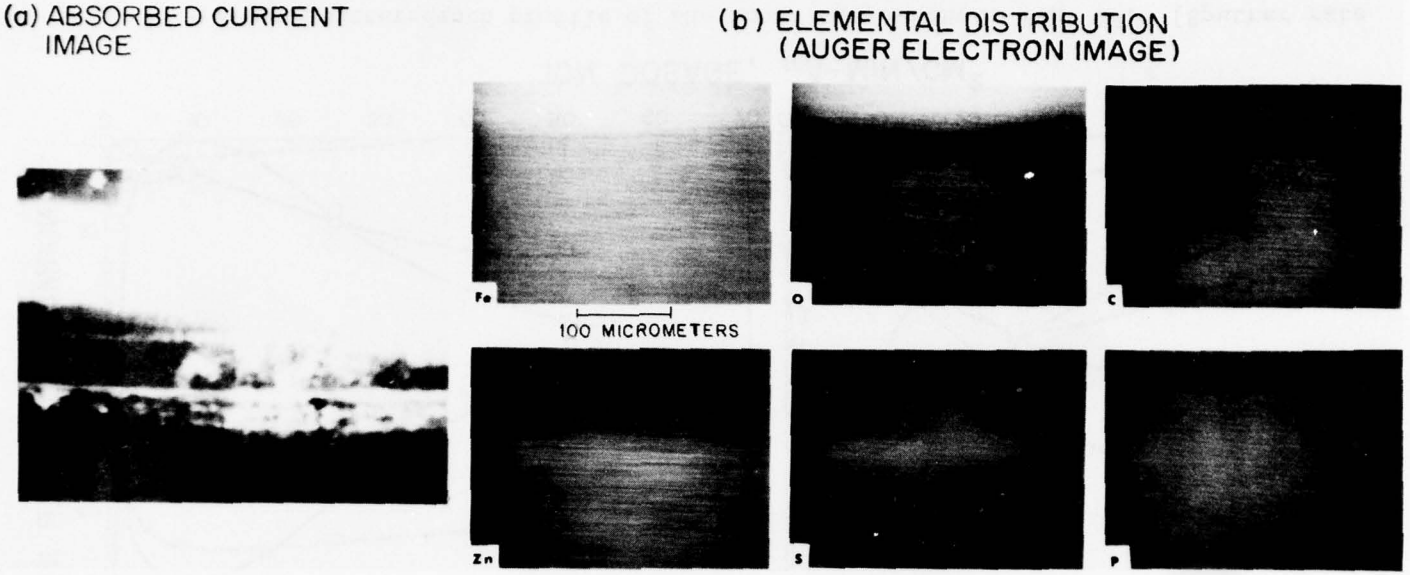


Fig. 18 - (a) Scanning-electron micrograph of an inner race from a disassembled bearing, No. 801. The bright horizontal band in the top of the micrograph locates the wear track. (b) The six micrographs on the right show a scanning Auger measurement of the elemental distribution of Fe, O, C, Zn, S, and P about a point on the edge of the wear track; the lower third is well below the wear track.

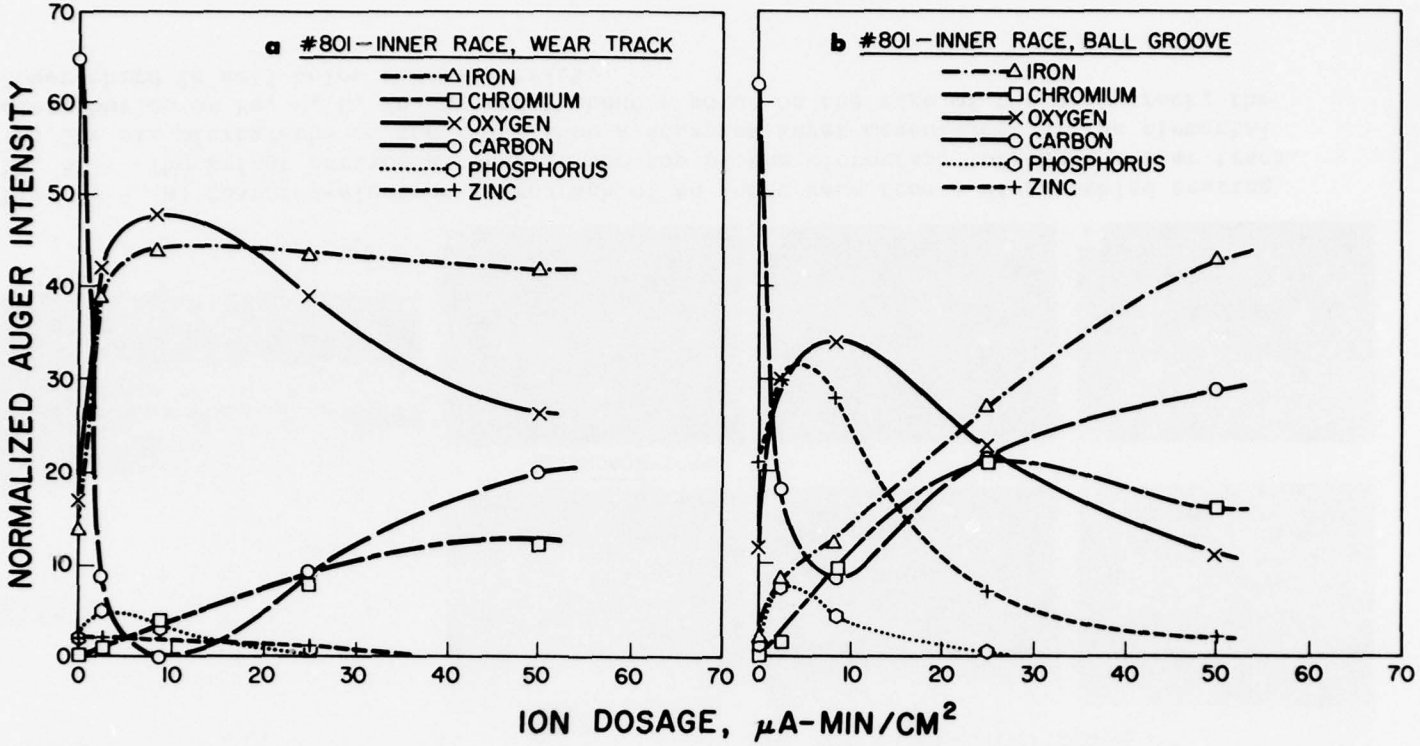


Fig. 19 - Auger sputter-depth profile of the inner race shown in Fig. 18. [Sputter rate $\sim$ 2 Å/(μA/cm^2).] (a) Composition observed at a point well into the wear track corresponding roughly to the upper portion of the pictures in Fig. 18(b). (b) Composition observed at a point below the wear track corresponding roughly to the lower portion of the picture in Fig. 18(b).

layers, and a monolayer of carbonaceous material covering that. The thicker oxide is probably due to the mechanical stresses imposed by the ball or shadowing of the ion beam etchant by greater surface roughness. In the few layers with phosphorus the Auger lineshape is consistent with an oxygen phosphorus moiety.

The ball groove outside the wear track is quite different (Fig. 19b). It contains the same carbonaceous overlayer but beneath it lies a layer with considerable amounts of zinc (30 at %), phosphorus (7 at %) (as an oxygen-phosphorus moiety) and little iron. This is interpreted to mean that the ball groove outside of the wear track retains a ZDTP-promoted overlayer which is formed during the soak treatment. On the basis of the observed elemental distribution, it is postulated that the mechanical action of ball on ball groove serves to remove most of the ZDTP-promoted overlayer from the wear track and to restore an oxide composition similar to that found on lapped buttons, albeit thicker and with about 5 atomic percent phosphate and 2 atomic percent zinc in the first few atom layers. The improved performance observed after the ZDTP treatment could be ascribed to the formation of a persistent phosphate layer in agreement with the postulated action of TCP. The ZDTP-promoted overlayer in the regions outside the wear track may serve as a storehouse of reactant available to restore any wear damage to the wear track phosphate layers.

The recorded histories for the M1C and M999B bearings indicate that for each bearing either an IR or an OR showed poor wetting characteristics after running. Unfortunately, the record does not indicate which race was bad on either bearing. One can ask, however, if Auger can indicate any differences between the IR and OR which might have correlated with poor wetting. The answer is yes: in both bearings the outer race shows larger Cr, Fe, O and less C than the inner race. In fact for all three bearing sets the Cr, Fe, O signal intensities are larger on the OR and the C signal smaller. The miscellaneous parts on the other hand, which have never been run as bearings, do not show this difference between OR and IR.

The inner race of the M999B bearing also shows inhomogeneous surface composition related to wear track chemistry. The scanning Auger micrographs in Fig. 20 show that, in contrast to the 801 inner race, the cleanest surface is the ball groove well away from the wear track. A pronounced carbon film is evident at the edge of the wear track. This corroborates Draper observations of lubricant breakdown (LBD) residues collecting at wear track edges. Sputter profiles have been measured for the wear track and the wear track edge (Fig. 21) and show that the pile of debris is very thick. The wear track itself has only a slightly thicker carbonaceous overlayer than did the 801 bearing wear track.

No scanning or profile data was taken for the M1C bearing, but one of the miscellaneous inner races was sputter profiled. The data, presented in Fig. 22, show a significantly thick overlayer of a carbonaceous residue is found in the ball groove. The layer is not uniform as evidenced

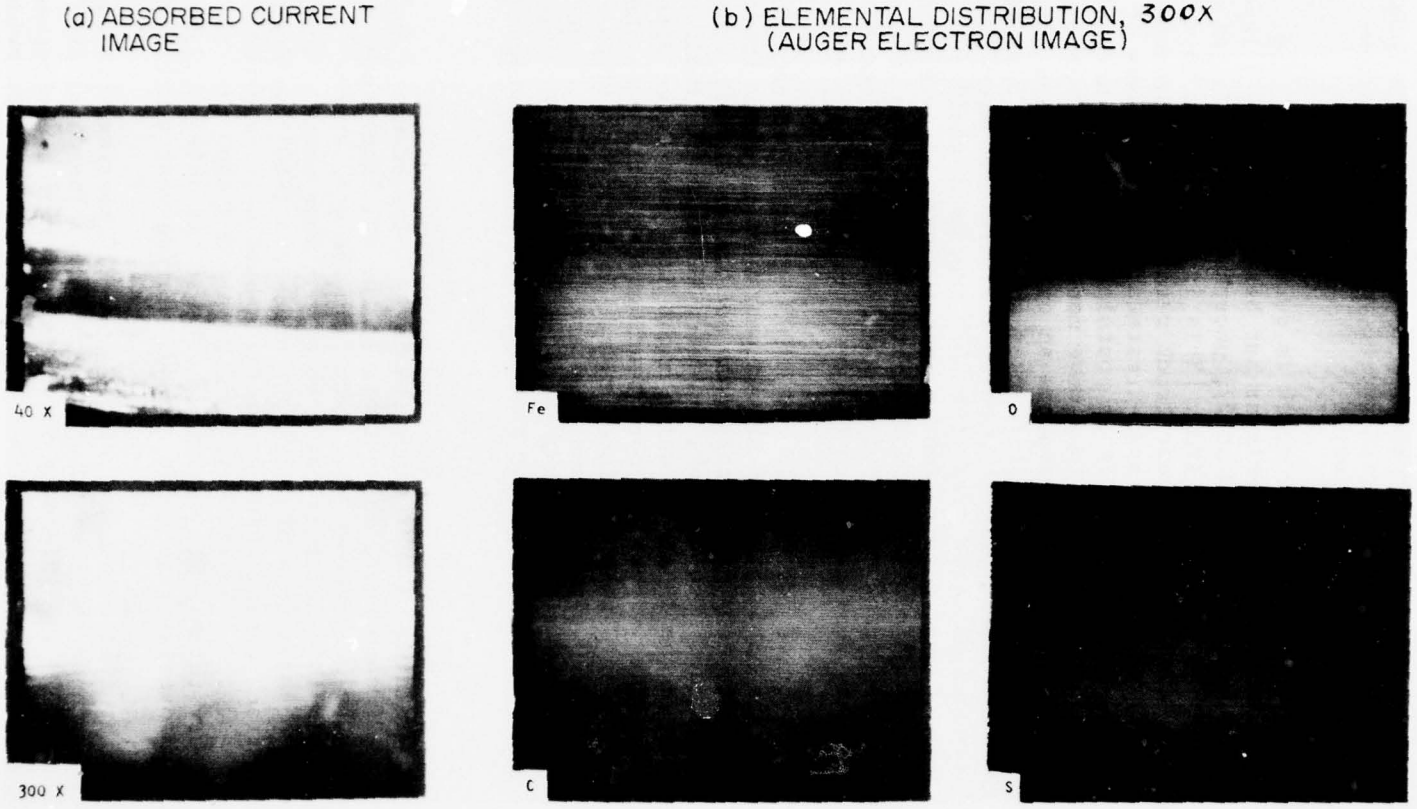


Fig. 20 - (a) Scanning-electron micrographs of a inner race from a disassembled bearing, No. M999B. The bright band at the top of the lower micrograph (300X) corresponds to the wear track. (b) These four micrographs show the scanning Auger measurement of the elemental distribution of Fe, O, C, and S for the same area as shown in the 300X SEM micrograph.

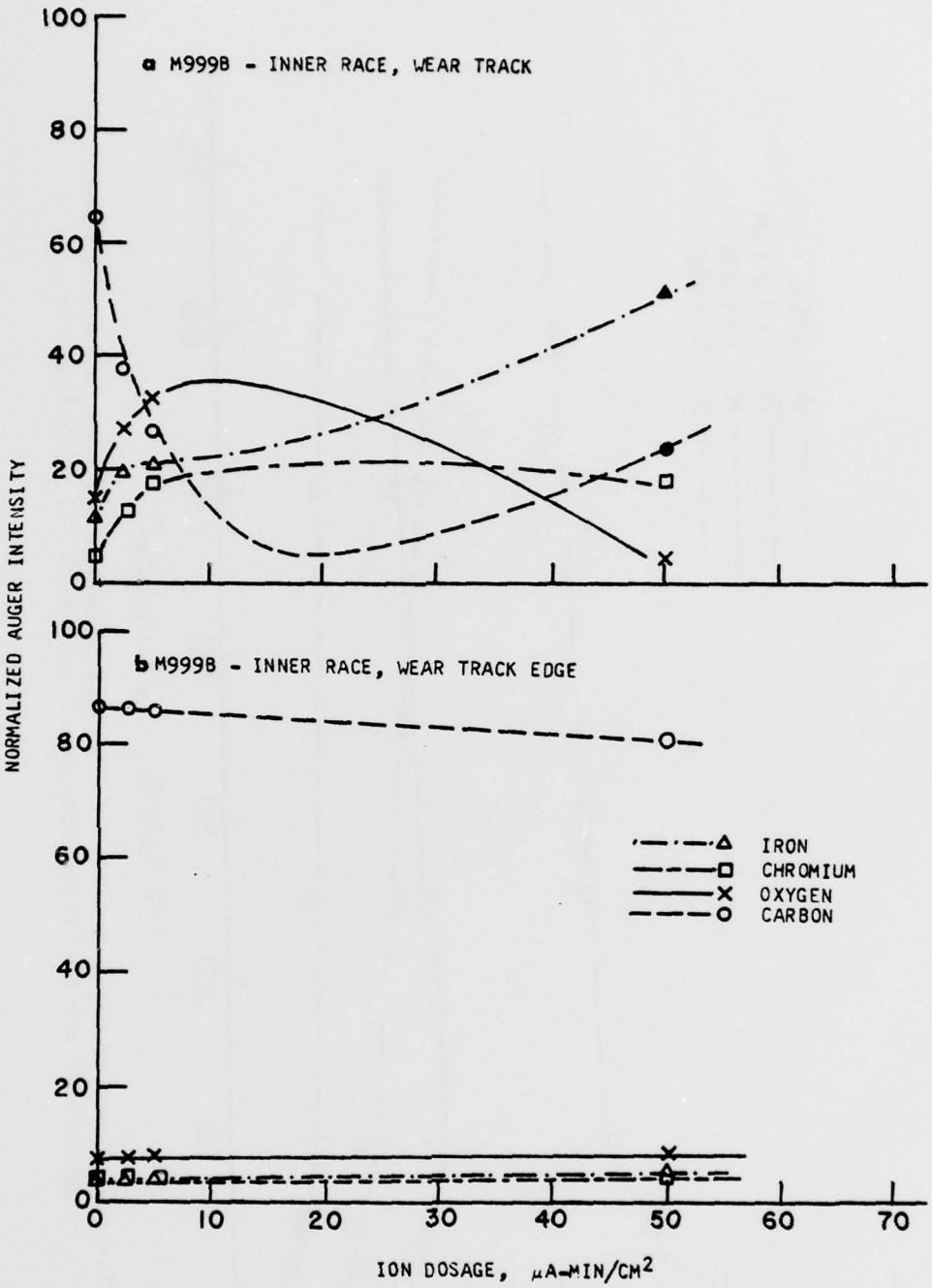


Fig. 21 - Auger/sputter depth profiles of the inner race shown in Fig. 20. [Sputter rate ∿ 2 Å/(μA min/cm^2).] (a) Composition observed in the wear track. (b) Composition observed at a point just below the wear track.

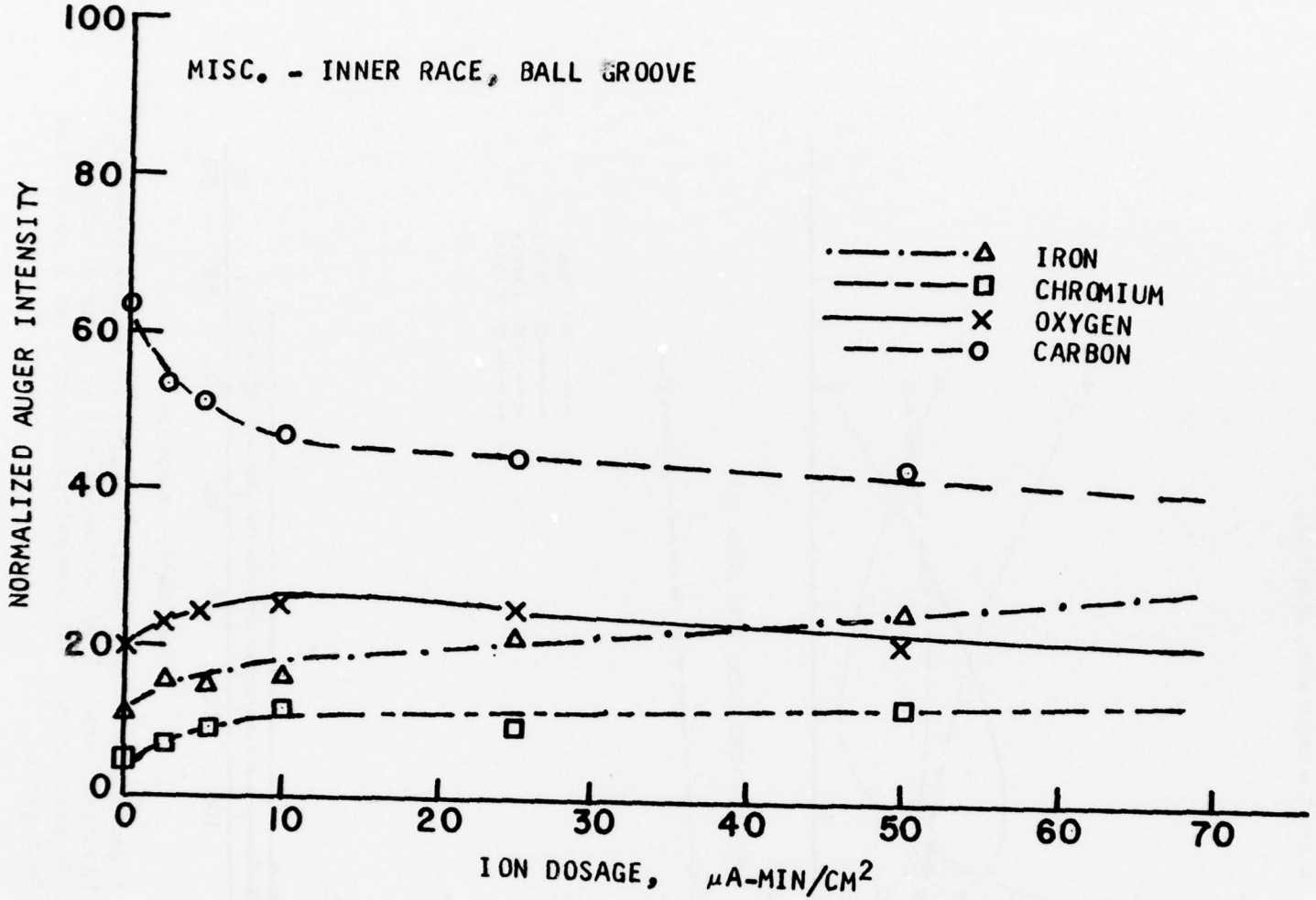


Fig. 22- Auger/sputter depth profile of the ball groove of an inner race which was rejected for use by Draper because it failed an oil spreading test.

by the observation of some substrate material even prior to sputtering. Those areas which are covered, however, have a fairly thick layer. The miscellaneous parts failed their lubricant wetting/spreading test; this layer may be the cause of that failure.

C. Studies of Bearings in Final Production Stages

1. General Observations

The usefulness of Auger spectroscopy as a measurement tool for quality control of bearing manufacturing processes depends on the kinds of information available from the technique. The work presented in this section illustrates some of the kinds of practical information that can be obtained. The surface compositions of bearing components - inner races, outer races, and balls - have been measured for components removed at two stages of production: (1) after the last metal removal step and (2) after the components have been assembled into a complete bearing. It was not thought necessary to probe surface composition earlier in the production process since any metal removal process would strip off a thicker layer of material than Auger spectroscopy examines. Three samples of inner and outer races were extracted by Draper personnel from the production line after the last metal removal step. The samples were solvent-cleaned (TSC) and placed into the sample carrousel. Three packages of assembled bearings, taken from the same production run, were also selected, disassembled, cleaned twice by hexane to remove the preservative oil, solvent-cleaned (TSC), and added to the carrousel. An identified set of IR, OR and ball was used from each bearing assembly. Additionally, separate samples of balls were also received from two manufacturers. These balls also were cleaned by hexane to remove the preservative oil, three-solvent cleaned and mounted in the carrousel.

Examination of the various components in the SEM mode of the scanning Auger system showed obvious irregularities in the topographical structure of the inner races and balls. The outer races are of lesser interest in this regard, not because we found fewer irregularities but because only a small area of the ball groove was observable in our instrumentation. Before pursuing the irregularities let us first examine the surface compositions of an area seen by the SEM as featureless (spatial resolution of the SEM mode in the scanning Auger was on the order of 10 microns). The surface composition of featureless areas on various components is presented in Table 21. Since vacuum system contamination is known to occur (see Section II A) one ball was selected for analysis immediately after insertion in the vacuum system and then rechecked on following days. The ball started very clean; a constituency of C, S, Cl in fact did build up and to a larger degree than observed in other earlier sample sets. This presumably reflects electron-beam-stimulated or thermal desorption from carbonaceous residues on the sample carrousel

Table 20

Legend of Bearing Components From Various Manufacturing Stages

Part	Number of Pieces	Company	Description of Production Stage
Outer Race	3	A	From packaged bearing assembly, same batch as ALMR
	3	A	Immediately after last metal removal (ALMR)
Inner Race	3	A	From packaged bearing assembly, same batch as ALMR
	3	A	Immediately after last metal removal
	4	A	From packaged bearing assembly
Ball	2	B	Machine finished, good quality balls
	2	B	Machine finished, poor surface conditions
	2	B	Tumbled finished, poor surface conditions
	2	C	Acceptable surface finish, stored over 10 years

Table 21

Surface Composition* of Bearing Components: Featureless Areas

Part Analyzed	Date Analyzed	Number of Spots	Normalized Auger Intensities Fe	O	C	S	Cl	Ca	P	Na/Zn	Ba	Mg	Al
Parts Ready for Assembly													
Balls (Company B, good)	5/5	2	49	50	-	-	-	-	-	-	0.8		
	5/6	1	42	40	16	2	0.3	-	-	-	-		
	5/7, 18	3	31	27	39	1	1	-	-	-	0.7(2)		
Inner Race (ALMR)	5/6	3	33	30	36	1	-	-	-	-	1(2)		
Outer Race (ALMR)	5/7	3	28	28	39	1	-	-	2	0.8	0.6		
Parts from Disassembled Bearing													
Balls	5/6	4	40	38	21	0.4	0.3(1)	0.7	0.6(1)	-	-		
Inner Race	5/6	3	40	35	23	0.7	0.2(1)	0.3	-	-	0.5(2)		
Outer Race	5/7	3	30	31	37	1	0.3(2)	0.8	-	-	0.4(1)		
Miscellaneous Balls (Unacceptable)													
Company B, machine finished, bad	5/5	1	49	50	-	-	-	-	-	-	0.7		
	5/7	2	34	32	32	0.9	0.5	-	-	-	0.8		
Company B, tumble finished, bad	5/5	1	42	46	11	0.1	-	-	-	-	1.1		
	5/7	1	34	31	33	0.9	0.7	-	-	-	0.9		
Company C, old	5/5	1	36	44	6	-	0.2	1.3	-	-	4.5	2.7	5.7
	5/7-18	3	27	32	29	2	0.4	1	-	-	2	2	5

* Some elements are not detected at each spot analyzed. Where this happened the number of occurrences is included in parenthesis following the percentage.

or some other source of mobile contaminant which was not present during the sample transit from Massachusetts to NRL. The vacuum system had been baked in the normal fashion prior to this sample set so it should not have been any greater source of contaminant than in previous experience. This observed contamination shows that the amounts of C, S, and Cl must be viewed with caution in any comparisons; however, other elemental constituencies reflect differences in bearing surface composition.

The presence of barium was detected on most of the components, the principal exception being the balls from the disassembled bearings. The barium presumably originates in an anti-corrosion additive. It is most pronounced on those balls which had been a long time in storage. Calcium appears on all components from the disassembled bearings; its source is not known. Phosphorus, with a lineshape consistent with a phosphorus-oxygen moiety, was observed on the outer races procured at the last metal removal step; its source is also unknown.

2. Balls

Fig. 23 shows absorbed current scanning electron micrographs of 52100 balls taken from assembled bearings or supplied by a manufacturer in a ready-for-assembly status; these balls are referred to as acceptable. Fig. 24 shows micrographs of balls which were identified by their manufacturers as having unacceptable surface conditions or very long storage times. The judgment on surface conditions was based on topographical criteria. The featured areas were examined by Auger spectroscopy to determine how, if at all, their surface composition differed from each other and from the featureless areas. The concentric gradation of brightness seen on the balls is believed due to changing secondary emission characteristics as the angle of incidence goes from 90° to 0°. The bright horizontal lines and diffuse white rectangles are caused by changes in surface composition induced by the primary electron beam. In addition to these features there are obvious brighter and darker imperfections located on many balls. From Figs. 23 and 24 it would appear that the acceptable balls have a greater number of these imperfections than do their rejected companions. This attribute is believed due to the more varied chemical environments received by the balls removed from assembled bearings.

Auger analysis of the surface composition in featureless areas of balls showed that they were relatively free of carbonaceous contaminant. Sputter profile measurements of the featureless areas confirmed that the oxide layers of the balls (52100 steel) were approximately the same thickness as the 52100 solvent cleaned buttons. The principal difference from the 52100 button studies was the presence of barium on all balls which had not been assembled into a bearing. The barium layer was particularly pronounced on the balls (Fig. 24 a,b) which had been in storage for longer than ten years. The source of the barium is presumed to be an anti-corrosion additive to oils such as barium dinonylnaphthalene sulphonate.

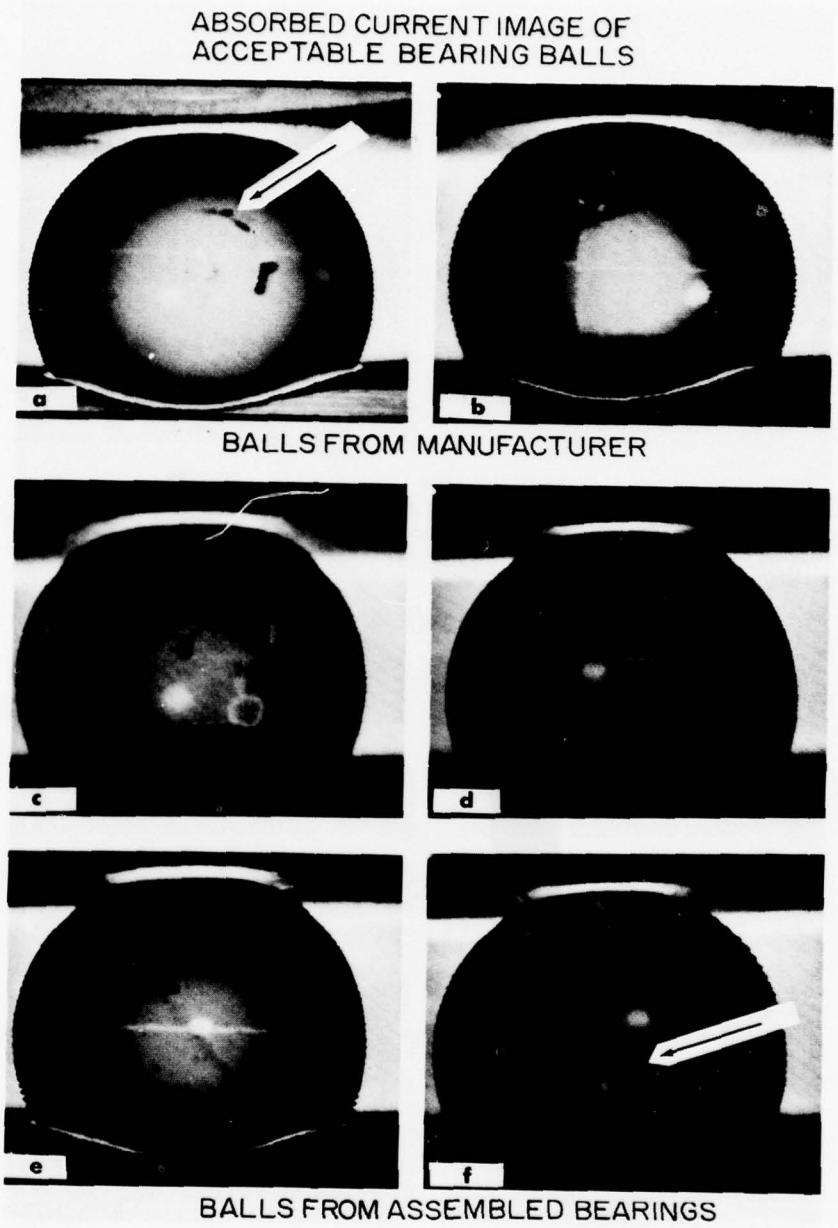


Fig. 23 - Scanning electron micrographs (30X) of bearing balls. The identity of the ball vis a vis Table 20 is: (a - b) Company B, good quality; (c - f) Company A, from packaged bearing assemblies.

ABSORBED CURRENT IMAGE OF
UNACCEPTABLE BEARING BALLS

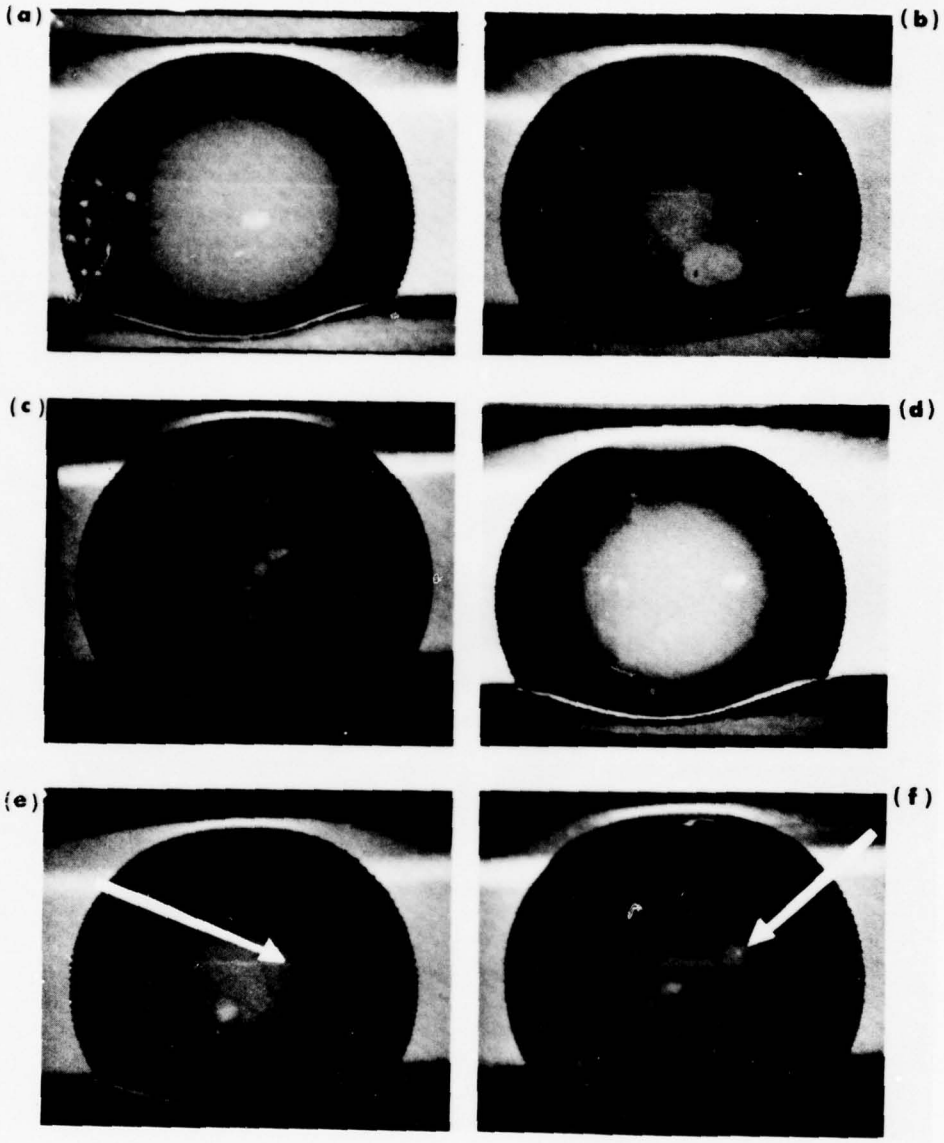


Fig. 24 - Scanning electron micrographs (30X of bearing balls. The identity of the balls vis a vis Table 20 is: (a - b) Company C, stored 10 years; (c - d) Company B, machine finished, poor; (e - f) Company B, tunble finished, poor.

The black imperfection indicated in Fig. 23a is shown by the scanning Auger images in Fig. 25 to be an imbedded alumina particle. Alumina, rather than aluminum, is concluded because this spot was highly insulating, such that no spectra could be observed in a non-rastered electron beam mode due to charging problems.

The varied features indicated in Fig. 23c are enlarged in Fig. 26 and the composition of the various spots are presented in Table 22. The black spots, Fig. 26 points a) and b), are once again imbedded alumina. It is believed that the bright areas in the SEM image, Fig. 26 point c, contains silicon, probably in the form of an oxide. A scanning image of silicon could not be formed due to charging problems. The two remaining black spots, c) and d) of Fig. 26 are attributable to inclusion of Na and Si, and Zn and Ca respectively.

The circular deposit observed on the ball in Fig. 24b was examined by scanning Auger (see Fig. 27). Three spots were analyzed in detail; the data in Table 22 shows considerable Ba, Mg and Al in all three locations. The dark, circular band (Fig. 27, point b) appears best correlated with the absence of carbon. The bright area external to the band (point c) correlates with the presence of carbon.

The black spots evident on the ball shown in Figs. 23f and 28a correlate with the presence of Ca and P. These imperfections are quickly removed by sputter etching and therefore must be due to thin deposits. A dark vein not evident in the micrograph of Fig. 24c, but shown at the edge of the ball in Fig. 28b contains a small amount of Na, Ba, and K. These materials are also quickly removed under sputter attack. A similar dark vein seen in Fig. 24e and magnified in Fig. 28c has similar composition and sputter etch characteristics.

A bright spot on the ball in Fig. 24f was examined by scanning Auger (see Fig. 29). It also proved to be an imbedded Al particle (see Table 22) and shows very clearly the inclusion of C and S in the same hole where the Al particle was observed.

The balls held in storage for 10 years, i.e. the "old" balls, showed Al, Mg and Ca even in the featureless areas analyzed; sputter profile data shows that at least the Al_2O_3 appears to be particulate. Since the surface SEM image and Auger studies of the old balls argue for a homogeneous composition, the particulates must be small (< 10μ) and plentiful.

3. Inner Races

The SEM images of the inner races show one common feature with the ball images - the components analyzed after last metal removal (ALMR, see Fig. 30) show less features than do those removed from assembled bearings (see Figs. 31, 32, and 33). Various features observed in the SEM micrographs were analyzed for identification. The results are listed in Table 23.

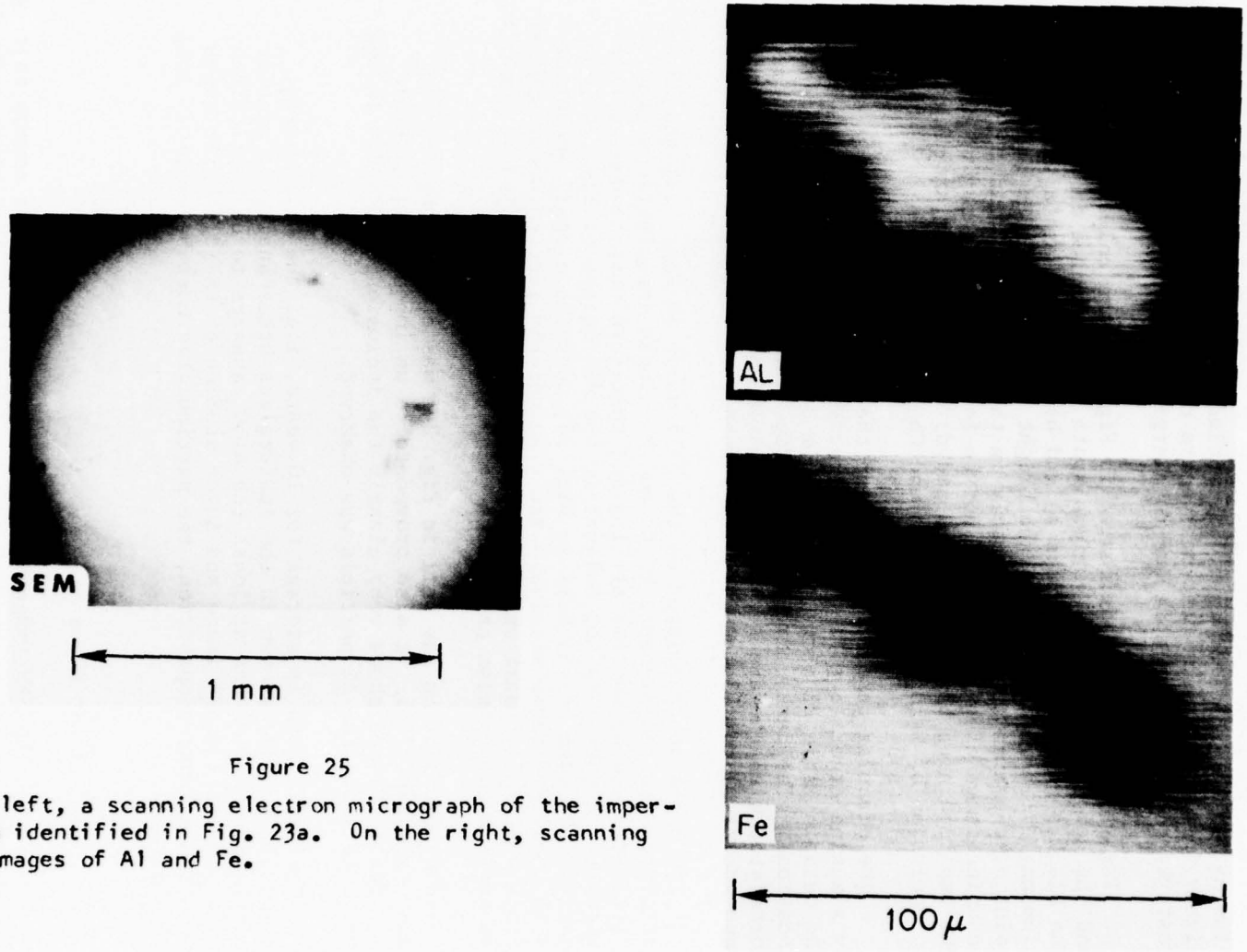


Figure 25

On the left, a scanning electron micrograph of the imperfection identified in Fig. 23a. On the right, scanning Auger images of Al and Fe.

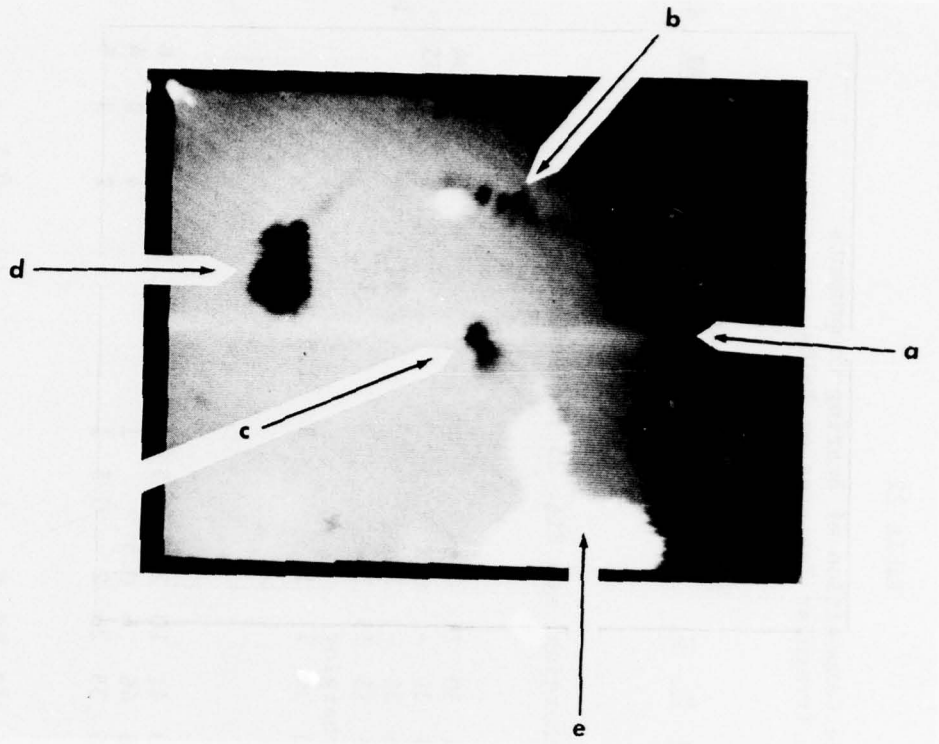


Fig. 26 - A scanning electron micrograph (100X) of the center portion of the ball in Fig. 23c. The compositions of spots a - e are given in Table 22.

Table 22

Surface Composition of Bearing Components
Irregular Features on Balls

Part and Figure Identification	Normalized Auger Intensities													
	Cr	Fe	O	C	S	Cl	Ca	P	Na/Zn	Ba	Mg	Al	Si	Cu
Acceptable Balls														
ALMR														
Fig. 23a		charging, see Fig. 25 for scanning image												
Disassembled														
Fig. 23c, Fig. 26a		14	30	21	0.6							34		
Fig. 23c, Fig. 26b		14	31	-	0.2							55		
Fig. 23c, Fig. 26c		25	26	-	2				32				14	
Fig. 23c, Fig. 26d		36	15	15	3				14^{n}_{z}					18
Fig. 23c, Fig. 26e		charging												
Fig. 23f		43	36	5	1		3	1.5						
Unacceptable Balls														
"Old"														
Fig. 24b, Fig. 27a		33	41	10	2	0.5	1			3	3	6		
Fig. 24b, Fig. 27b		36	46	6	0.5		1			4	3	4		
Fig. 24b, Fig. 27c		26	35	26	2	0.5	1			2	3	5		
Tumble Finish														
Fig. 24c		25	22	47	2	1			1_{n}	0.5				
Fig. 24e		29	27	40	2	1			0.3_{n}	0.5				
Fig. 24f, Fig. 29	2	10	9	73	0.9	0.5						5		

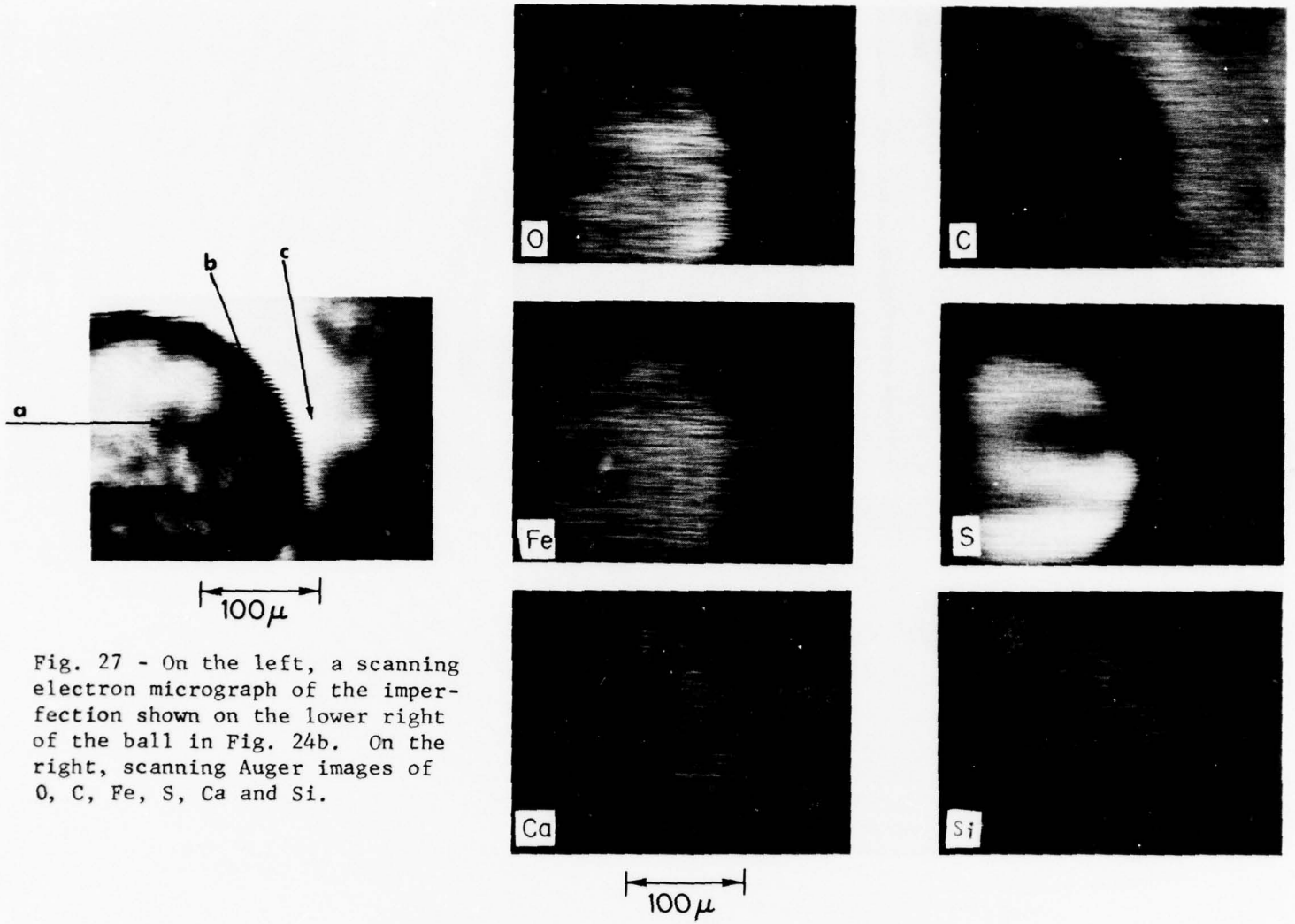


Fig. 27 - On the left, a scanning electron micrograph of the imperfection shown on the lower right of the ball in Fig. 24b. On the right, scanning Auger images of O, C, Fe, S, Ca and Si.

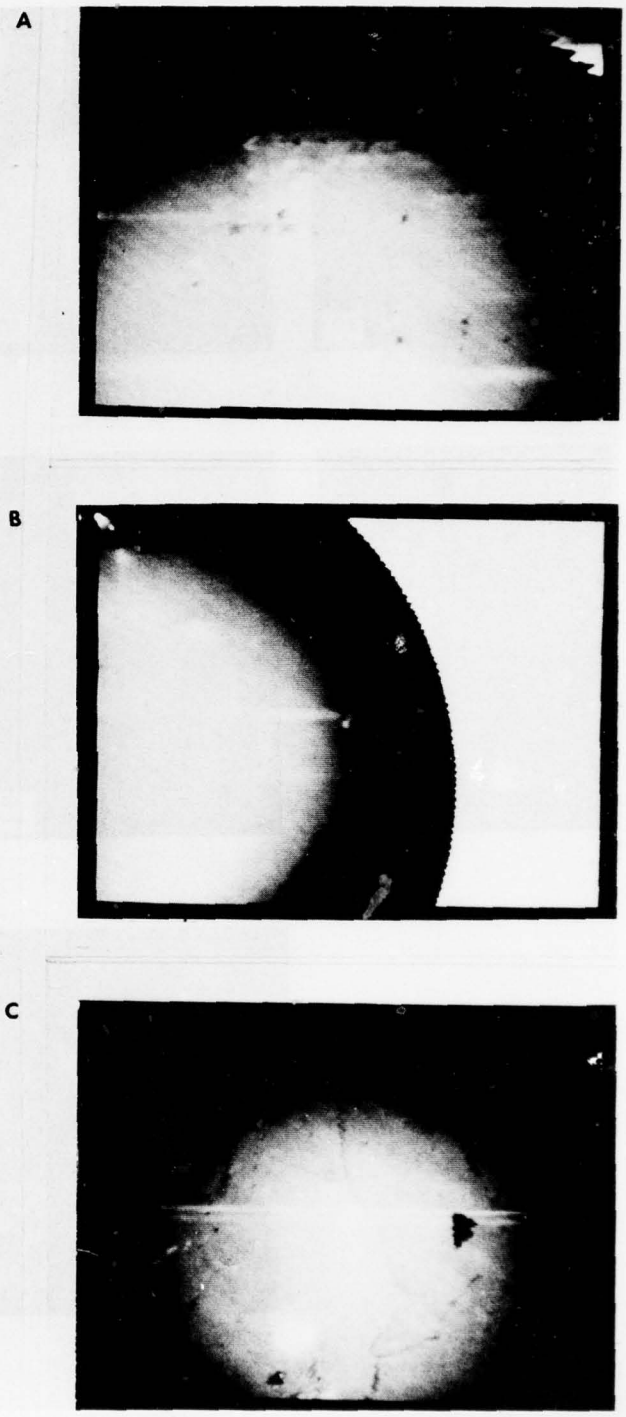


Fig. 28 - Scanning electron micrographs at 60X of balls shown in (a) Fig. 23f, (b) Fig. 24c, and (c) Fig. 24e.

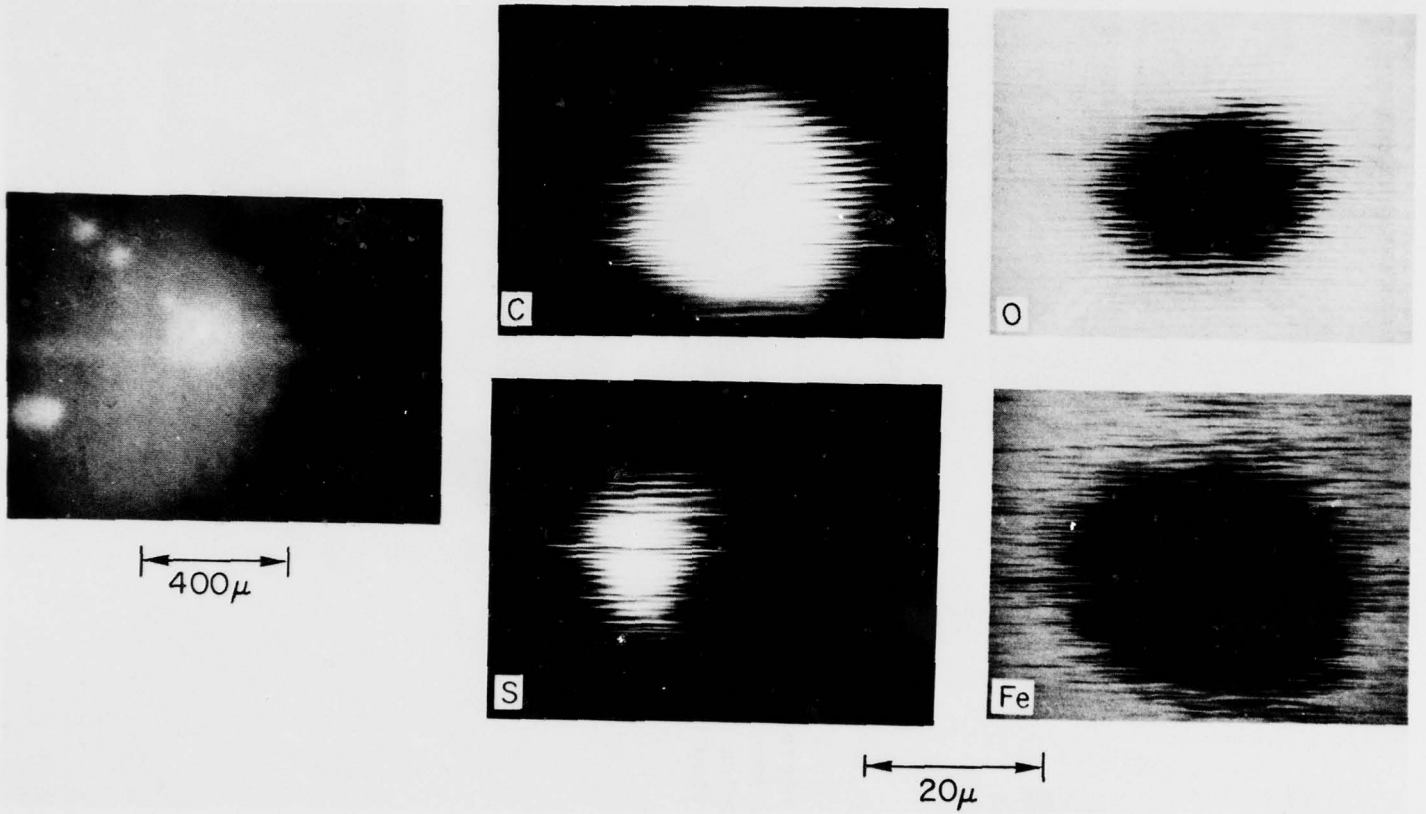


Fig. 29 - On the left, a scanning electron micrograph of the spot indicated in Fig. 24f. On the right, scanning Auger images of C, S, O and Fe. Although not shown, Al is also present in the area where the C is predominant.



Fig. 30 - SEM micrographs (40X) of three inner races examined after the last metal removal step of manufacture.

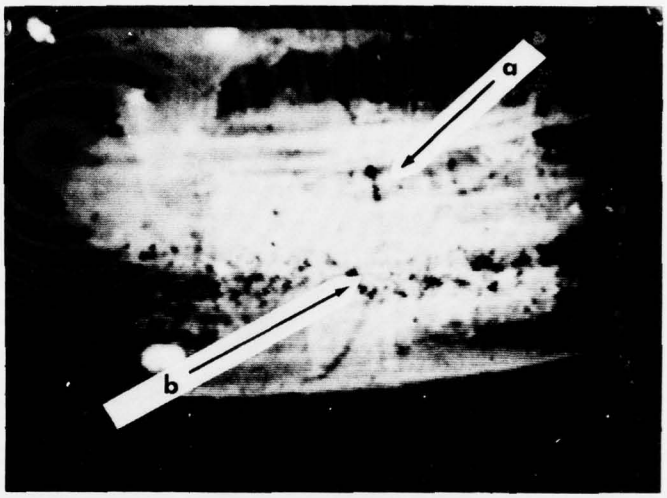


Fig. 31 - SEM micrograph (40X) ot an inner race removed from an assembled bearing

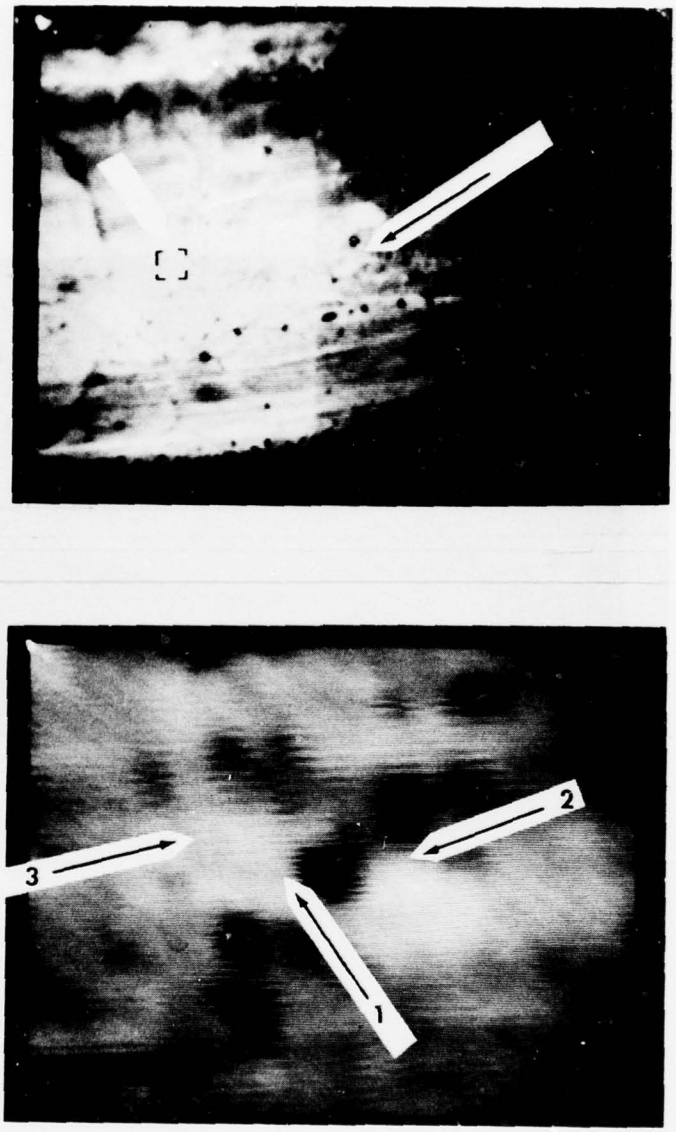


Fig. 32 - SEM micrographs of an inner race removed from an assembled bearing: (a) 40X magnification; (b) 300X magnification of the boxed area in (a).

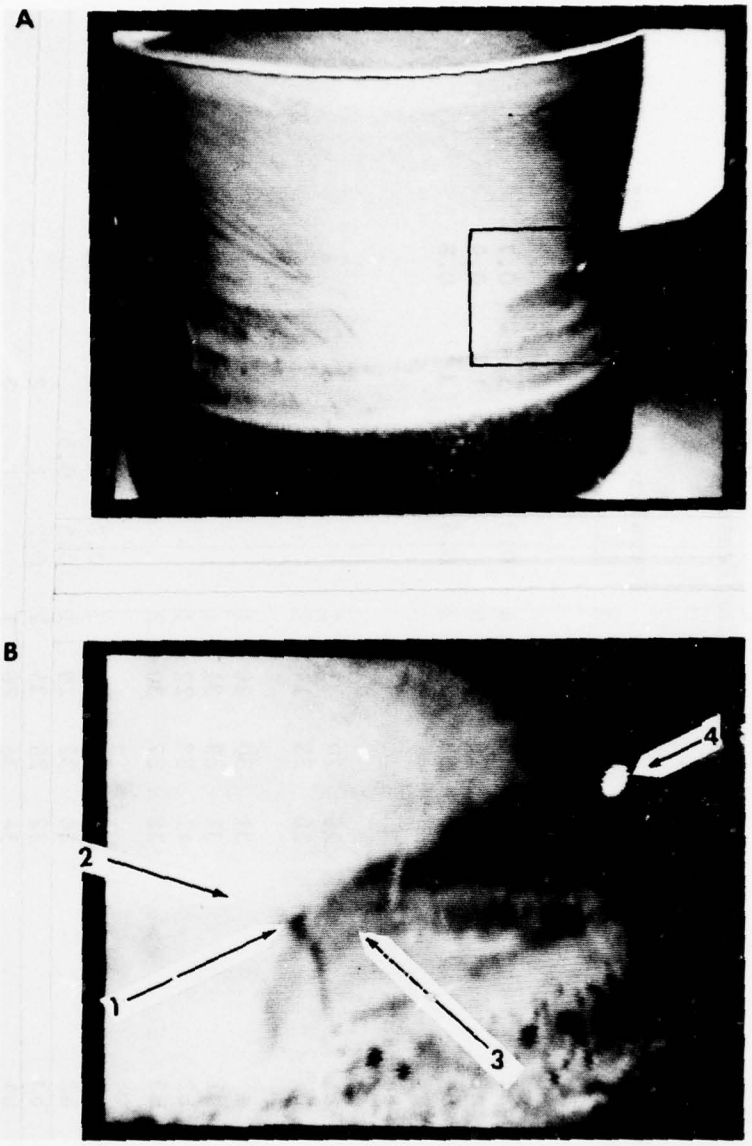


Fig. 33 - SEM micrograph of an inner race removed from an assembled bearing: (a) 12X magnification; (b) 50X magnification of the boxed area in (a).

Table 23

Surface Composition of Bearing Components
Irregular Features on Inner Races

Part and Figure Identification	Normalized Auger Intensities												
	Fe	O	C	S	Cl	Ca	Ba	Zn/Na	K	Al	Mg	Si	P
After last metal removal													
Fig. 30 a1	30	24	40	4	0.3		1	0.7					
a2	31	26	36	6			1	0.9					
30 b	35	33	25	2	0.4	0.4	3	0.8					
Disassembled bearings													
Fig. 31 a	29	29	31	2		8							1
b	26	25	14	1		4		5		22			3
Fig. 32 a	31	30	30	1		5							2
b1	32	29	31	1		5							2
b2	41	33	22	1		1	0.5						1
b3	28	27	30	2		11		0.7					2
Fig. 33 b1	34	32	27	2	0.7	2	2	0.3					
b2	36	32	29	1	0.5	0.5							
b3	32	28	35	2	0.2	1	2						
b4	34	36	26	1		1	2						

The white features in Fig. 30a are correlated with sodium or zinc and sulfur; the black spot in 30b appears to have considerable Ba.

The black spots on the disassembled inner races (Figs. 31 and 32) are usually associated with Ca and P deposits; this correlates with the observations on the ball (Fig. 23e and 28a) removed from an assembled bearing. The lesser defined feature seen in Fig. 33 appears to have both Ba and Ca.

It is presumed that the balls and inner races from disassembled bearings show up more features in the SEM images because they are exposed to a more varied chemical environment. This, in turn, provides a greater opportunity for chemical deposits on the surface which change the secondary emission patterns.

Sputter profile data were taken for several spots on the inner races. The data add no new information.

IV. SUMMARY AND CONCLUSIONS

The goal of this work was to build a data base from which bearing surface chemical states could be identified and correlated with bearing performance. With the limited time available, the study was necessarily a cursory examination of a wide range of samples. It was successful in producing a picture of the natural oxide layers on 52100 and 440C bearing steels, of fingerprints of several common preparation procedures, and of bearings as they come off the manufacturing line. In no case, not even with the TCP study, can one say that the full potential of surface analysis has been realized. This work should be viewed as a beginning, not as an end. The description of the normal oxide layers established in Section IIC and the work on the G-200 bearing components reported in Section III B2 show that a combined performance/surface analytical study has great potential for improving our understanding of the relation of surface chemistry and bearing performance.

As a quality control tool in a manufacturing line, the scanning Auger can provide tremendous amounts of information, as is shown in Section III C. The new surface-sensitive analytical tools have opened a kaleidoscope of new observations. What are the effects of the Ba, Ca, P, Mg, Al, etc. deposits which are observed on the various components?

440C steel will be used in the future bearings instead of 52100 steel because the former better resists corrosion. But it has been shown (Section II C) that the natural oxide layers of 440C seem to differ with the preparation of the metal. Further, 440C bearing components (Section III B2) show different surface compositions among themselves and are different from the reference samples, nominally prepared by similar techniques. These observations suggest that the surface chemistry of 440C may be quite uncontrolled with unknown consequences for corrosion and wear.

The studies have been able to identify some of the chemical modifications associated with good or bad performance. The beneficial treatments of TCP and ZDTP were shown to produce layers with an $\sim$ 5% P content in the form of a phosphorus-oxygen moiety. The glow discharge treatment which led to slightly diminished performance was shown to produce thicker oxide layers which appeared rich in oxygen content. Silicones which were shown by Draper to be relatively innocuous, were in fact hard to detect by AES. The small changes they induced on the surface evidently could be easily removed by the action of ball against ball groove. For the case of Joy exposure, which Draper showed produced the worst behavior, appropriate samples have not been examined to establish the change in surface chemistry.

The scanning Auger studies of the 801 and M999B inner races (Section III B2) have proven the capability for Auger spectroscopy, with its small area of analysis, to detect changes which occur directly within a wear track. The increasing ability to chemically interpret Auger spectra (32) (some of which resulted from this bearing program) provides an important tool for the study of wear track chemistry.

APPENDIX A

Auger Spectroscopy/Experimental Procedure

Auger Composition Measurement

The Auger spectrometer is a standard Physical Electronics System, Model 12-100, using a single pass cylindrical mirror analyzer and a three (3) kilovolt electron beam. A beam current of 5-10μA focused into a 200 micron diameter spot was used for all of the data taken, except for the Scanning Auger studies. Degradation of the surface composition due to the beam was observed in several cases and is noted in the appropriate spots.

Auger spectroscopy is sensitive to the outermost 5 to 30 Å of a solid surface. The surface selectivity is determined by the inelastic mean free path of the Auger electron emitted from the surface atoms. The kinetic energies of the Auger electrons can be used to identify the element from which they came. All elements except H and He can be detected with a variation in sensitivity of less than ten-fold across the periodic table. There is chemical information in the Auger spectra, but it is difficult to interpret. Auger is at best presently a semi-quantitative analytical tool; this point is addressed in more detail in the following paragraph. Several excellent reviews of Auger spectroscopy are available in the literature (34, 35, 36).

Auger in its present stage of development is semiquantitative. The task of making it quantitative is complicated by the presence of several factors each of which depends on the composition and structure of the surface being analyzed. The thrust of the present work is to establish a feel for the kinds of information Auger can provide to bearing technology; the effort to make the data quantitative has been at a very simplistic level.

To facilitate interpretation of the Auger results in terms of surface composition, the authors chose to convert the raw Auger data into a normalized form. Auger electron signal intensities are proportional to atomic concentration and to several other factors. The "other factors" can be divided into two classes - sample dependent and sample independent. The sample independent factors include such things as core ionization cross section, probability for Auger deexcitation, different Auger lineshapes for different elements and the spectrometer response function. The sample dependent factors, i.e. matrix effects, include such things as the distortion of a non-uniform composition in the measured sample volume by electron mean free path effects and variations in signal intensity induced by chemical changes in the valence electron density of states.

To the extent that the surface composition is homogeneous, the measured Auger signal intensities I_i can be related to the atomic concentration by sensitivity factors S_i (34). The sensitivity factors may be estimated from calibrated spectra published by Palmberg et al. (37) provided the experimental conditions are similar (34). Variations of selected S_i from sample to sample or in different materials have been measured by several investigators and the variations have been less than $\pm$ 50% (16, 18, 19). However, for Auger transitions involving the valence electrons, this variation can be larger. For instance, the sensitivity factor for carbon (270 eV line) in graphite is estimated to be one half that of carbide; for iron (650 eV line) in metallic iron, 20% larger than in Fe_2O_3; for phosphorus (120 eV) in phosphide, $\sim$ 60% larger than in PO_4^{3-}. The Auger intensities presented in this paper have been normalized according to the relation $I_i^N = S_i^{-1} I_i / \Sigma S_i^{-1} I_i$. The sensitivity factors S_i used on the data are recorded in Table A1.

The normalized intensities I_i^N can be interpreted as atomic concentrations in the limit of homogeneous surface composition. Observed Auger electrons with energies of 0-600 eV originate predominantly from within 10-15 Å of the surface. The surface composition of the samples observed here does change within that dimension, but with the exception of the initial carbonaceous overlayer, the change is relatively slow. As a result, the normalized intensities reported in the tables and figures may be interpreted as atomic concentrations recognizing the uncertainties discussed above.

Composition Depth Profiling by Sputter/Auger

The sputter etching was accomplished by means of a 2 keV Ar ion beam. For the buttons the angle of incidence was 70-75° from the sample normal; for the bearing components the angle of incidence varied due to the curvature of the sample. The ion current density was measured for the various sputtering conditions by means of a Faraday cup.

Composition depth profiling can be performed by etching away the surface layers while monitoring the surface composition via Auger spectroscopy. The etching process in this work is accomplished by 2 keV ion bombardment of the surface. There are many problems associated with sputter/Auger measurements; these have been adequately described in the literature and won't be discussed here (38, 39, 40, 41). As implied by the heading, the sputter/Auger technique provides information on the atomic composition as a function of depth into the material.

a) Uniform Overlayer

If a uniformly thick, homogeneous overlayer is present on a substrate, the sputter/Auger profile can provide a measure of the overlayer thickness. The Auger spectrometer derives 60% of its signal intensity from Auger electrons emitted within an electron mean free path of the surface. This path is between 5 - 20 Å for commonly used Auger

transitions. As long as the overlayer is thicker than the mean free path, the Auger signals from the elements within the overlayer will be constant (subject to the difficulties discussed in Ref. 38-41). If the sputter yield of the material is known, then an overlayer thickness may be deduced from the ion dosage required to reach the point where the Auger intensities begin to decrease. The conversion from the ion dosage ($\mu A\text{-min/cm}^2$) to Angstroms of material removed depends on the material composition and several other parameters (38). The films under measurement here vary in composition and the variations in the sputter yield are not known but they are principally an iron oxide. For an electro-chemically grown Ta_2O_5 film of 800 Å thickness, the conversion factor was measured as 1 Å per $\mu A\text{-min/cm}^2$ for the same sputtering conditions used on the bearing steels. Betz, Wehner, and Toth (42) estimate the conversion factor to be 0.6 Å per $\mu A\text{-min/cm}^2$ for 2 keV Ar ions normally incident on stainless steel oxide layers. Seo, Lumsden and Staehle (9) estimate 4 Å per $\mu A\text{-min/cm}^2$ for 600 eV Ar ions with unspecified angle of incidence on iron oxides. A value of 2 Å per $\mu A\text{-min/cm}^2$ will be assumed for this report.

When the overlayer is a uniform monolayer coverage or less a simple theory of sputtering (removal rate proportional to the product of sputter yield surface coverage) predicts an exponential decay of the Auger intensity from overlayer constituents. The halflife defined from a plot of signal intensity versus ion dosage provides a measure of the sputter yield. This simple model presumes a uniform overlayer. For the films present in this report the overlayers are probably not spatially, or compositionally uniform. Spatial variations in overlayer thickness or composition will in general make the signal-intensity decrease non-exponential. Further the signal halflife will reflect the spatial variation of the thickness as well as the sputter yield. This fact is utilized in the report to explain the variation in decay halflife seen for the various oxide films.

Scanning Auger Microscopy

The scanning Auger microscope allows one to raster the primary electron beam over a square 400 microns to a side and to energy-analyze the secondary electrons emitted from the area. This permits one to select out only the Auger electrons from a designated element. The electron current from that element is used to modulate the intensity of a cathode ray tube monitor whose scan is synced with the primary beam. Elemental images may thereby be formed.

The electron beam spot size determines the resolution of the elemental and SEM images taken with this instrument. The spot size for this work is estimated to be on the order of 10 microns. When this work was accomplished, the suspension of the spectrometer was inadequate to prevent building vibrations from jiggling the sample. The wavy features of the scanning images are due to this wiggling and can be precluded by better isolation mounts.

Table A1

Auger Sensitivity Factor, S(1)

Atomic No.	Element	Ref.	n(2)	Auger Line (eV)	λ(3)	S=λ/n
5	B	B	1.3	179	9.2	7.1
6	C	C	10	272	7.3	.7
7	N	TaN	5.0	381	12.2	2.4
8	O	MgO	5.3	512	34.2	6.3
11	Na	$Na_{0.7}WO_3$	0.8	990	2.25	2.8
12	Mg	Mg	4.3	45	28	6.5
				1186	6.7	1.6
13	Al	Al	6.0	68	13.1	2.2
				1396	3.3	0.6
14	Si	Si	5.2	92	32.1	6.2
				1619	3.0	.6
		SiO_2		78		
15	P	GaP	2.5	120	15.8	6.3
16	S	CdS	2.0	152	43.5	21.8
17	Cl	KCl	1.6	181	17.9	11.2
19	K	KCl	1.6	252	26.2	16.4
20	Ca	Ca	2.3	291	30.7	13.1
21	Ti	Ti	5.6	418	29.3	5.2
24	Cr	Cr	8.2	529	20.5	2.5
				571	7.6	.9
26	Fe	Fe	8.5	651	13.3	1.6
28	Ni	Ni	9.1	848	17.1	1.9
29	Cu	Cu	8.5	920	16.0	1.9
30	Zn	Zn	6.6	994	13.0	2.0
31	Ga	GaP	2.5	55	2.0	0.8
				1070	5.9	2.4
33	As	InAs	1.8	91	0.9	0.5
				1228	2.7	1.5

Atomic No.	Element	Ref.	n(2)	Auger Line (eV)	λ(3)	S=λ/n
34	Se	Se	3.7	99	1.8	0.49
				1315	7.2	1.9
40	Zr	Zr	4.2	147	10.5	2.5
47	Ag	Ag	5.9	351	67.2	11.4
48	Cd	Cd	4.6	376	64	13.9
		CdS	2.0		29.5	14.8
	Sn	Sn	3.0	425	40	13.3
56	Ba	Ba	1.5	73	7.8	5.2
				584	7.6	5.1

APPENDIX B

Sample Preparation Procedures

1. Three Solution Cleaning (TSC)

   All solvents reagent grade

   a. Ultrasonic clean for 5 min in toluene, vacuum dry
   b. Ultrasonic clean for 5 min in Freon (TF or PCA), vacuum dry
   c. Ultrasonic clean for 5 min in methanol, vacuum dry
   d. Dip in solution of 50% methanol and 50% acetone, vacuum dry

2. Glow Discharge

   a. Pumpdown to 8×10^{-7} torr.

   b. Backfill to 200 microns with Ar as measured with a thermocouple gauge.

   c. GDC at 200 ma for 15 minutes

   d. Pump to 8×10^{-7} torr

   e. Backfill to 200 microns O_2

   f. GDC at 200 ma for 15 minutes

   g. Pump to 8×10^{-7} torr

   h. Vent with N_2

3. Passivation (Chromic-Nitric Acid)

   a. Submerge sample for 30 min in a 115°F bath of

      800 ml Distilled H_2O

      200 ml Nitric acid

      20 mg Sodium dichromate

   b. Rinse twice in hot distilled H_2O

   c. Air dry

4. Chromerge (Chromic-Sulfuric Acid) Treatment

   a. Submerge in Chromerge at 150°F for 15 min.

   b. Rinse copiously with distilled H_2O

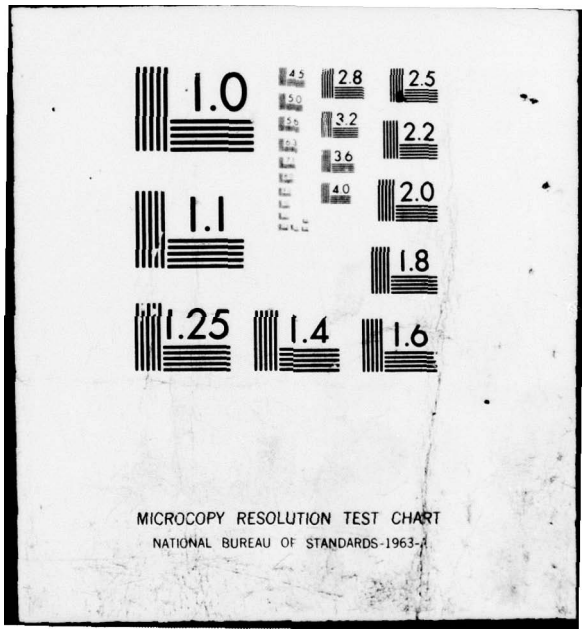
   c. Vacuum dry

AD-A060 834 NAVAL RESEARCH LAB WASHINGTON D C F/G 13/9
SURFACE CHEMISTRY OF BALL BEARING STEELS II.(U)
AUG 78 J S MURDAY, E G SHAFRIN
UNCLASSIFIED NRL-MR-3850 NL

2 OF 2
AD
A060834

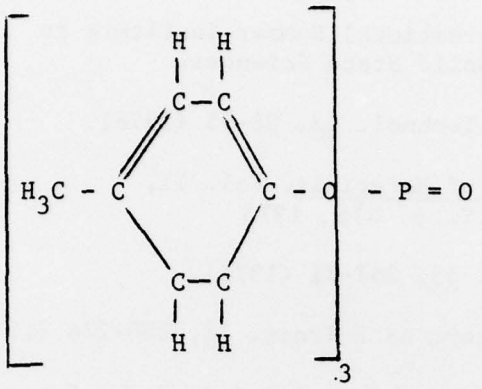


END
DATE
FILMED
1-79
DDC


1.0
1.1
1.25
1.4
1.6
1.8
2.0
2.2
2.5
2.8
3.2
3.6
4.0
4.5
5.0
MICROCOPY RESOLUTION TEST CHART
NATIONAL BUREAU OF STANDARDS-1963-A

5. Tricresyl Phosphate (less than 2% ortho)

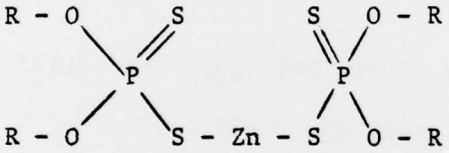
Tri-p-cresyl phosphate



a. Submerge in TCP at 225°F for 4 days

b. Three solution clean

6. Zinc Dialkyldithiophosphate



(where R = alkyl group)

a. Submerge in ZDTP at 125°F for 4 days

b. Three solution clean

7. Silicone Treatments

a. Cover surface with a copious amount of silicone at 70°F for 1 hour.

b. Three solution clean.

REFERENCES

1. W. E. Jamison, J. Vac. Sci. Technol. 13, 76-81 (1976).

2. T. E. Fischer, Proc. of International Summer Institute in Surface Science, Critical Reviews in Solid State Sciences.

3. D. H. Buckley, J. Vac. Sci. Technol. 13, 88-95 (1976).

4. D. Tabor in Surface Physics of Materials, Vol. II, J. M. Blakely, ed., Academic Press, N.Y., p. 475, 1975

5. J. S. L. Leach, Surface Sci. 53, 257-71 (1975).

6. R. L. Cottington and H. Ravner, ASLE Trans. 12, 280-286 (1969).

7. "Final Report Gyro Bearing Improvement Program, Tasks 8 to 10 NAS 9-3079", MIT/DL R-674, October 1970.

8. J. S. Murday, E. G. Shafrin, E. P. Kingsbury and S. Allen. "Surface Chemistry of Ball Bearing Steels I", NRL Memorandum Report 3047, April 1975.

9. M. Seo, J. B. Lumsden and R. W. Staehle, Surf. Sci. 50, 541-552 (1975).

10. M. Suleman and E.B. Pattinson, Surf. Sci. 35, 75-81 (1973).

11. K. Ueda and R. Shimizu, Surf. Sci. 43, 77-87 (1974).

12. G. Ertl and K. Wandelt, Surf. Sci. 50, 479-492 (1975).

13. G. W. Simmons and D. J. Dwyer, Surf. Sci. 48, 373-392 (1975).

14. G. C. Allen and R. K. Wild, J. Electron Spectrosc. Relat. Phenom. 5, 409-415 (1974).

15. C. Leygraf, G. Hultquist and S. Ekelund, Surf. Sci. 51, 409-432 (1975).

16. W. E. Boggs, R. H. Kachik and G. E. Pellissier, J. Electrochem. Soc. 112, 539-546 (1965); W. E. Boggs and R. H. Kachik, ibid. 116, 424-430 (1969).

17. J. P. Coad and J. G. Cunningham, J. Electron Spectrosc. Relat. Phenom. 3, 435-448 (1974).

18. T. W. Haas, J. T. Grant and G. J. Dooley in Adsorption-Desorption Phenomena, F. Ricca, ed., Academic Press, N.Y., 1972.

19. J. Ferrante, "Auger Electron Spectroscopy and Depth Profile Study of Oxidation of Modified 440C Steel", NASA TN-7789, Oct. 1974.

20. Military Specification MIL-B-81793, U.S. Dept. of Defense, "Bearing, Ball, Precision, for Instruments and Rotating Components", 23 November 1973.

21. A. C. Edwards, "Final Report on the Gyro Spin-Axis Bearing Program", MIT/IL R-418, September 1963.

22. H. B. Singer, "The Effect of TCP Treatment on the Low-Speed Performance of Ball Bearings", MIT/IL E-2317, September, 1968; presented at the Dartmouth Bearings Conference, Dartmouth College, Hanover, N.H., 3-6 September 1968.

23. C. H. Hannan, "The Effect of Tri-Cresyl-Phosphate Coating on Reducing Torques in Low-Speed Bearings", presented at the Dartmouth Bearings Conference, Dartmouth College, Hanover, N.H., 3-6 September 1968.

24. S. Allen, "Final Report, Gyro Bearing Program", Tasks 1 to 6, NAS 9-3079", MIT/DL R-586, June 1970; "Tasks 8 to 10, NAS 9-3079", MIT/DL R-674, October 1970.

25. S. Allen, "Effect of Surface Condition of Instrument Ball Bearings", MIT/DL E-2766, May 1973.

26. D. Godfrey, ASLE Trans. 8, 1-11 (1965).

27. E. E. Klaus and H. E. Bieber, ASLE Trans. 8, 12-20 (1965).

28. H. E. Bieber, E. E. Klaus and E. J. Tewksbury, ASLE Trans. 11, 155 (1968).

29. R. L. Cottington and H. Ravner, ASLE Trans. 12, 280-286 (1969).

30. R. L. Jones, H. Ravner and R. L. Cottington, ASLE Trans. 13, 1-10 (1970).

31. G. D. Galvin, D. W. Morecroft and A. G. Patterson, Trans. ASME 90F, 850 (1968).

32. M. K. Bernett, J. S. Murday and N. H. Turner, J. Electron Spectrosc. and Related Phenomena 12, 375-393 (1977).

33. H. L. Hughes, R. D. Baxter and B. Phillips, IEEE Trans. Nucl. Sci. NS-19, 6, 256 (1972).

34. C. C. Chang in Characterization of Solid Surfaces, P. F. Kane and G. B. Larrabee, eds., Plenum Press, New York, 1974.

35. E. N. Sickafus, J. Vac. Sci. Technol. 11, 299 (1974).

36. J. C. Riviere, Contemp. Phys. 14, 513 (1973).

37. P. W. Palmberg, G. E. Riach, R. E. Weber and N. C. MacDonald, Handbook of Auger Electron Spectroscopy, Physical Electronics Industries, Inc., 6509 Flying Cloud Drive, Eden Prairie, Minn. 55343. (1972)

38. G. K. Wehner in Methods of Surface Analysis, A. W. Czanderna, ed., Elsevier Scientific Publishing Co., New York, 1975.

39. J. W. Coburn, J. Vac. Sci. Technol. 13, 1037-1044 (1976).

40. D. M. Holloway, J. Vac. Sci. Technol. 12, 392-399 (1975).

41. J. W. Coburn and E. Kay, CRC Critical Reviews in Solid State Sciences 4, 561-590 (1974).

42. G. Betz, G.K. Wehner, L. Toth, and A. Joski, J. Appl. Phys. 45, 5312-5316 (1974).